SYNTHESIS AND CHARACTERIZATION OF BIO-DEGRADABLE   STARCH BASED GRAPHENE NANOCOMPOSITES

A dissertation submitted to the Department of Physics, Bangladesh University of Engineering and Technology, Dhaka in partial fulfillment of the requirements for the degree of Master of Science (M.Sc) in physics

**Submitted
By
Md. Shafiqul Islam Mollik
Roll NO: 0417142504F
Session: April-2017**

**DEPARTMENT OF PHYSICS
FACULTY OF ENGINEERING
BANGLADESH UNIVERSITY OF ENGINEERING AND TECHNOLOGY (BUET)
DHAKA-1000, BANGLADESH
JULY, 2019**

BANGLADESH UNIVERSITY OF ENGINEERING AND TECHNOLOGY (BUET)

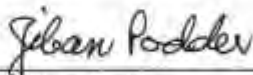## DEPARTMENT OF PHYSICS, DHAKA-1000, BANGLADESH

CERTIFICATION OF THESIS

The thesis titled **"SYNTHESIS AND CHARACTERIZATION OF BIODEGRADABLE STARCH BASED GRAPHENE NANOCOMPOSITES"** submitted by **Md. Shafiqul Islam Mollik**, Roll No.:0417142504F, Session: April'2017, has been accepted as satisfactory in partial fulfillment of the requirement for the degree of **Master of Science** (M. Sc.) in Physics on 09 July, 2019.

BOARD OF EXAMINERS

1. _____   Chairman
Dr. Muhammad Rakibul Islam (Supervisor)
Assistant Professor, Department of Physics, BUET

2. _____   Member (Ex-Officio)
Dr. Md. Forhad Mina
Professor and Head, Department of Physics, BUET

3. _____   Member
Dr. Jiban Podder
Professor, Department of Physics, BUET

4. _____   Member
Dr. Mohammed Abdul Basith
Professor, Department of Physics, BUET

5. _____   Member (External)
Dr. Khandker Saadat Hossain
Professor, Department of Physics, University of Dhaka

DECLARATION

It is hereby declared that the work for this thesis has not been presented elsewhere by the author

for any degree or diploma.

Md. Shafiqul Islam Mollik
Roll No. : 0417142504F
Session: April- 2017
Department of Physics
BUET, Dhaka-1000

ACKNOWLEDGEMENT

Abstract

Biopolymers with nano-scale fillers based nano-composites have gained significant research interest as an alternative to the conventional plastics. The synthetic plastics are detrimental to health and are a great threat to wildlife due to its low quality degradation and fabrication of biodegradable starch is therefore much needed. Starch, a natural polysaccharide, is considered as one of the most promising biopolymers to the alternatives of fossil resources because it possesses a number of unique specialties such as renewability, abundance, low cost and biodegradability. The physical properties of biopolymer can be improved by incorporating various nano-materials as fillers in the polymer matrix. In this study, Graphene oxide (GO), and Reduced graphene oxide (RGO), derivatives of Graphene, has been used as a nanofiller for plasticized starch (PS) matrix. Biodegradable PS has been extracted from potato and a solution casting technique was used to fabricate GO/PS and RGO/PS nanocomposite. After synthesis, the structural, chemical, mechanical, optical, dielectric and electrochemical properties of the nanocomposite has been studied. The structural properties of the nanocompopsite shows the presence of the same crystal type for PS, GO/PS and RGO/PS. Chemical analysis indicates formation of hydrogen bonding between graphene and PS in nanocomposite. The optical properties shows that incorporation of GO and RGO enhanced the absorbance of the nanocomposite. The tensile strength of PS increased with the amount of graphene nanofiller, proves that GO/RGO had an obvious reinforcing effect on the PS matrix. Furthermore, the dielectric constant of the nanocomposite increases with the filler concentration indicating interfacial and space charge polarization in the nanocomposite. The electrochemical properties shows that incorporation of GO or RGO nanofiller significantly enhance the specific capacitance of the nanofiller. PS/GO (0.5%) shows a higher dielectric constant of almost 5000 and a specific capacitance of 116.5 f/g while PS/RGO (1%) offers a remarkable value in dielectric constant of 60000. The enhanced dielectric constant & specific capacitances of graphene based PS nanocomposite originate from the synergistic effect of PS and graphene. The starch based graphene nanocomposite with improved mechanical, dielectric and electrochemical properties synthesized from a simple, low-cost process will pave a way to the production of economic and bio-friendly energy storage devices.

CONTENTS

CHAPTER ONE: INTRODUCTION

CHAPTER TWO: LITERATURE REVIEW

CHAPTER THREE: EXPERIMENTAL DETAILS

CHAPTER FOUR: RESULTS & DISCUSSION

CHAPTER FIVE: CONCLUSION

List of figures

CHAPTER ONE

INTRODUCTION

1.1 Introduction

Plastic is considered as one of the greatest innovation of 20th century because of its resilience against degradability, flexibility, ease of manufacture, imperviousness to water and cost effectiveness and are used in lots of products of different sizes, from paper clips to spacecraft. Plastic has replaced the traditional materials, such as, wood, stone, horn and bone, leather, metal, glass and ceramic. But this wonder-product, which has transformed our lives in so many positive ways, has some serious environmental flaws in both its production and disposal and become a great concern for human health and the environment.

Bio-nanocomposites offer an environment- friendly strategy for the production of novel materials and has a potential to replace conventional plastic. These systems are comprised by a continuous biopolymer matrix loaded with nanofillers, usually inorganic in nature [1-3].While the biopolymer matrix ensures the material"s biodegradability, nanofillers provide the required thermal, mechanical, and electrical properties, usually very poor in the biopolymer alone [4-5].Although polymer collection for recycling is widely carried only a small proportion is actually remade into materials. The majority is incinerated to reclaim energy. There are many other reasons that motivate industries and researchers to find alternatives to non-renewable resources; however it is noted that all replacements for current plastics should meet some important conditions, they need to be low cost, renewable, sustainable and biodegradable [6-7].

Among different biopolymers, starch is very appealing because of its cost effectiveness and easy availability from different natural sources such as vegetables and cereals. Besides the nourishing value, the film forming ability has given to starch a more remarkable role, for example in food packaging. Starch-based films are biodegradable and edible and, therefore, potential substitutes for many synthetic packaging materials and pose negligible harm to the environment. Unfortunately, the starch-based biocomposites exhibit many disadvantages (e.g. strong hydrophilic character, poor mechanical properties and low thermal stability) compared to conventional polymers, which make it unsatisfactory for practical applications [8-10]. Moreover, the utilization of nano-sized fillers can also increase dispersibility in polymer resin and lead to improved mechanical, thermal and dielectric properties [11-12].

The nanometer-scale fillers are often introduced into a plasticized starch (PS) matrix to improve the tensile strength and properties, and to add to the functional properties. Recently, carbon materials have also been used as filler in the preparation of PS-based composites. Carbon

nanotube (CNT) has been incorporated into PS matrix resulting in enhanced mechanical strength and electrical conductivity. Carbon black was also added into PS matrix to obtain electrically conductive composites, prepared by both melt extrusion and microwave radiation. The composites prepared using microwave radiation exhibited better properties, including reinforcing effect, conductivity and water vapor barrier, than those from melt extrusion. Graphene is a two-dimensional carbon sheet exfoliated from graphite, which has recently emerged as one of the most attractive and creative materials because of its remarkable chemical and physical characteristics. These properties include a large surface area, good thermal and electrical conductivity, and extremely high mechanical properties. These properties make graphene a promising material for many industrial applications, such as field effect transistor, memory device, hydrogen storage, conducting electrode, ultra-capacitor, and solar cell [13].

Although various studies have indicated that graphene is a good reinforcement for polymer resin, many unresolved problems restrict its development. For instance, the pristine graphene sheets have a tendency to agglomerate in a polymer matrix, which leads to difficulties in material processing and high cost of device fabrication. Considered as the precursor of graphene, graphene oxide (GO) contains reactive functional groups, including hydroxyl, carboxyl, carbonyl, and epoxy groups on the basal plane and edge. With these functional groups, GO possesses unique characteristics and various potential applications, such as good dispersion stability in water and other common organic solvents and low manufacturing cost. These intrinsic properties of GO make it a suitable nanofiller for polymer matrix composite materials [14-15].

In this study, PS/GO biocomposite films were prepared by solution casting method. The aim of this work is to study the influence of GO& RGO loading on the morphologic, thermal stability, mechanical, dielectric properties and to further evaluate the applicability of GO/PS and RGO/PS composites for supercarpacitors, the electrochemical properties of pure PS and GO/PS were fully characterized by cyclic voltammetry (CV), galvanostatic charge-discharge (GCD) and cycling life measurement. The biocomposites were analyzed by Fourier transform infrared (FTIR), X-ray diffraction (XRD), thermal gravimetric analysis (TGA) and tensile tests. The fundamental structure–property relationship of GO/RGO-based starch biocomposites was also discussed.

Recently, the conducting polymers (CPs) have recently received special attention in the areas of nanoscience and nanotechnology because of their controllable chemical and electrochemical properties, reversible doping/dedoping process and unusual conducting mechanism. But these polymers are costly and rarely abundant. We studied starch and expect a closer result to CPs, if the electrochemical properties can be enhanced, PS/GO & PS/RGO nanocomposites can also be used as supercapacitor. We also studied dielectric properties of the nanocomposites as it is viable in electrical and electronics engineering.

1.2. OBJECTIVES

- ➢ Synthesis of Graphene oxide (GO) and reduced Graphene oxide (RGO).
- ➢ Preparation of GO/Starch nanocomposites and RGO/Starch nanocomposites.
- ➢ Investigation of the structural properties of the nanocomposites by X-ray diffraction (XRD) technique.
- ➢ Investigation of tensile strength of the composites by universal testing machine (UTM)
- ➢ Analysis of the surface morphology of the composites.
- ➢ Investigation of optical properties of the composites by FTIR and UV-VIS spectrum
- ➢ Study the dielectric properties of the nanocomposites by impedance analyzer
- ➢ Investigations the electrochemical properties by electrochemical workstation.

1.3. Organization of the thesis:

- ✓ Chapter one – In this chapter, a brief introduction my thesis work has been given.
- ✓ Chapter two- The literature review in brief has been provided, which I studied through my journey to make my work fruitful.
- ✓ Chapter three- Material synthesis & experimental part have been discussed in this chapter
- ✓ Chapter four- properties of PS/GO nanocomposite has been presented
- ✓ Chapter five- properties of PS/RGO nanocomposite has been presented
- ✓ Chapter six- conclusion and suggestions for future work are narrated here.

REFERENCES

[1]   Rodríguez,F.J.,Galotto,M.J.,Guarda,A., and Bruna.J.E.,"Modification of cellulose acetate films using nanofillers based on organoclays," Journal of Food Engineering,vol.110, pp.262–268,2012.

[2]   Liu,D., Chang,P.R.,"Fabrication and characterization of zirconium hydroxide-carboxymethyl cellulose sodium/plasticized TrichosanthesKirilowii starch nano-composites," Carbohydrate Polymers,vol.86,pp.1699–1704, 2011.

[3]   Liu,Z., Zhao,L., Chen,M., and Yu,J., "Effect of carboxylate multi-walled carbon nanotubes on the performance of thermoplastic starch nanocomposite," Carbohydrate Polymers, vol.83, pp.447–451,2011.

[4]   Dallas,P., Sharma,V.K., and Zboril,R.,"Silver polymeric nano-compositesasadvanced antimicrobial agents: Classification, synthetic paths, applications,and perspectives," Advances in Colloid and Interface Science, vol.166,pp. 119–135,2011

[5]   Kumar,S., Raj,S., Jain,S., and Chatterjee,K., "Multifunctional biodegradablepolymernano-composite incorporating graphene-silver hybrid for biomedicalapplications," Materials & Design, vol.108,pp. 319–332,2016.

[6]   Zhang,M., Li,Y., Su,Z., and Wei,G.,"Recent advances in the synthesis andapplications of graphene–polymer nano-composites," Polymer Chemistry, vol.6, pp.6107–6124,2015.

[7]   Feng,Y.,Zhang,X., Shen,Y.,Yoshino,K., and Feng,W.A.,"Preparation and characterization of a photocatalytic antibacterial material: Graphene oxide/TiO_2/bacterial cellulose nanocomposite" carbohydrate polymer,vol.174, pp.1078-1086,2012.

[8]   Potts,J.R., Dreyer,D.R.,Bielawski,C.W., and Ruoff,R.S., "Graphene-based polymer nanocomposites," polymer,vol.52, 2011.

[9]   Li,G.H., Liu, K.,& Ma,Z.W., "Flexible Solid-State Supercapacitors Based on Carbon Nanoparticles/MnO_2Nanorods Hybrid Structure"*ACS Nano*,2012, vol.6, pp. 656–661, 2011.

[10]   Torres, F. G., Commeaux, S.,Troncoso, O. P., Starch "Starch-based Biomaterials For Wound-dressing Applications," Starch,vol.65, pp.543,2013.

[11]   Baier, G., Baumann, D., Siebert, J. M., Musyanovych, A., Mailander, V.,Landfester, K.,"Suppressing unspecific cell uptake for targeted delivery using hydroxyethyl starch nanocapsules," Biomacromolecules,vol.13, pp.2704,2012.

[12] Jaber-Ansari,L.,&Hersam,M.C.,"Influence of Electronic Type Purity on the Lithiation of Single-Walled Carbon Nanotubes,"Acs Nano,vol.8,3, pp.2399-2409, 2012.

[13] Wang, Y., Shi, Z., Huang, Y., Ma, Y.,Wang, C., Chen, M., Chen, Y. J., "Supercapacitor Devices Based on Graphene Materials," Phys. Chem. C, vol.113, pp.13103−13107,2009.

[14] Saha, A., Basiruddin, S. K., Ray, S. C., Roy, S. S., Jana, N. R, " Fabrication of microcellular polymer/grapheme nanocomposite foams," Nanoscale, vol. 2, pp. 2777−2782,2010.

[15] Wu, Q.,Xu, Y., Yao, Z., Liu, A., Shi, G.,"Supercapacitors Based on Flexible Graphene/PolyanilineNanofiber Composite Films," ACS Nano,vol. 4,pp.1963−1970, 2010.

CHAPTER TWO

LITERATURE REVIEW

2.1 BIOPOLYMER

Polymer science or macromolecular science is the subfield of materials science concerned with polymers, primarily synthetic polymers such as plastics. The field of polymer science includes researchers in multiple disciplines including chemistry, physics, and engineering. Polymer is a large molecule composing, hundreds of thousands of atoms formed by successive linking of one or two, occasionally more types of small molecules into chain or network structures. Biopolymers are a class of polymers produced by living organisms. Cellulose and starch, proteins and peptides, and DNA and RNA are all examples of biopolymers, in which the monomeric units, respectively, are sugars, amino acids, and nucleotides.

2.2 NATURAL BIODEGRADABLE POLYMERS

Biopolymers are polymers formed in nature during the growth cycles of all organisms; hence, they are also referred to as natural polymers. Their synthesis generally involves enzyme-catalyzed, chain growth polymerization reactions of activated monomers, which are typically formed within cells by complex metabolic processes.

2.2.1 Cellulose

It is widely known that polysaccharides are produced by plants. These are a linear polymer with very long macromolecular chains of one repeating unit, cellubiose. Cellulose is crystalline, infusible and insoluble in all organic solvents [16]. Biodegradation of cellulose proceed by enzymatic oxidation, with peroxides secreted by fungi. Cellulose can also be degraded by bacteria. As for starch degradation products are non-toxic [17]. Cellulose is the most common biopolymer and the common organic compound on Earth and about 33 percent of all plant matter is cellulose. The total cellulose content in cotton is 90 percent and in wood it is 50 percent.

Cellulose esters represent a class of polymers that have the potential to participate in the carbon cycle via microbiologically catalyzed de-esterification and decomposition of the resulting cellulose and organic acids. Cellulose acetate is currently used in high volume applications ranging from fibers, to films, to injection moulding thermoplastics. It has the physical properties

and relatively low material costs that have exerted to exclude other biodegradable polymers from being widely accepted in the marketplace.

2.2.2 Chitin and Chitosan

Chitin is the second most abundant natural biopolymer. It is a linear copolymer of *N*-acetyl glucosamineand *N*-glucosamine with *β*-1,4 linkage. These units are randomly or block distributed throughout the biopolymer chain depending on the processing method used to obtain the biopolymer. Chitin is usually found in the shells of crabs, shrimp, crawfish and insects. It could be considered as amino cellulose. Recent advances in fermentation technology suggest that the cultivation of fungi can provide an alternative source of chitin [18]. The study reports the exploitation of both sources to produce chitin. The protein content in chitin obtained from these two methods is different. It is less than 5% for the chitin extracted from shells and reaches 10 – 15% for the chitin produced by fungi. The molecular weights for all chitin samples were in the same range. A review of chitin and chitosan has been recently published [19]. The distribution of chitin and chitosan in nature and the biosynthesis of chitin and chitosan by applying microorganisms are discussed there. Chitinase, an enzyme, degrades chitin. As chitin has a poor solubility, it is often substituted for many applications [20].

Chitin is processed to chitosan by partial alkaline *N*-deacetylation. In chitosan glucosamine units are predominant. The ratio of glucosamine to acetyl glucosamine is reported as the degree of deacetylation. This degree may range from 30% to 100% depending on the preparation method and it affects the crystallinity, surface energy and degradation rate of chitosan. Chitosan is insoluble in water and alkaline media. This is due to its rigid and compact crystalline structure and strong intra and intermolecular hydrogen bonding. Chitosan can only soluble in few dilute acid solutions. Then chitosan is dissolved in acidic solutions before its incorporation into biodegradable films [21]. Enzymes such as chitosanase or lysozymes are known to degrade chitosan. The applications of chitin and chitosan are limited because of their insolubility in most solvents. As chitosan has amino and hydroxyl reactive groups, chemical modifications can widely be employed. Modified chitosan have been prepared as *N*-carboxymethyl chitosan or *N*-carboxyethyl chitosan. They have been prepared for use in cosmetics and in wound treatment [22].

2.2.3 Lignin

Wood is composed of many chemical components, primarily extractives, carbohydrates, and lignin, which are distributed non-uniformly as the result of an atomical structure. Lignin is derived from the Latin term lignum, which means wood [23]. In 1838 Anselme Payen was the first to recognize the composite nature of wood and referred to a carbon rich substance as the "encrusting material" which embedded cellulose in the wood. In 1865 Schulze defined this encrusting material as lignin. Lignin has been described as a random, three-dimensional network polymer comprised of variously linked phenyl propane units [24]. Lignin is the second most abundant biological material on the planet, exceeded only by cellulose and hemicelluloses, and comprises 15-25% of the dry weight of woody plants. This macromolecule plays a vital role in providing mechanical support to bind plant fibers together. Lignin also decreases the permeation of water through the cell walls of the xylem, thereby, playing an intricate role in the transport of water and nutrients. Finally, lignin plays an important function in natural defense of a plant against degradation by impeding penetration of destructive enzymes through the cell wall. Although lignin is necessary to trees, it is undesirable in most chemical paper making fibers and is removed by pulping and bleaching processes.

2.2.4 Fiber

Since ancient Egypt natural fibers were already being used as reinforcement materials. These natural fibers are divided in three main categories: straw-fibers, non-wood fibers and wood fibers. The non-woods fibers won the interest of industry due to the mechanical and physical properties. Inside this category, another classification depending on the plant origin is made: as bast for kenaf, flax, jute and hemp; leaf for sisal, henequen and pineapple leaf fiber; and seed for cotton; fruit coconut.

The application of the natural fiber composites depends on the production cost and their functional properties. Generally natural fibers cannot provide the same mechanical properties as carbon fiber, but some of them can achieve the same behavior as fiberglass. In composite materials, before being used, natural fibers are subject to preparation for operations and modification of its surface. Following the latter, the fibers should have: good adhesion between

fiber and matrix; suitable degree of polymerization and crystallization; resistance to humidity and homogenous physical properties; and nonetheless should be non-inflammable.

2.2.5 Protein

Proteins are thermoplastic hetero polymers. They are constituted by both different polar and non-polar α-amino acids. Amino acids are able to form a lot of intermolecular linkages resulting in different interactions. These offer a wide possibility of chemical functionalities and functional properties. Most of the proteins are neither soluble nor fusible, especially fibrous proteins as silk, wool and collagen. So they are used in their natural form. Casting of film-forming solutions allows the preparation of films. To process protein based bio-plastics, classical way is the thermoplastic processing, which consists of mixing proteins and plasticizers. Flexibility andextensibility of films are improved by the use of plasticizers [25, 26]. The biodegradation of proteins is achieved by enzymes, as protease, and is an amine hydrolysis reaction. Grafting of protein is a mean to control the rate of biodegradation.

2.2.6 Alginic acid

Many polysaccharides in solution form gels upon the introduction of counter ions. The degree of cross-linking is dependent on various factors such as pH, type of counter ion, and the functional charge density of these polymers. Alginates have been studied extensively for their ability to form gels in the presence of divalent captions. Alginate is a binary linear hetero polymer containing 1, 4-linked α-L-guluronic acid and β-D- mannuronic acid. Alginic acid forms water-soluble salts with monovalent cations, low molecular weight amines, and quaternary ammonium compounds. It becomes water insoluble in the presence of polyvalent cations such as Ca^{2+}, Be^{2+}, Cu^{2+}, Al^{3+} and Fe^{3+}. Alginate gels have been used widely in controlled release DDS. Alginates have been used to encapsulate various herbicides, microorganisms and cells. Some polysaccharides structures are depicted in Figure .
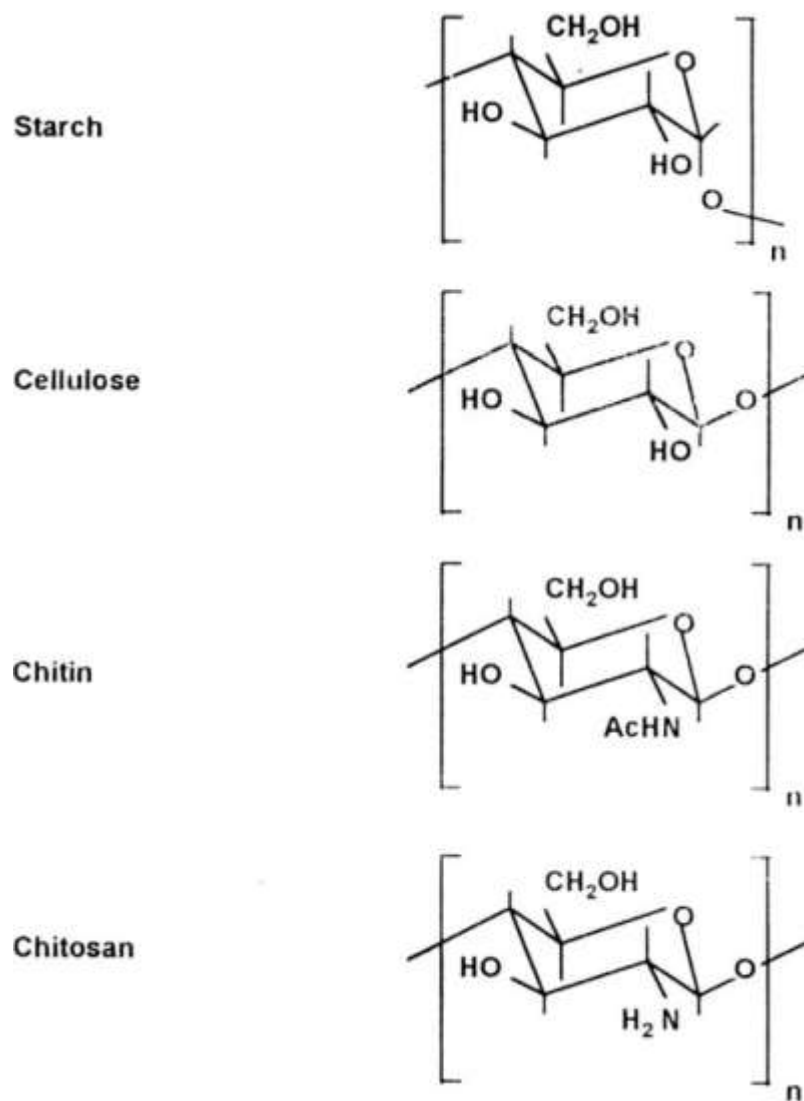
Figure 2.1: Structures of some natural bio-degradable polymers.

2.2.7 Starch

Starch, can be produced at low cost and at large scale. It is an abundant and cheap agricultural source of starch. Starch is not a real thermoplastic material but, in the presence of a plasticizer, high temperatures and shearing, it melts and fluidizes, like thermoplastic polymer. We, therefore, used starch in this work.

2.2.7.1 Introduction to Natural Starch

Starch is a carbohydrate material that can be hydrolyzed into small molecules by specific enzymes during animal metastasis, generating biological energy for animals. Many plants, in their fruits, seeds, tubers or rhizomes, grow with starch. Potato, corn, wheat and rice are major resources for production of starch worldwide.

2.2.7.2 Compositions of Natural Starch

Starch contains two major components: one is amylose, which is a linear polymer, and the other is amylopectin, which is a highly branched polymer. The repeat units in both amylose and amylopectin are identical (so-called α-D-glucosyl residues) but connected in different ways, as given in Figure 2.3. Most starch contain 20—30 wt % of amylose, although some waxy starches contain very little amylose. In amylose, *α-D*-glucosyl residues are linked by an α [1→4] bond. Typically, the molecular weights of extracted amylose are in the order of 105—106 g/mol [27]. Amylose generally is recognized as linear macromolecule. However, it has been reported that there is a slight degree of branching (9—20 branch points per molecule) in amylose from various botanical sources [28]. The length of side chains ranges from 4 to over 100 repeat units [29]. There is no effective way of separating the branched amylose from the linear amylose.

Side chains on branched amylose form small clusters rather than a random comb structure. Note that amylopectin also forms clusters by its branched side chains, which will be elaborated on later. Branched amyloses still have properties, such as iodine binding capability, which amylopectin does not have. In aqueous solutions, amylase molecules can form extended chains with a hydrodynamic radius of 7-22 nm. In natural starch, the amylose molecules tend to have a rather stiff left-handed single helical structure or form an even stiffer parallel double left-handed helix [30].

The helix consists of six *α-D*-glucosyl residues per turn with a pitch of 0.8 nm. Figure 2.4 shows a single helix structure of amylose molecule. On each of the glucose residues, hydroxyl groups connecting with carbons on position 2 and 6 (C2 and C6) point outward of the helix, while the hydroxyl group connecting with carbon on position 3 (C3) points inward of the helix, which makes the inner surface of the helix more hydrophobic than the outer surface. Thus, amylose with a helix structure can hold the hydrocarbon portion of glycerides and fatty acid in its helix cavity to form a V-helix complex. The distinct capability of amylose to bind with iodine is also by holding iodine ions in its hydrophobic helix cavity

amylopectin
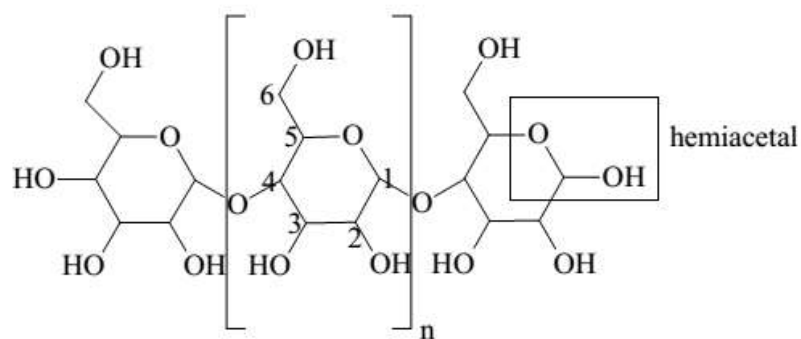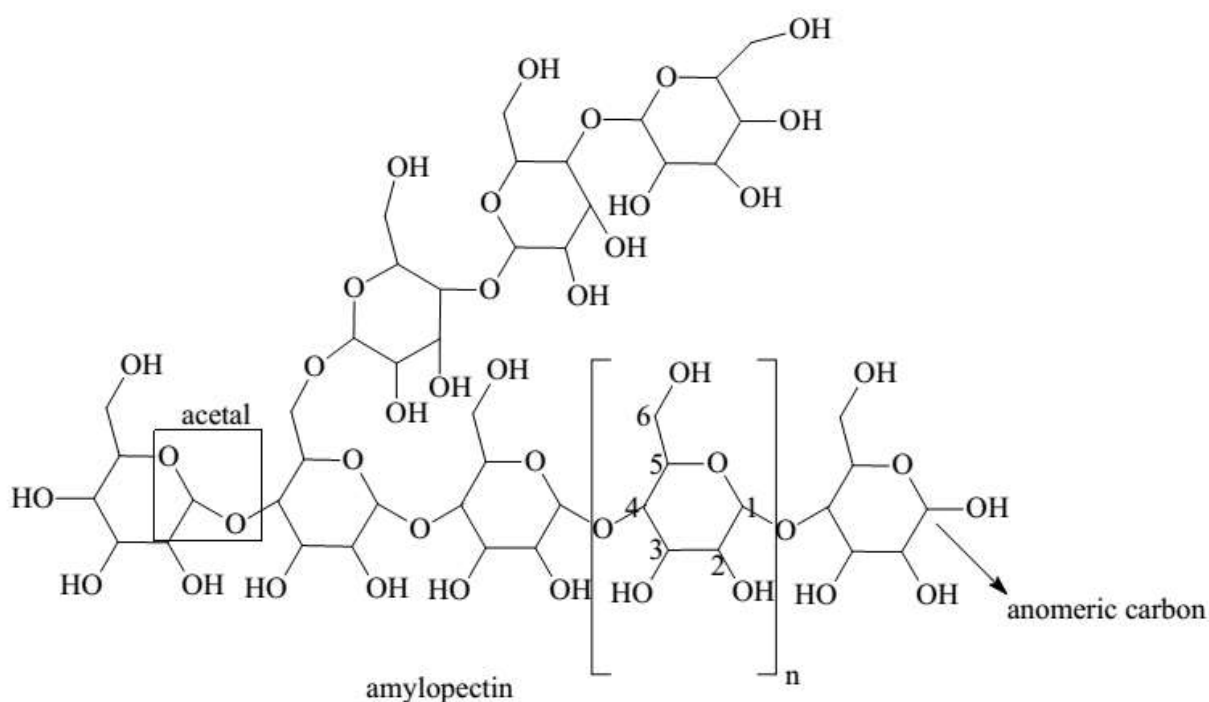
amylose

Figure 2.2: Chemical structure of amylose and amylopectin

Amylopectin is a highly branched component of starch. The α-D-glucosyl residues are mainly linked by α [1→4] bonds but with 5-6% of α [1→6] bonds at the branch points. Its molecular weight ranges 107-109 g/mol.
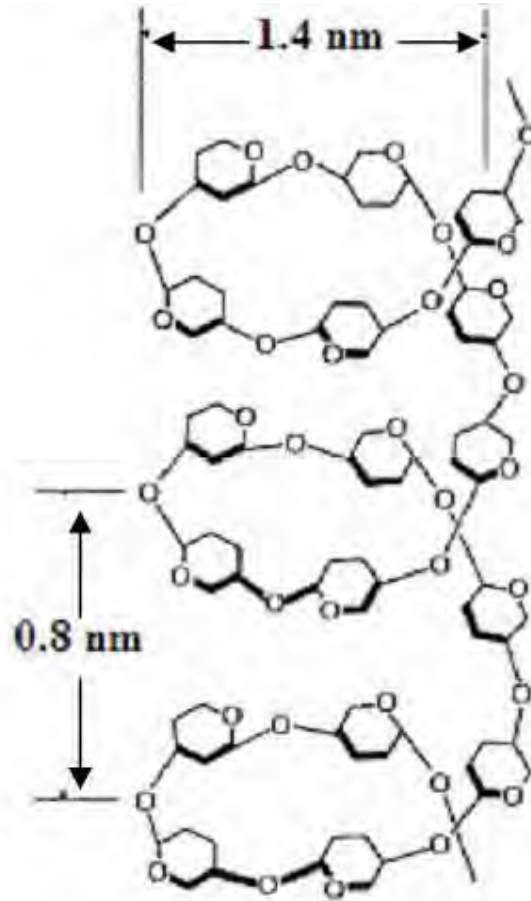
Figure 2.3: Single helix structure of amylose.

The amylopectin molecular chains can be classified into three categories by their ways of connecting with each other: the C chain carries the sole reducing end of the molecule; the A chain (unbranched) is only linked to the rest of the molecule through its potential reducing end; and the B chains carry one or more A chains and/or B chains. Figure 2.5 shows a schematic describing this classification.
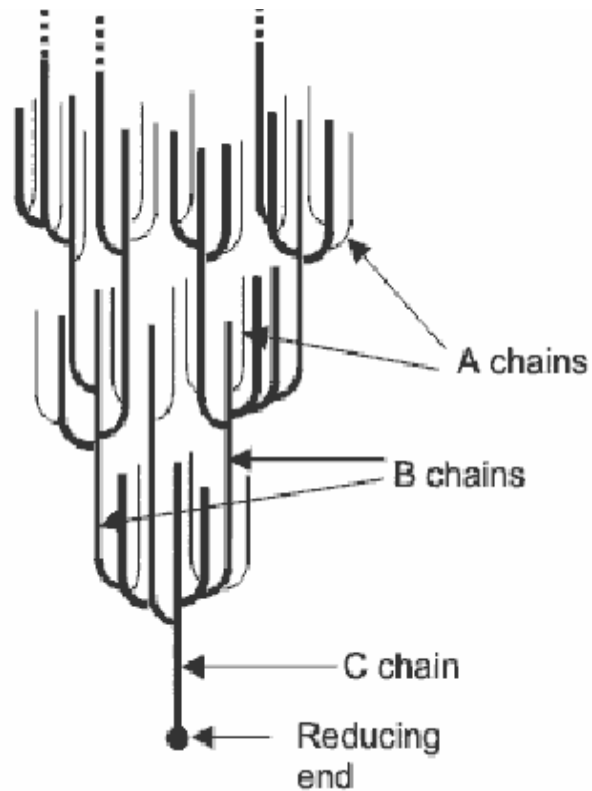
Figure 2.4: Structure of branched amylopectin

In most experiments, the C chain is not distinguished from B chains. According to their positions in the cluster structure, B chains are further subdivided: B1 is a short chain, being components of only one cluster while B2, B3, etc. are long chains that span over two, three, or more clusters, thereby interconnecting them. The branching points on the amylopectin molecules are not randomly distributed but periodically clustered. The distance between two clusters on the same B chains is 2-2-α-D-glucosyl residues on average. Most short chains (the average degree of polymerization ranges from 14 to 18) are organized within clusters, while long chains (the average degree of polymerization is more than 55) usually span more than one cluster. The molar ratio of short to long chains, influenced by the source of starch, varies from 5 in potato starch amylopectin to 8—10 in cereal amylopectin. The distribution of chain length in amylopectin critically influences the inner assembly structure of starch granules and the interaction with the water or solvent.

2.2.7.3. Corn starch

The word „corn" is used in the United States as the common name for the cultivated member of the grass family (Gramineae) known to botanists as Zeamaysl. More specifically, „corn" means the seed produced by this plant. Outside of the United States, this crop is commonly known as maize. The mature corn kernel is composed of four principle parts: tip cap, 0.8%; pericarp, 5.3%; germ, 11.9%; and endosperm, 82%. The most important genetic change in corn for starch production was development of waxy maize (corn) hybrids. Starch from waxy maize, which contains 100% of the branched starch fraction, amylopectin, has become a major food starch. This corn must be grown in fields isolated from dent corn to prevent crosspollination, and generally will be grown under identity-preserved contracts to ensure delivery of uncontaminated shipments of maize to the wet-milling establishment and to provide adequate supply. The milling properties of waxy maize are similar to those of regular corn, except that the yield of soluble is a little higher, starch yield is lower and starch and gluten slurries filter and dry a little more slowly than those from normal dent corn. This characteristic has been shown to be caused by the presence of a small amount of a phytoglycogen. The addition of a small amount of an amylolytic enzyme to the slurries results in normal filtering and drying characteristics [30]. High-amylose corn having starch which contains 55 – 80% of the linear starch fraction, amylose, has also been developed [31] and must also be grown under contract. Production of amylomaize is even smaller than it is for waxy hybrids because of limited uses for the starch. Starch yields of high-amylose corn are lower than those of dent corn [32].

2.2.7.4 Wheat starch

Starch comprises 54-72% of the dry weight of wheat kernels [33, 34]. Starch content is positively associated with grain yield, but inversely related to protein content [35, 36]. Normal wheat starch is comprised of 25% amylose and 75% amylopectin. Amylose is a mixture of linear and lightly branched (0.2 – 0.8% of linkages) molecules having a number average degree of polymerization of 1000 – 5000, whereas amylopectin is monodisperse and highly branched (4 – 6% of linkages) with a DP of about 10 000 or more. The detailed structural features of amylose and amylopectin are dependent on the source of starch, even among wheats. Moreover, the proportions of amylose and amylopectin in starch may vary within a plant source, due to genetic

mutation. Amylose and amylopectin are readily isolated and purified, but branched and linear amylose molecules from wheat starch have not been separated and isolated.

2.2.7.5 Tapioca starch

Tapioca starch is obtained from the roots of the cassava plant, which is found in equatorial regions between the Tropic of Cancer and the Tropic of Capricorn. Typically, cassava starch contains 17 – 20% amylose. Unlike corn (0 – 70% amylase content) and rice (0 – 40% amylose content), no significant variation of amylase content has been found in cassava starch. Similar to other starches, the amylase molecules of cassava starch are not completely unbranched as indicated by their beta-amylolysis limit, a value lower than that for corn, potato, rice and wheat starches. In addition, cassava amylose has a higher molecular weight than other starches. Each fraction can be classified in terms of its chain length (degree of polymerization, DP) and position in amylopectin molecules [37].

2.2.7.6 Potato starch

In some potato starch applications, as with applications of other native starches, the presence of amylose is undesirable. After gelatinization, it forms crystals which reduce paste clarity. Amylose retrogradation can be prevented by chemical modification; a new type of potato has been bred to solve this problem. This potato contains only amylpectin, it can be developed in two ways. One way consists of treating a mutation-sensitive potato with radiation or chemicals and selecting the desired variety. After successful selection the normal plant cross-fertilization method to produce starch potatoes is used. The second way involves genetic modification of the potato with an antisense technique to eliminate the formation of amylose. By this method, no materials are introduced into the potato which is not normally present, and the amylopectin potato starch contains no genetically manipulated substances. This method avoids the time consuming (10 years) cross-fertilization program. Amylopectin starches, like waxy maize starch, are mostly used by the food industry. However, amylopectin potato starch has specific properties which are not available in current commercial starches.

Native potato starch, which is used in the food, paper and textile industries, is often not optimal for a particular application. Modifications are done to obtain the properties needed for specific uses. More than 500 modifications of potato starch are currently known. Potato starch

and its derivatives have special properties, such as a low gelatinization temperature and a high paste consistency. Potato starch is preferred in the food industry, because its pastes have a good clarity (due to a small amount of lipid sand protein) and a neutral flavor. In the paper industry, there is also a preference for potato starch. The reason for this is the high molecular weight of its amylose and its good solubility. Cationic potato starches are preferred for internal sizing due to the concurrent presence of phosphate groups. Potato starch dextrins also have an advantage over other starches as an adhesive, because of the good remoisten ability [38] and a desirable rheology resulting in a perfect direct tack. Textiles are manufactured better with potato starch due to its film properties [39], paste penetration depth [40] and adhesive power [41].

2.3 SYNTHETIC BIODEGRADABLE POLYMERS

Biodegradable synthetic polymers such as poly (glycolic acid), poly (lactic acid) and their copolymers, poly (*p*-dioxanone), and copolymers of trimethylene carbonate and glycolide have been used in a number of clinical applications.

2.3.1 Polyesters

A vast majority of biodegradable polymers studied belongto the polyester family. Table 2.2 lists the key polymersin this family. Among these poly (α-hydroxy acids) such as poly (glycolic acid) (PGA), poly (lactic acid) (PLA), and a range of their copolymers have historically comprised the bulk of published material on biodegradable polyesters and have a long history of use as synthetic biodegradable materials [42-46] in a number of clinical applications. These polymers have been used as sutures [47] plates and fixtures for fracture fixation devices [48] and scaffolds for cell transplantation [49].

2.3.2 Poly (glycolic acid), poly (lactic acid) and their copolymers

Poly (glycolic acid) (PGA) is a rigid thermoplastic material with high crystallinity (46-50%). The glass transition and melting temperatures of PGA are 36ºC and 225ºC, respectively. Because of high crystallinity, PGA is not soluble in most organic solvents; except highly fluorinated organic solvents such as hexafluoro isopropanol.

The attractiveness of PGA as a biodegradable polymer in medical application is that its degradation product glycolic acid is a natural metabolite. Numerous studies [50-52] have

established a simple degradation mechanism via homogeneous erosion. The degradation process occurs in two stages, the first involves the diffusion of water into the amorphous regions of the matrix and simple hydrolytic chain scission of the ester groups. The second stage of degradation involves largely the crystalline areas of the polymer, which becomes predominant when the majority of the amorphous regions have been eroded.

Poly (lactic acid) is present in three isomeric forms d (-), l (+) and racimic (d, l) and the polymers are usually abbreviated to indicate the chirality. Poly (l) LA and poly (d) LA are semi-crystalline solids, with similar rates of hydrolytic degradation as PGA. PLA is more hydrophobic than PGA, and is more resistant to hydrolytic attack than PGA. For most applications the (l) isomer of lactic acid (LA) is chosen because it is preferentially metabolized in the body. Poly (lactic-glycolic acid) (PLGA) copolymers and PGA are among the few biodegradable polymers with Food and Drug Administration (FDA) approval for human clinical use.

2.4 THERMOPLASTIC STARCH (TPS)

The term "thermoplastic" indicates that these materials melt on heating and may be processed by a variety of moulding and extrusion techniques. The most common thermoplastics are polyethylene, polystyrene and polymer chloride together with a number of more specialized engineering polymers. If one of the reacting substances in a step polymerization possesses more than two functional groups, then the reaction will lead naturally to branched structures. As these intercom bines, random three-dimensional networks are developed. Ultimately the network extends throughout the mass of polymerized material, which therefore in effect constitutes a single giant molecule. Such structures are by their very nature incapable of melting or of truly dissolving. Important examples are the phenolic and amino resins. Similar thermo set network structures may be formed by cross linking linear chains in a second post polymerization or 'curing' reaction, which may be free radical initiated.

The production of TPS (also known as plasticized starch, PS) basically involves three essential components, namely: starch, plasticizer and thermo-mechanical energy. The thermo-plasticization of starch entails the collapse of starch crystallinity (which in general is about 15-45% of the granule molecular order) through the formation of hydrogen bonds between the plasticizer and starch in the presence of some energy, invariably severing the hydrogen bonds

between the hydroxyl groups of the starch molecules to form TPS [53]. Therefore, the crystallinity observed in TPS is due to the hydrogen bonds formed between starch and the plasticizer molecules and according to [54], this degree of crystallinity is expected to be rather low. It is important to mention that there must be sufficient amount of plasticizer (30% wt for glycerol-PS) for the formation of a homogeneous (continuous) phase to occur, otherwise some starch granules will remain intact in the TPS, a condition that can make the TPS fracture under tension at very low strains. Plasticizers impart pliability by modifying the free volume of the matrix such that starch chains enjoy more mobility [55]. The use of starch alone is not encouraged because of its lack of melt-processability and humidity-resistance which in turn militates against its suitability for extrusion or injection molding [56].

The most common plasticizers used are water and glycerol, which often times are used together. The TPS thus produced exhibits two major drawbacks, namely, poor mechanical properties and water resistance. To this end, four areas of consideration are being explored; these include plasticizers, starch forms (in relation to chemical modification and amylose/amylopectin ratio), reinforcements (organic and inorganic), polymer orientation and blends with other synthetic polymers (discussed in the following sections). Accordingly, materials such as ethylene bisformamide, urea [57], formamide [58], sorbitol [59] and xylitol [60] have been investigated for their plasticizing abilities. Using corn starch [61], reported that extruded ethylene bisformamide-PS showed better water resistance than glycerol-PS but rather lower corresponding tensile strengths at plasticizer contents measured, with both decreasing in strength with increase in contents. The glass transition of the ethylene bisformamide-PS was found higher than that of glycerol-PS (63.3oCagainst 38.3oC) since ethylene bisformamide form stronger hydrogen bonds with starch than glycerol. Thunwall *et. al.* [62] reported that glycerol plasticized potato starch produced using hydroxypropylation/oxidation modified starch exhibited a modestly higher resistance than that of native starch. However, increase in glycerol content reduced the moisture resistance of the TPS regardless of the type of starch used. Modified native potato starch and high amylose starch offered reduced viscosity levels (measured at 140oC) for starch melts containing 30% (dry mass) glycerol.

In comparison with high polyethylene Thunwall*et.al.* further noted that polyethylene melt at 180oC had lower viscosity than native potato PS and hydroxypropylation/oxidation-modified

high amylose PS but higher than that of hydroxypropylation/oxidation modified native potato PS, all at 140oC. They also discovered that starch melt drawability, a crucial property in film production, generally increased with glycerol and chemical modification but decreased with temperature, but in comparison with PE melt, PS melt was very much lower in extensibility. It is important to mention that it is rather difficult to make thin blown films with granular starches as fillers in polymer composites due to their big particle size range (5-100 μm). Hence the preference for TPS [63] approached the issue slightly differently by blending cassava starch (74.70±1.76%) plasticized with water and glycerol, and another with water and Buriti oil, all in ratio 50:15:35 (mass/vol/vol) with polystyrene in different ratios by mass. It was observed that blends with TPS plasticized by buriti oil were apparently more thermally stable than those by glycerol.

A reduction of up to 60% in the water uptake of TPS could be achieved by replacing glycerol with sugar/water mixture as plasticizer though with a concomitant reduction in the TPS crystallinity [64]. One property peculiar to TPSs plasticized with polyols (such as glycerol, sorbitol, glycol and sugars) is their retro gradation (recrystallization due to reformation of hydrogen bonds between starch molecules) propensities as they age, a condition that leads to embrittlement. This phenomenon could be inhibited using formamide as plasticizer (since it could form stronger or more stable hydrogen bonds with starch –OH groups) but with a reduction in tensile strength and modulus against a simultaneous increase in elongation at break and energy break vis-a-vis glycerol plasticized starch [65]. Amides generally form stronger hydrogen bonds with starch -OH groups than polyols in the following order: urea > formamide > acetamide > polyols [66]. Though with a compromise on tensile stress, similar result of inhibited retro gradation coupled with reduced shear viscosity (improved fluidity) of TPS, improved elongation, thermal stability and water resistance at high relative humilities was achieved by yu et. al. [67] when glycerol plasticized TPS was modified with citric acid in comparison with the unmodified glycerol TPS. Torres *et. al.* [68] explored some natural fibers reinforcing potentials for thermoplastic starch in their work published recently. Three material variables were considered, namely: starch (sweet potato, corn and potato starches), plasticizer (ethylene glycol, glycerol, chitosan, water and propylene glycol) and fiber (jute, sisal and cabuya with fiber lengths of 5±1 mm).

22

All these factors coupled with process (compression molding) conditions such as time and temperature were found to affect the tensile strength of the TPS. Individual assessments (done keeping other variables constant) shows that potato starch, sisal and ethylene glycol gave the highest tensile strength results whereas water and cabuya fiber give the highest impact strength.

Besides discrete macro fibers as reinforcements for TPS, cellulosic nanofibers, such as cellulose microfibrils [69] and tunicin whiskers [70] have also been investigated. Two types of wood pulps (bleached Kraft pulp from Eucalyptusuro grand is and unbleached thermo mechanical pulp of Eucalyptus grandis) were evaluated by De Carvalho et. al. [71] in reinforcing TPS produced with corn starch (28%amylose) and glycerol. It was found that though increase in glycerol (above 30%) decreased both the tensile strength and modulus, increase in fiber (pulp) contents (from 5-15% of matrix mass) remarkably increased both the tensile strength and modulus in all cases. On the other hand, the tensile strains of the composites decreased with the addition of fiber or glycerol to the raw matrix. Interestingly, regardless of glycerol amounts, fiber breakage as against debonding was observed on all fracture surfaces, an indication of a strong fiber-matrix interfacial bonding.

In agreement with similar work, the equilibrium water absorption of the TPS matrix increased with glycerol and was found higher than those of TPS-fiber composites (thus, implying improved moisture resistance by fiber inclusion), which were similar irrespective of formulation. Besides organic materials like natural fibers, the potentials of inorganic minerals such as hydroxyapatite [72] as reinforcement materials for TPS have been reported. The reinforcing potentials of clay were examined by Hwan-Man [73] whereby TPS/clay nano-composites produced from native potato starch and natural montmorillonite (clay) were found to possess higher tensile strength and thermal stability, and lower water vapor transmission rate than ordinary TPS. In addition their recent study of the effectiveness of fly ash in reinforcing corn PS prepared with glycerol and formamide-urea combination as plasticizers observed considerable increase in the tensile stress, Young''s modulus and water resistance, though with a corresponding decrease in ductility. Fly ash was also found to inhibit retro gradation.

Lastly, Yu, L*et. al.* [74] exploited polymer orientation technique in improving extruded corn TPS sheet. The orientation was achieved by drawing at different speeds TPS sheet

extrudates from the die under positive tension by a three-roller system in front of the die after which the mechanical properties were measured along and across the extrusion direction. Unlike elongation, both tensile modulus and yield strength improved in both directions.

However, the effect of orientation was influenced by amylose/amylopectin ratio, such that differences in modulus and yield stress in the two directions widened with increase in amylase while differences in elongation became pronounced at higher amylopectin contents. These directional differences in tensile properties are much higher in conventional polymers and for instance, may be in the order of 10 times in polypropylene. On a broader view, amylose contents have actually been found to proportionately influence mechanical properties such as tensile modulus, tensile strength and elongation of TPS [75, 76].

2.5 GELATINIZATION OF STARCH

Gelatinization of starch is usually known as the disruption of the crystalline structure and ultimately the destruction of the starch granular structure when heat and water (or other effective solvents) are applied. In the presence of excessive water (usually > 90 wt %), starch granules start to swell because the amylose molecules are preferentially solubilised in the water. Below a characteristic temperature known as gelatinization temperature, the crystalline region, mainly composed of high molecular weight and branched amylopectin molecules, still maintains its integrity. Above the gelatinization temperature, the crystalline region starts to lose its order and swell irreversibly [77]. If approximately treating starch granules as a polymer network, the swelling of the starch before the occurrence of gelatinization can be considered as a reversible equilibrium. In this equilibrium, the affinity between the polymer network and the solvent generates osmotic pressure (favoring the swelling), which is equal to the restoring force (disfavoring the swelling), from the stiffness of polymer network. Obviously, enhancing the temperature or choosing the solvent that has a high affinity with starch will increase swelling. Swelling above the gelatinization temperature is profoundly irreversible.

2.6 POLYMER NANO-COMPOSITE

Polymer composites in which the size of the reinforcement is on the order of nanometers are called polymer nano-composites. These materials are generally lightweight, are often easy to process and provide property enhancements extending orders of magnitude beyond those realized with traditional polymer composites. Examples of commonly used reinforcements, often termed nano-fillers, include carbon nanotubes (CNTs) [78-79], layered silicate clay nanoparticles [80-82], cellulose nanocrystals [83], graphite nanoflakes [84-86] etc. These nano-fillers have at least one characteristic dimension on the order of nanometer sand can range from isotropic elements to highly anisotropic needle-like or sheet-like elements. While CNTs and cellulose nanocrystals are generally cylindrical in shape, clay nanoparticles are disk-shaped with a high aspect ratio. The structures of some of these nano-fillers are shown in Figure 2.6.

Over the last 2 decades, clay nanoparticles have attracted great interest in academia and industry because of the relatively easy processibility, low cost and fairly predictable stiffening behavior when introduced into polymers [87-93]. A clay nanoparticle is composed of stacked structures of 1 nm thick silicate layers with a variable basal distance. Montmorillonite (MMT), shown in is an example of a clay nanoparticle generally used in polymer-clay nano-composites because it is readily available and has exceptional mechanical properties [94]. The in-plane modulus of elasticity has been estimated to be 270 GPa by Monte Carlo simulations [95]. MMT, a member of the smectite family, is 2:1 clay, meaning that its crystal structure consists of layers made up of two tetrahedrally coordinated silicon atoms fused to an octahedral sheet of aluminum. Each silicate layer, around 1 nm thick, is regarded as a rigid inorganic polymer consisting of mainly silicon and oxygen, and a small amount of aluminum, magnesium and other metal ions.
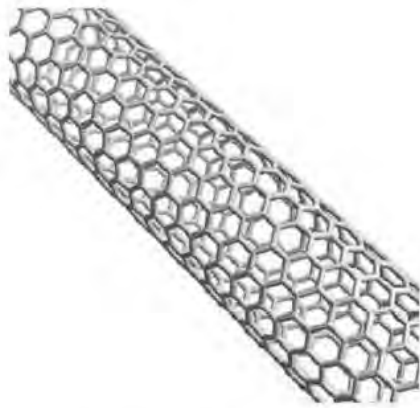
Single-walled carbon nanotube
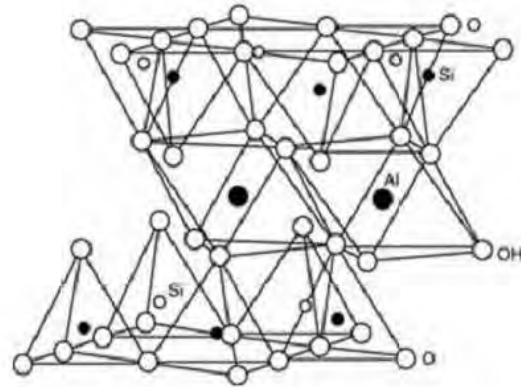
Layered silicate
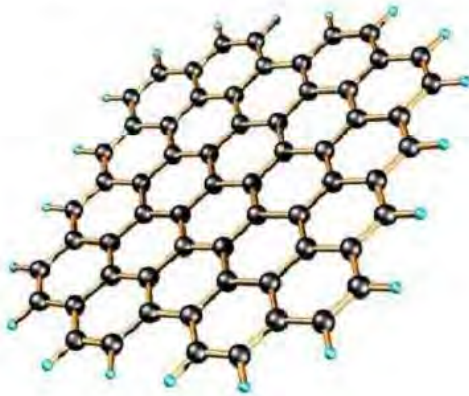
Graphene sheet
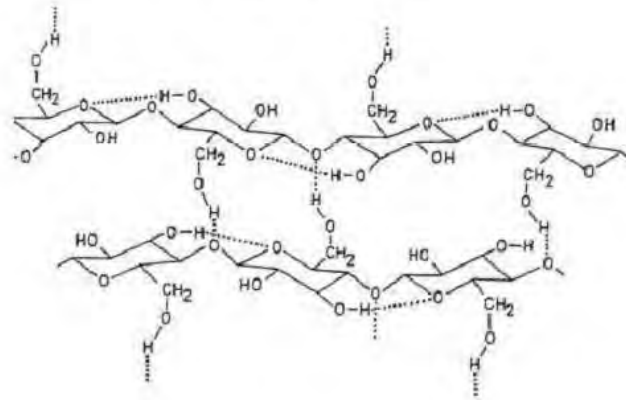
Cellulose nanocrystals

Figure 2.5: Structures of commonly used nano-fillers

An alkali metal cation (typically, Na+) holds the silicate layers together by an intermolecular force. In a polar solvent, such as water, this intermolecular force is broken and the basal distance of the silicate layers expands by solvation of the cation leading to exfoliation of silicate layers into individual sheets. The individual sheet of silicate layer contains a negative charge and has an aspect ratio of 100: 1 to 1000: 1.

The use of clay nanoparticles as precursors to nano-composite formation has been extended into various polymer systems including nylon 6 [96-97]; epoxys; polyamides; polystyrenes polyurethanes ; polyolefins such as polypropylene , polyethylene ; among others. Although the first clay-reinforced resin known as Bakelite was introduced in early 1900"s, the

26

research on polymer-clay nano-composites was stimulated by the pioneering work at Toyota. Kojima et al. [98] showed a combined enhancement of modulus, strength and toughness in a Nylon 6-clay nano-composite.

At a loading of 4:2 wt.% (>1:5 v.%) clay, the modulus doubled and the ultimate tensile strength increased more than 50%. These results sparked the research in the nano-composites area and since then the manufacture of polymer nano-composites has received much attention both by academics and industry [99].

2.7 PROPERTIES OF POLYMERIC MATERIALS

Types of polymer 'properties' can be broadly divided into several categories based upon scale. At the nano-micro scale, properties directly ascribe from the chain itself. These can be thought of as polymer structure. At an intermediate microscopic level, properties describe the morphology of the polymer matrix in network space. At the macroscopic level, properties describe the bulk behavior of the polymer. The bulk properties of a polymer are those most often of end-use interest. These are the properties that dictate how the polymer actually behaves on a macroscopic.

2.8. GRAPHENE

Graphene, or mono-layer graphite, is a single-atom-thick sheet of 2-D bonded carbon atoms which are tightly packed in a hexagonal crystalline structure (Park &Ruoff 2009). Pioneering research in 2004 by Geim and Novoselov (2010 Nobel Prizewinners in Physics) of the University of Manchester led to the isolation of a single sheet of graphene which was prepared by using the scotch tape method on the top of a silicon wafer. Today, graphene is the subject of much research in the scientific community; further, it can be utilized in several industrial applications because of its outstanding electronic, optical, thermal conductivity and mechanical properties (Balandin et al. 2008,Jung, Dikin et al. 2008, Wang, Zhang et al. 2008). Due to the remarkable low-energy electronic structure of single-layer graphene, white light can be absorbed by ~ 2.3% where α is the fine-structure constant) (Kuzmenko, van Heumen et al. 2008).This confirms how important the structure of graphene is for applications in development of optical electronic materials. In general, graphene synthesis can be carried out *via* four different methods:

(1) chemical vapor deposition (CVD) (Eizenberg & Blakely 1970);

(2) scotch tape method- which mechanically exfoliates graphene sheets from highly-oriented graphite flakes(Novoselov, Geim et al. 2004);

(3) epitaxial growth of graphene films on an electrical insulating substrate (e.g. Si) (Berger, Song et al. 2004); (4) chemical reduction of graphene oxide derivatives from natural graphite flakes (Stankovich, Piner, Chen et al.2006, Stankovich, Piner, Nguyen et al. 2006). These methods originated in several distinct research efforts at different times in the history of the material. In the early1970s, the pioneers of the production of mono-layer graphite through the CVD were surface scientists and chemists (Eizenberg & Blakely 1970). In the 1950s and 1960s,extensive research on aqueous suspensions of mono-layer graphite oxide (GO) sheets was conducted by Boehm and co-workers (Boehm, Clauss et al. 1962, Boehm, Eckel etal. 1967). "Graphite Oxide", which can be used to extract the graphene oxide sheets typically by oxidation treatment of natural graphite flakes, was identified as early as the19th century (Brodie 1860, Staudenmaier 1898, Hummers & Offeman 1958).

Ultrasonic sonication, a much more recently discovered process, can be utilized to exfoliate the graphite flakes and generate aqueous suspensions of oxidized graphene sheets having abroad range of physical and mechanical properties (Park & Ruoff 2009).Ruoff and co-workers reported bulk production of chemically modified graphene(CMG) sheets in colloidal suspensions that have many applications in composites andenergy storage materials and devices (Stankovich, Dikin et al. 2006, Park & Ruoff2009). Tour and his colleagues proposed a comparable green process to bulk graphene oxide (GO) sheet synthesis (see figure 1.2). The method is a modified version of Hummers" technique, which utilizes potassium permanganate (KMnO4), sodium nitrate(NaNO3) and sulfuric acid (H2SO4) for graphite oxide fabrication. However, Tour"smethod has advantageously excluded the potassium permanganate (KMnO4), generating less toxic gases and wastes (Marcano, Kosynkin et al. 2010). Graphene platelet (GPL) consists of few-layer graphene sheets and can be produced in bulk quantities through thermal reduction of graphite oxide (GO) flakes. The term platelet primarily refers to the multiple-layer structure of graphene sheets. In 2006,Aksay and co-workers reported the mass production of functionalized graphene sheets(FGS) using a thermal shock process (up to 1050 °C) of GO flakes derived from natural graphite flakes (Schniepp, Li et al 2006, McAllister, Li et

al 2007). This thermal shockprocessing of GO results in wrinkled GPL structures that can play a critical role in composite processing. Choucair et al. also synthesized bulk amounts of carbon nanosheets through a novel process involving heating sodium and ethanol at ~ 220 °C. The reaction process leads to a solid product that is pyrolysed and washed to yield an array of single-layer graphene sheets (Choucair et al. 2009). In this thesis, we have used a thermal exfoliation process to prepare GPLs for epoxy composite applications. Due to the excellent electrical properties of graphene sheets, it is very important to synthesize large-area graphene thin films on substrates for graphene-based electronic devices applications.

In 2009, Ruoff's group established a fundamental process of mono layer graphene fabrication on copper (Cu) substrate (because the solubility of C in Cu isvery low) by utilizing methane (CH4) gas and the CVD technique (Li, Cai et al. 2009). In2010, a group of scientists led by the Suimo Ijima have successfully scaled up the Ruoff's method for industrial applications (mainly for LCDs). Ijima's group was able toproduce a 30-inch single sheet of graphene (thickness 0.34 nm) by using a roll-to-rollapproach for touch-screen electronics (Bae, Kim et al. 2010).
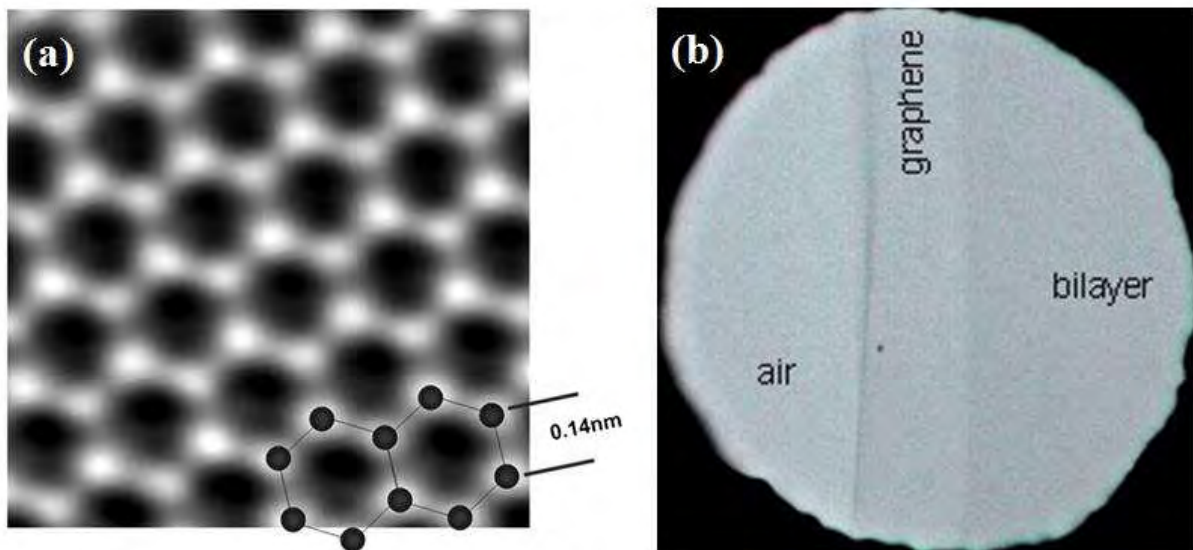

Figure 2.6: a) TEM image of a graphene sheet illustrating the crystalline lattice (bond length ~

0.14 nm) (Dato et al. 2009), b) A single sheet graphene can be visualized by eye due to its capacity to

absorb 2.3% of white light (Kuzmenko, van Heumen et al. 2008).

2.8.1. Graphene Synthesis

In spite of outstanding achievements of the physicists, chemists and materials scientists in the production of high quality graphene samples in the lab, it is still a grand challenge to use graphene-based materials and devices for large-scale industrial applications (Ruoff 2008). The performance of high quality graphene materials and devices is mainly based upon the number of individual layers (e.g. mono-/bi-/multi-) andthe quality of the crystal lattice (Yan, Henriksen et al. 2008, Meyer, Geim et al. 2007,Castro, Novoselov et al. 2007, Morozov, Novoselov et al. 2008). Synthesis of monolayer graphene can be achieved by overcoming the van der Waals bonding in graphite. The mechanical exfoliation of highly oriented graphite flakes through a scotch tape method is the primarily solution and was pioneered by Geim and Novoselov in 2004,indicating a reliable approach to the fabrication of the highest quality single sheets ofgraphene to date (Novoselov, Geim et al. 2004, Novoselov, Jianing et al. 2005).Stankovich et al. later proposed a method to exfoliate graphene oxide sheets by ultrasonication of graphite oxide flakes in a liquid phase and subsequent reduction of thefilms in a hydrazine hydrate solvent (Stankovich, Piner, Chen et al. 2006, Stankovich,Dikin, Piner et al. 2007). Lotya et al. reported mono-/few- layer graphene synthesis *via*ultrasonic sonication of graphite powders in a sodium dodecylbenzene sulfonate (SDBS)solution (Lotya, Hernandez et al. 2009). Unfortunately, graphene materials produced using liquid phase exfoliation are not of sufficient quality for electronic applications dueto defect formation during the oxidation and reduction processes (Choi, Lahiri et al.2010).Somani et al. synthesized the planar structure of few-layer graphene by using a thermal CVD process (Somani et al. 2006). The HRTEM images confirmed few-layer graphene sheets fabricated using the thermal CVD technique, but note that it is a great challenge to apply this method if less than 5-10 graphene layers are required. Obraztsovet al. synthesized few-layer graphene sheets using the thermal CVD on a Ni substrate(Obraztsov et al. 2007). However, large scale mono-layer graphene fabrication is still achallenge, and has been a major interest of the scientific community within the past fewyears (Obraztsov 2009, Wang, You, Liu, Li et al. 2009). Reina et al. recently grew the single-/few-layer graphene sheets on a large area Ni substrate enhancing the substrate transferring property (Reina, Jia et al. 2009). In 2004, plasma enhanced chemical vapor deposition (PECVD) was the method used to fabricate a bi-/few-layer graphene structure on a range of different substrates (Wang, Zhu et al. 2009, Wang, Zhu, Outlaw et al.2009). The highest quality of mono-layer graphene sheets produced by the

thermal CVD process was reported by Ruoff‟s group on a Cu foil (Li, Cai et al. 2009). This processhas been commercialized by Ijima‟s group to produce 30-inch graphene film for touchscreen LCD applications (Bae, Kim et al. 2010).Graphene sheets can be made *via* approaches, including chemical exfoliation,thermal decomposition on a substrate, and unzipping of CNTs. Horiuchi et al. reported detecting mono-layer graphene films extracted from natural graphite flakes using alchemical process (Horiuchi et al., 2004). Using thermal decomposition of 6H-SiC on its(0001) plane, graphene configuration is successfully achieved by hydrogen etching and subsequent heating to 1450 °C (Wu, Ren, Gao et al. 2009). The process is of great interest to researchers engaged in further study for semiconductor industries. V´azquezde Parga et al. also reported the synthesis of single-layer graphene on a (0001) plane of ruthenium single crystal (V´azquez de parga et al. 2008). The above outlines the majority of graphene research to date. It is clear that scientists are working towards the production of fewer layers of high quality graphene sheets in gram quantities, or synthesizing large-area mono-layer graphene on the substrates in very large sizes.

2.8.2. Properties and Applications of Graphene

Mono-/Bi-/Multi- layer graphene sheets can be extensively utilized for applications in electronics, semiconductors, gas absorbers, sensors, solar cells, fuel cells, optic devices, and composites due to the outstanding properties of sp2-bonded carbon atoms ina 2-D network. The signature of electron diffraction pattern (DP) corresponding to the graphene‟s (002) plane is found in its solid form (Kasuya, Yudasaka et al. 2002). Graphene can be characterized by SEM, TEM, optical microscopy, SPM, AFM, STM,Raman spectroscopy and FTIR. Scanning tunneling microscopy (STM) has been extensively utilized to investigate the graphite‟s electronic topography (Batra et al. 1987,Rabe et al. 1991, Soler et al. 1986, Stolyarova et al. 2007). Although it is difficult toreach a precise estimate of the number of graphene layers under the microscopy instruments, it can be approximated based upon the shape and position of G and 2Dbands in Raman spectra (Kim, Zhao, Jang, Lee et al. 2009).Mono-layer graphene demonstrates exceptional electronic, thermal, quantum-Hall effect, strength, and biocompatibility properties, making it a suitable material forindustrial applications (Novoselov, Geim, Morozov et al. 2005, Novoselov, Jiang, Zhanget al. 2007, Sakhaee-Pour 2009, Chen, M¨uller et al. 2008, Katsnelson, Novoselov et al.2006, Rao, K. Biawas et al. 2009, Castro Neto et al. 2009). The 2D

structure of themono-layer graphene also creates an enormous specific surface area, which introduced graphene as an efficient gas absorber to fabricate next-generation chemical sensors(Schedin et al. 2007). In addition, graphene"s extraordinary electrical property makes it an excellent material to fabricate field-effect transistors (FET) possesses a distinct reaction to external electric fields (Novoselov et al. 2004). De Heer and coworkers have proven that graphene-based transistors and loop devices are more efficient for next generation electronic systems (Berger et al. 2004, Bullis 2008). Echtermeyer et al.reported enhanced on-off ratio (~ 6 OM) in graphene-based field effect electronics through chemical modification of the graphene layers (Echtermeyer et al. 2008). Despite the issues facing the production of mono-layer graphene, special properties like high carrier mobility and low noise make it a high potential material for FETs. In 2007, Chen et al. developed a technique to transfer the single-layer graphene sheet from the Si-based substrate onto a plastic-based one, which has more flexibility for wide operations in theFETs (Chen, Ishigami et al. 2007). Carrier mobility of graphene, which makes it an outstanding semiconducting material, has been theoretically predicted and experimented via E-Beam lithography technique (Novoselov, Geim et al. 2008, Novoselov, Geim et al.2005, Wallace 1947, Slonczewski & Weiss 1958).In more recent research, Ruoff and co-workers have successfully synthesized functionalized chemically-modified graphene (CMG) to develop the next-generation high performance ultracapacitors with greater energy storage density (Stoller et al.2008). Antibody-functionalized graphene sheets (AFGS), with modified surface chemistry and enormous surface area, have been fabricated and used in Bio-MEMS(Nihar & Berry 2008). Shan et al. has publicized glucose properties of graphene sheets and suggested an innovative solution for the graphene electrochemical biosensors (Shen,Yong, Song et al. 2009). Anti-bacterial materials, such as metal ions and ammonium compounds, are extremely important in human life. However, because of several disadvantages, like complex processing and environmental challenges, related to the current anti-bacterial materials, it is very important to develop high performance anomaterials for these novel applications (Ramstedt et al. 2007, Allison et al. 2007, Stewart et al. 2001, Adolfsson-Erici et al. 2002). For instance, Hu et al. recently studied the anti-bacterial property of GO paper in killing food poisoning bacteria (e.g. E. coli)and has successfully shown that it is an effective inhibitor in the food packaging industry(Hu, Peng, Luo et al. 2010).Other two-dimensional materials, such as single-layer h-BN, can be broadly utilizedto study fundamental physics of materials for high potential applications

in transparent electronics and optoelectronics (Ci, Song, Jin, Jariwala et al. 2010). By using the dopingprocess, the p-/n- type graphene with semiconducting properties has been experimentally fabricated and carbon atoms effectively substituted with those of boron or nitrogen(Martins, Miwa et al. 2007, Lherbie et al. 2008). Ajayan''s group at Rice University has reported the large area production of few-layer h-BN (white graphene) through the CVD process; h-BN can be extensively utilized as dielectric substrate in electronics (Song, Ci,Lu et al. 2010). Graphene fillers can be exfoliated from the natural graphite flakes in bulk quantities to be utilized for polymer composite processing. Different types of polymers, such asPMMA, polyester, polypropylene (PP), and polystyrene (PS), have been used to make nanocomposites by adding different types of graphene fillers (Ramanathan et al. 2008,Stankovich, Dikin et al. 2006, Fang, Wang et al. 2009, Higginbotham et al. 2009, Das etal. 2009). Researchers recently dispersed graphene fillers into polymers by using a melt blending technique (graphene fillers and a melted polymer are mixed using a shear mixing technque), and fed the mixture into an extruder machine (Zhang, Zheng et al.2010, Kim, Jeong et al. 2010, Kim, Do et al. 2010, Kalaitzidou et al. 2007). In anotherapproach, emulsion polymerization method (by incorporation of water and a monomer)was utilized to create an aqueous colloidal suspension of graphene oxide sheets for applications in latex-based polymers (Hu, Wang et al. 2010, Zheming et al. 2009, Tkalyaet al. 2010).Our research on the mechanical properties of graphene/epoxy composites started in2009, and to the best of our knowledge we were the first group in the US which used graphene fillers to enhance the fracture, fatigue and strength properties of epoxy polymers. Herein we report the fracture toughness (KIc), fracture energy (GIc), and fatigue crack propagation rate properties of epoxy composites with different weight fractions of GPL fillers (see Chapter 2). In Chapter 3, we compare the mechanical properties of epoxy nanocomposites with GPL, SWNT, and MWNT fillers at the same loading fraction of ~ 0.1 wt.%. In Chapter 4, we demonstrate that unzipping MWNTs into graphene nanoribbons (GNRs) results in an enhancement in load transfereffectiveness in their epoxy composites. We show that this unzipping effect can be used to transform carbon nanotubes into graphene nanoribbons, which are far more effective than the baseline nanotubes in composites. In Chapter 5, we describe the mechanical properties of fullerence (C60) epoxy nanocomposites at different loading fractions(wt.%) of fullerene fillers in the pristine epoxy. In Chapter 6 and 7 we explore beyond polymer (epoxy) matrices and study the mechanical properties of graphene ceramic(silicon nitride) matrix and graphene metal

(alumnimum) matrix nanocomposites. The goal of the present thesis is to investigate the effectiveness of different carbon-based materials, including C60s, SWNTs, MWNTs, GNRs and GPLs to enhance the fatigue, fracture and strength properties of nanocomposite materials for high performance structural applications.

2.9 NON- BIODEGRADABLE POLYMER AND THEIR IMPACTS ON ENVIRON-MENTAL POLLUTION IN BANGLADESH

In all stages of a synthetic polymer life, from manufacturing to disposal, negative social and environmental impacts are evident. The planet"s environment, including its soil, water and air, is affected directly in numerous ways, beginning with the extraction and use of fossil fuels during the manufacturing process of plastic bags. Emissions resulting from this process are also very harmful to both humans and the physical environments, and the transportation of plastic bags from their origin to their place of use also contributes significantly to the environmental pollution. Further negative impacts are found during the use and immediate disposal of synthetic polymer products especially plastic bags, particularly in non-industrial nations where waste management services are not well-developed. In these regions, plastic bags are found everywhere, from remote tourist destinations to city streets where they can risk the society in varieties way.

Polyethylene materials are not bio-degradable. Whenever a polyethylene bag is thrown away, it does not decompose through natural process. It contributes to the accumulation of non-destructive waste of permanent nature. If anybody looks at any garbage dumping site, he will observe this fact that although other garbage matter get decomposed and merged into the soil but polyethylene bags remain intact with their different colors. Polyethylene remains intact in the soil and disturbs the flow of nutrients to the soil and hinders entering sunlight. It destroys the beneficial bacteria of soil and losses soil fertility. It hinders the way of soil compaction, which in the long run effects the construction of foundation of the different structure.

Using Polyethylene is not environment friendly. Medical reports find it as an agent of cancer, skin diseases and other health problems. The users are more exposed to these types of health hazards when polyethylene is used to pack bread, biscuits, potato chips or other food items. In

the developed countries, food is wrapped in food-graded plastic or polyethylene, but in Bangladesh this was not strictly followed and sometimes colorants are used, some of which may be carcinogenic.

Polyethylene industries for shopping bag production emerged in Bangladesh in early 80's and within a decade the industry reached in such a level that the jute bag production forced to be almost closed. The use of polyethylene shopping bags had been so enormous that one could find the polyethylene bags everywhere i.e in the street, dumpsites, drains, ditches, open-fields, roof tops, hanging from trees and overhead cables, floating on ponds, canals, rivers. Survey report showed that near about 10 million polyethylene bags were used every day and every year about 3000 million bags were dumped in Dhaka City alone. The steadily growing use of polyethylene bags posed an ominous environmental problem in the city as well as in rural areas. This enormous use of polyethylene bags led to severe environmental impacts like soil degradation, loss of soil fertility, blocking up of drainage and sewerage systems, causing water logging and the spread of harmful microbes and bacteria. The worst example of adverse effect caused due to polyethylene bags was the delaying process of recession of flood water in Dhaka city during 1998.The question of plastic bags ultimately comes down to the issue of use. If people are willing and able to use environmentally-friendly alternatives, such as reusable cloth or plastic bags, the decreasing use of plastic bags will reduce their overall footprint. However, without educating the public concerning the impacts of plastic grocery bags or constructing barriers to their use, business will continue as usual. Many governments have chosen the route of taxes or levies on plastic bags, to great success. Perhaps in a culture where convenience often comes before environmental concern, speaking to consumers" pocketbooks may be the only way to effectively deal with this ever-increasing problem.

2.9.1 Anti-polythene Campaign

Environment and Social Development Organization (ESDO), an environmental NGO for the first time started campaign against polythene shopping bags in Bangladesh in 1992. It drew attention of the press as well as of the Government. A number of non-government organizations and public leader came forward to support the campaign. Some organizations demanded banning of production and use of polythene shopping bags. Based on the popular demand, in 1993, Ministry of Environment and Forest took an initiative to ban the production and trade of

polythene bags outside Export Processing Zone (EPZ) with the approval of the cabinet, but it was not materialized. However, anti-polyethylene campaign was picking up steadily and spreading from the capital city to other cities and towns.

The campaign reached to its peak in the aftermath of 1998 flood, when two third areas of the country including a large part of the Dhaka City was under knee deep water for nearly two months. Clogging of city drains by polyethylene bags was the reason for delaying process of recession of flood water of Dhaka City. The people realized that indiscriminate use of polythene has been the root cause of their suffering. In 1999, Ministry of Environment again started campaign against polyethylene through its Sustainable Environment Management Program, which led to the formation of a task force by the government under the ministry to work towards framing a strategy for phasing out of polythene shopping bags. The task force recommended for undertaking a detailed study on the production, marketing and use of polythene shopping bags and its socio-economic impacts before making the final decision.

2.10. Dielectric properties

Dielectrics are non-conductors of electricity, but because they consist of positively and negatively charged particles bound together, their interaction to applied electrical field is significant. The fundamental action of the field is to separate positive and negative charges of the entire volume of the dielectric, causing what is known as the polarization of the dielectric. Fig 1 shows the effect of the polarization. We see that the net polarization charges are produced at the faces of the dielectric, a positive charge on the right and a negative on the left; inside the medium there is no excess charge on the in any given volume element. The medium as a whole remains neutral, and the positive charge on the right is equal in magnitude to the negative charge on the left. These charges create their own electric field E_p which is directed to the left, and thus oppose the external field E_0. When we add this polarization field E_p to the external field E_0, so as to obtain resultant field E, we find that $E < E_0$. Thus the Polarization of the medium reduces the electric field in its interior.
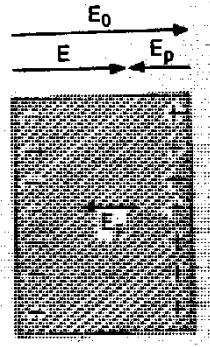
Fig 2.7: Effect of polarization in dielectric materials

It must be noted here that during polarization the charges in the dielectric are displaced from their equilibrium positions by distances that are considerably less than an atomic diameter. There is no transfer of charge over macroscopic distances such as occur when a current is set up in a conductor.
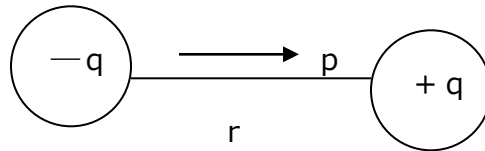
The electric moment is therefore equal to one of the charges times the distance between them. Now, if each of the particles of a solid possesses a dipole moment, the total dipole moment of the sample would be

$$p = \sum_i q_i r_i \qquad \ldots(2)$$

The polarization P in a solid is defined as the dipole moment per unit volume:

$$P = \frac{p}{V}. \qquad \ldots(3)$$

It has the same units as the surface charge density and is, in fact, equivalent to it, since a polarized object will have induced surface charge at the two ends. The electric field E is defined as the force F per unit charge acting on a test charge q:

$$E = \frac{F}{q}. \qquad\qquad ....(4)$$

Measurement of E in empty space is easy because all we have to do is to place a small test charge there and observe the force on it. But how to measure it in a solid medium? In solids we cut a long needle-like cavity parallel to the field and place a test charge in it; the force on this test charge will gives us the field E. This is because the field in such a cavity is equal to the field in the medium.

Dielectric Constant:

Consider a parallel-plate capacitor consisting of two plane parallel plates of area A and separation d, charge with a surface charge density σ. If the space between the plates is vacuum and if d small compared with he dimensions of the plates, there will result an electric field between the plates, its strength being given by

$$E_{vac} = \frac{\sigma}{\varepsilon_0}.$$

The p. d. between the plates is equal to

$$V_{vac} = E_{vac}d,$$

and the capacitance of the capacitor is defined by

$$C_{vac} = \frac{A\sigma}{V_{vac}}.$$

Suppose now that the space between the plates is filled with an insulating substance, the charge on the plates being kept constant. It is then observed that new p. d. V is lower than V_{vac} and the capacitance C of the capacitor is increased. The dielectric constant ε is then defined by

$$\varepsilon = \frac{V_{vac}}{V} = \frac{C}{C_{vac}}.$$

Thus, the field strength is reduced from the value E_{vac} to the value E, where $\frac{E_{vac}}{E} = \varepsilon$, or, in other words, the effective surface charge density on the plates in now changed from

$$\sigma = E_{vac} \times \varepsilon_0 \text{ to } \sigma' = E \times \varepsilon_0 .$$

The effect of introducing the insulating substance (i.e. dielectric) is thus to reduce the surface charge density by an amount

$$\sigma - \sigma' = E_{vac} \times \varepsilon_0 - E \times \varepsilon_0 = \varepsilon E \times \varepsilon_0 - E \times \varepsilon_0 = (\varepsilon - 1)\varepsilon_0 E. \quad (5)$$

The above explanation of the induction of charge at the surface of the dielectric is an accord with that considered earlier.

Polarizability:

All these quantities are macroscopic and measurable. But if we want a microscope theory to explain these properties, we need microscopic properties. Polarizability α defined as

$$\alpha = \frac{p}{E_{loc}}.$$

is such a property. Here p is the dipole moment that an atom acquires in a local electric field E_{loc}. The local field E_{loc} is the field that is actually effective in polarizing the atoms of a solid. The polarizability of a dielectric is the quantity that is experimentally determined, α is the quantity about which we are theoretically concerned; **we will find out how α arises, and how it depends on frequency and temperature**. In the next section we shall see that α is related to ε. The polarizability has dimensions of volume and, in fact, turns out to be closely related to the atomic volume.

acting on a test charge q assumed at the centre of the sphere in the direction of **r**. Hence, the field dE_s at the centre due to this charge element is

$$dE_s = \frac{dF}{q} = -\frac{P\cos\theta\, dS}{r^2}. \qquad \ldots(10)$$

Now resolving dE_s into components parallel and perpendicular to the direction of P, we easily see that the perpendicular component will be cancelled due to an equal contribution from another symmetrically situated surface element. Thus only the component of dE_s along the direction of P will contribute to the integral of eqn. (10) over the entire surface. Thus

$$E_s = -\int \frac{P\cos\theta\, dS}{r^2}. \qquad (11)$$

Now the appropriate surface element dS in this case is the ring shown in fig. 4 so that $dS = 2\pi r\sin\theta\, rd\theta = 2\pi r^2 \sin\theta\, d\theta$, and the limits of integration with respect to θ are from 0 to π. Thus

$$E_s = \int_0^\pi \frac{P\cos^2\theta\, dS}{r^2} 2\pi r^2 \sin\theta\, d\theta$$

$$= 2\pi P \int_0^\pi \cos^2\theta\sin\theta\, d\theta.$$

This integral can be evaluated directly by making the substitution $z = \cos\theta$ and $dz = -\sin\theta\, d\theta,$

so that
$$E_s = 2\pi P \int_1^1 z^2\, dz$$

or
$$E_s = \frac{4\pi P}{3} \qquad \text{.(12a)}$$

$$E_s = \frac{P}{3\varepsilon_0} \qquad \text{in SI unit} \qquad \text{.(12)}$$

We thus have, finally, from eqn.(9)

$$E_{loc} = E + \frac{4\pi P}{3} \qquad \text{...(13a)}$$

$$E_{loc} = E + \frac{P}{3\varepsilon_0} \qquad \text{...(13)}$$

This shows that E_{loc} is indeed different from E, as we have expected: the former field is larger than the latter, so the molecules are more effectively polarized than that our earlier discussion have indicated. **Eqn. (13) is known as the Lorentz relation.**

Dipolar Polarizability

Consider a dipolar system in which the dipoles are able to rotate freely. Without an external field, the dipoles will be oriented at random and the system as a whole will have no resultant dipole moment. But an external field E will exert a torque on each dipole and will tend to orient the dipoles in its direction, according to fig. 7.
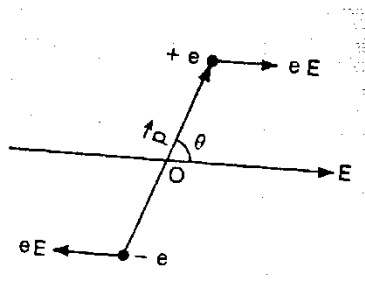

Fig. 2.8. Torque applied by an electric field on a dipole.

On the other hand, this ordering effect of the field will be counteracted continuously by the thermal motion of the dipoles. Therefore, an equilibrium state will reach in which different, torque applied by a field on dipole dipoles will make *zero* to π radian angles with the field direction, producing a net polarization in the direction of the field. It is this polarization that we are going to calculate.

Frequency Dependence of Dipolar Polarizability

Let us now discuss ac dipolar polarizability. To begin with we consider the situation in a dc field. In the absence of the field, the dipole orientations are randomly distributed; these orientations change continuously as a result of phonon collisions. When the field is switched on, the dipoles tend to line up with the field. But it takes time i.e, there is a lag in the attainment of equilibrium polarization. The time required to reach equilibrium polarization is expressed in terms of the relaxation time τ, which is defined as the time that makes the polarization attain nearly two-third of its equilibrium value. On account of this finite time, it is clear that if the applied field changes (say, it is switched off and on frequently) in a time short compared to τ, the dipole system cannot respond to the changes. Consequently, the polarizability dies off at high frequencies of the applied field. In particular, if $E(t) = E_0 e^{i\omega t}$, then polarizability approaches to zero value when $\omega >> \dfrac{1}{\tau}$ and to its dc value if $\omega << \dfrac{1}{\tau}$ i.e. if the oscillations are slow compared to τ.

In order to calculate the frequency dependence, we shall first give a description of the transient effects using the concept of the relaxation time and then proceed to consider the case of an alternating field. The equation which describes the transient effects of a dc field on the dipolar polarization is

$$P_d(t) = P_{ds}(t)\left(1 - e^{-t/\tau}\right) \qquad \ldots(25)$$

Hence $\qquad \dfrac{dp_d(t)}{dt} = \dfrac{1}{\tau}\left[p_{ds}(t) - p_d(t)\right] \qquad \ldots\ldots(26)$

Here $p_d(t)$ is the actual dipole moment at the instant t and $p_{ds}(t)$ is the equilibrium (or saturated) value of the moment; in fact $p_{ds}(t)$ is the value $p_d(t)$ obtained after the dc field has acted for a long time. Thus the moment rises towards its equilibrium value in an exponential fashion, much like the dc rise in an R-L electrical circuit of time constant τ when the battery has just been switched on. In the case of an alternating field, the appropriate equation is therefore

$$\frac{dp_d(t)}{dt} = \frac{1}{\tau}\left[p_{ds}(t) - p_d(t)\right].$$ ..(27)

Note that (27) has been obtained from (26) by replacing p_{ds} by $p_{ds}(t)$ representing saturation value which would be obtained in a static field equal to the value of the alternating field at an instant t. Let us now apply (27) to the case of an ac field.

$$E(t) = E_0 e^{i\omega t}.$$

The equilibrium moment is given by

$$P_{ds}(t) = \alpha_d(0)E(t)$$
$$= \alpha_d(0) E_0 e^{i\omega t}$$

where $\alpha_d(0)$ is the static polarizability. Eqn. (27) now reduces to

$$\frac{dp_d(t)}{dt} + \frac{p_d}{\tau} = \frac{\alpha_d(0)}{\tau} E_0 e^{i\omega t}.$$ ...(28)

It can be shown that (28) has

$$p_d(t) = \alpha_d(\omega)E_0 e^{i\omega t}$$ ..(29)

as its solution provided that

43

$$\alpha_d(\omega) = \frac{\alpha_d(0)}{1+i\omega t}. \qquad (30)$$

It can be seen that $\alpha_d(\omega)$, by definition the a.c. polarizability, is now a complex quantity; this in turn establishes the fact that the polarization is no longer in phase with the field.

Our final goal is to express the dielectric constant in terms of the frequency ω and the relaxation time τ. The definition of the electrical susceptibility used in eqn. (6) gives us for he dielectric constant

$$\varepsilon(\omega) = 1 + 4\pi\chi(\omega)$$
$$= 1 + 4\pi\chi_e(\omega) + 4\pi\chi_d(\omega) \qquad (31)$$

where $\chi_e(\omega)$ and $\chi_d(\omega)$ are the electronic and dipolar susceptibilities respectively. The ionic contribution is very small, and has therefore been ignored. Now in the frequency region in which frequency effects are significant (i.e. the microwave region), $\chi_e(\omega)$ is constant because the electrons are the light particles and thus they can respond to the field instantaneously. Under this condition $1 + 4\pi\chi_e(\omega)$ is equal to the optical dielectric constant. Finally, recalling from Maxwell"s theory that the optical dielectric constant is equal to n^2, where n is the index of refraction, we have from (31)

$$\varepsilon(\omega) = n^2 + 4\pi\chi_d(\omega). \qquad ....(32)$$

Since χ_d is proportional to α_d by definition, it follows that $\chi_d(\omega)$. has the same complex form as $\alpha_d(\omega)$ in (30), and we may then write (32) as

$$\varepsilon(\omega) = n^2 + 4\pi \frac{\chi_d(0)}{1 + i\omega\tau}$$

$$= n^2 + \frac{\varepsilon(0) - n^2}{1 + i\omega\tau} \tag{33}$$

Here $\chi_d(0) = [\varepsilon^{(0)} - n^2]/4\pi$ is the static value of the dipolar susceptibility. This is the equation we set out to seek; it expresses clearly the frequency dependence of the dielectric constant. Now, from the definition of the complex dielectric constant

$$\varepsilon(\omega) = \varepsilon'(\omega) - i\varepsilon''(\omega)$$

the following expressions result

$$\varepsilon'(\omega) = n^2 + \frac{\varepsilon(0) - n^2}{1 + i\omega^2\tau^2} \tag{34}$$

$$\varepsilon''(\omega) = \frac{\varepsilon(0) - n^2}{1 + i\omega^2\tau^2}\omega\tau. \tag{35}$$

These equation are frequently referred to as the Debye equations. Fig. 10 shows these equations graphically. We note that the real part $\varepsilon'(\omega)$ is a constant, equal to $\varepsilon(0)$ for all frequencies in the range $\omega \ll \frac{1}{\tau}$; this frequency range usually covers all frequencies up to the microwave region. In the frequency range $\omega \geq \frac{1}{\tau}$, it decreases, eventually reaching the value n^2. This result is quite expected. The imaginary part $\varepsilon''(\omega)$ has its maximum at $\omega = \frac{1}{\tau}$, and decreases as the frequency departs from this value in either direction.

It may be added here that a part of the electrical energy is dissipated in the dielectric in the form of heat. This is a consequence of the fact that the polarization in alternating fields lags behind in phase relative to the applied field. It can be proved that the rate of this loss is proportional to $\varepsilon''(\omega)$, and is thus maximum at $\omega = 1/\tau$.
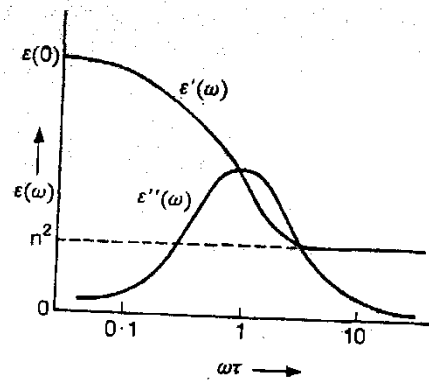
Fig. 2.9: Debye curves for ε' and ε'' for a dipolar substance.

Measurement of Dielectric Constant

Dielectric constant of a given substance is usually measured by comparing the capacity C_d of a condenser filled with the substance and the capacity C_0 of the empty condenser: the ratio the dielectric constant. The capacities C_d and C_0 may be measured conveniently by a resonance method shown in fig. 14, where C_s is a calibrated variable condenser and C is the condenser in which the given substance (taken in the form of a thin disc) may be placed.
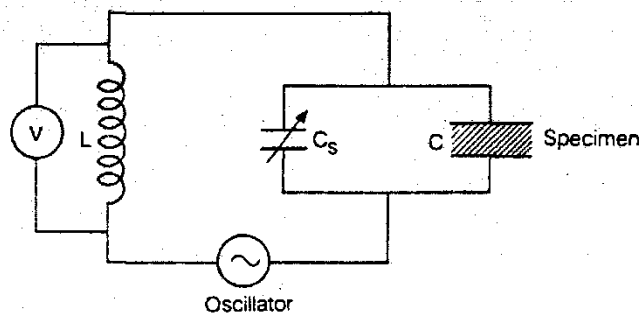
Fig.2.10. Principle of the resonance method for measureing C_0 and C_d

By varying C_s so as to keep the resonance frequency $\omega_0 = \dfrac{1}{\sqrt{[L(C_s + C)]}}$ constant when C is empty and then filled, we may determine C_0 and C_d, and hence ε. The voltmeter V measures the response of the resonant circuit.

This method of measuring dielectric constant is generally applicable to frequencies up to about 100 MHz. At the microwave region ($\sim 10^3$ to $\sim 10^5$ MHz) the frequencies are so high that the dimensions of the apparatus are comparable with, or greater than, the wavelength, and the specimen then can no longer be treated as if it were in quasi-static fields. Rather, it has to be thought of as a medium for the propagation of e.m. waves. Here one may measure the dielectric constant of the specimen by measuring essentially the wavelength of the microwave radiation in the specimen and using the relation

$$\frac{\lambda \: vacuum}{\lambda \: specimen} = (\varepsilon \mu)^{1/2}$$

where μ is the permeability. For majority of solids $\mu \simeq 1$. For optical and infrared frequencies, ε can be measured by measuring the refractive index, n, as

$$n^2 = \varepsilon \mu \simeq \varepsilon.$$

2.11. Electrochemical properties

Electrochemistry is a powerful tool to probe reactions involving electron transfers. Electrochemistry relates the flow of electrons to chemical changes. In inorganic chemistry, the resulting chemical change is often the oxidation or reduction of a metal complex. To understand the difference between a chemical reduction and an electrochemical reduction, consider the example of the reduction of ferrocenium $[Fe(Cp)2]+$ (Cp = cyclopentadienyl), abbreviated as Fc+, to ferrocene $[Fe(Cp)2]$, abbreviated as Fc:

• Through a chemical reducing agent: Fc+ + $[Co(Cp^*)2]$= Fc + $[Co(Cp^*)2]+$

• At an electrode: Fc+ + e− = Fc. Why does $[Co(Cp^*)2]$ (Cp* = pentamethylcyclopentadienyl) reduce Fc+?

Fig. 2.11. Electrochemical workstation in my laboratory

In the simplest explanation, an electron transfers from [Co(Cp*)2] to Fc+ because the lowest unoccupied molecular orbital (LUMO) of Fc+ is at a lower energy than the electron in the highest occupied molecular orbital (HOMO) of [Co(Cp*)2]. The transfer of an electron between the two molecules in solution is thermodynamically favorable and the difference in energy levels is the driving force for the reaction. In an electrochemical reduction, Fc+ is reduced via heterogeneous electron transfer from an electrode; but what is the driving force for this process? An electrode is an electrical conductor, typically platinum, gold, mercury, or glassy carbon. Through use of an external power source (such as a potentiostat), voltage can be applied to the electrode to modulate the energy of the electrons in the electrode. When the electrons in the electrode are at a higher energy than the LUMO of Fc+, an electron from the electrode is transferred to Fc+ . The driving force for this electrochemical reaction is again the energy difference between that of the electrode and the LUMO of Fc+. Changing the driving force of a chemical reduction requires changing the identity of the molecule used as the reductant.At its core, the power of electrochemistry resides in the simplicity with which the driving force of a reaction can be controlled and the ease with which thermodynamic and kinetic parameters can be measured.

Cyclic Voltammetry

Cyclic voltammetry (CV) is a powerful and popular electrochemical technique commonly employed to investigate the reduction and oxidation processes of molecular species. CV is also invaluable to study electron transfer-initiated chemical reactions, which includes catalysis.

Introduction to the Electrochemical Cell

In the experimental section of papers describing electrochemical measurements, a brief description is generally given for the experimental setup used to collect the data. The vessel used for a cyclic voltammetry experiment is called an electrochemical cell. The subsequent sections will describe the role of each component and how to assemble an electrochemical cell to collect data during CV experiments.
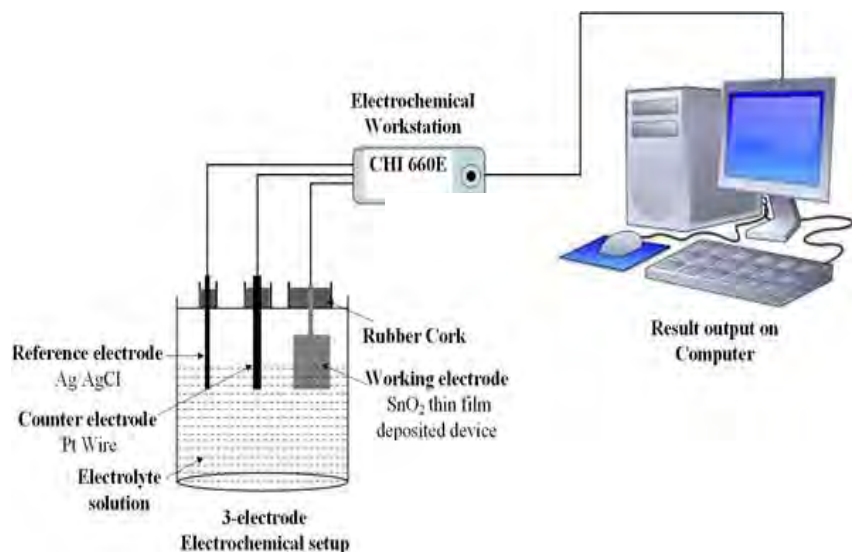

Figure 2.12. Schematic representation of an electrochemical cell for CV experiments

Preparation of Electrolyte Solution

As electron transfer occurs during a CV experiment, electric neutrality is maintained via migration of ions in solution. As electrons transfer from the electrode to the analyte, ions move in solution to compensate the charge and close the electrical circuit. A salt, called a supporting electrolyte, is dissolved in the solvent to help decrease the solution resistance. The mixture of the solvent and supporting electrolyte is commonly termed the "electrolyte solution." Solvent. A good solvent has these characteristics:

• It is liquid at experimental temperatures.

• It dissolves the analyte and high concentrations of the supporting electrolyte completely.

• It is stable toward oxidation and reduction in the potential range of the experiment.

• It does not lead to deleterious reactions with the analyte or supporting electrolyte.

• It can be purified.

A good supporting electrolyte has these characteristics:

• It is highly soluble in the solvent chosen.

• It is chemically and electrochemically inert in the conditions of the experiment.

• It can be purified.

Large supporting electrolyte concentrations are necessary to increase solution conductivity. As electron transfers occur at the electrodes, the supporting electrolyte will migrate to balance the charge and complete the electrical circuit. The conductivity of the solution is dependent on the concentrations of the dissolved salt. Without the electrolyte available to achieve charge balance, the solution will be resistive to charge transfer.

Working Electrode (WE)

The working electrode carries out the electrochemical event of interest. A potentiostat is used to control the applied potential of the working electrode as a function of the reference electrode

potential. The most important aspect of the working electrode is that it is composed of redox inert material in the potential range of interest. The type of working electrode can be varied from experiment to experiment to provide different potential windows or to reduce/promote surface adsorption of the species of interest. Because the electrochemical event of interest occurs at the working electrode surface, it is imperative that the electrode surface be extremely clean and its surface area well-defined. The procedure for polishing electrodes varies based on the type of electrode and may vary from lab to lab. When using electrodes such as glassy carbon or platinum, clean electrodes surfaces can be prepared via mechanical polishing .To remove particles, the electrode is then sonicated in ultrapure water. It is often also necessary to perform several CV scans in simple electrolyte across a wide potential window to remove any adsorbed species left over from the polishing procedure. This can be repeated until the scans overlap, and no peaks are observed. This procedure is sometimes referred to as "pretreating" the electrode. For glassy carbon electrodes, the surface is very reactive once activated via polishing. When impurities are present in the solvent, they can preferentially adsorb to the carbon surface of the electrode, leading to modifications of the voltammograms.

Reference Electrode (RE)

A reference electrode has a well defined and stable equilibrium potential. It is used as a reference point against which the potential of other electrodes can be measured in an electrochemical cell. The applied potential is thus typically reported as "vs" a specific reference. There are a few commonly used (and usually commercially available) electrode assemblies that have an electrode potential independent of the electrolyte used in the cell. Some common reference electrodes used in aqueous media include the saturated calomel electrode (SCE), standard hydrogen electrode (SHE), and the AgCl/Ag electrode. These reference electrodes are generally separated from the solution by a porous frit. It is best to minimize junction potentials by matching the solvent and electrolyte in the reference compartment to the one used in the experiment. In nonaqueous solvents, reference electrodes based on the Ag^+/Ag couple are commonly employed. These consist of a silver wire in a solution containing an Ag^+ salt, typically $AgNO_3$. Conversion tables exist which enable referencing of data obtained with an Ag^+/Ag electrode to other types of reference electrodes for several silver salt, solvent, and concentration combinations. The potential of Ag^+/Ag reference electrodes can vary between

experiments due to variations in [Ag+], electrolyte, or solvent used, so it is important to note the specific details of a nonaqueous reference electrode. To circumvent these problems, reduction potentials should be referenced to an internal reference compound with a known E0′. Ferrocene is commonly included in all measurements as an internal standard, and researchers are encouraged to reference reported potentials vs the ferrocene couple at 0 V vs Fc+/Fc.[20,21] Care should be taken to ensure that the potential window of the analyte‟s redox processes do not overlap with those of ferrocene and that the analyte does not interact with ferrocene. If this is the case, a number of other internal standards with well-defined redox couples can be used (such as decamethylferrocene). Since nonaqueous reference electrode potentials tend to drift over the course of an experiment, we recommend having ferrocene present in all measurements rather than adding it at the end of a measurement set.

Counter Electrode (CE)

When a potential is applied to the working electrode such that reduction (or oxidation) of the analyte can occur, current begins to flow. The purpose of the counter electrode is to complete the electrical circuit. Current is recorded as electrons flow between the WE and CE. To ensure that the kinetics of the reaction occurring at the counter electrode do not inhibit those occurring at the working electrode, the surface area of the counter electrode is greater than the surface area of the working electrode. A platinum wire or disk is typically used as a counter electrode, though carbon-based counter electrodes are also available. When studying a reduction at the WE, an oxidation occurs at the CE. As such, the CE should be chosen to be as inert as possible. Counter electrodes can generate byproducts depending on the experiment, therefore, these electrodes may sometimes be isolated from the rest of the system by a fritted compartment. One example is the oxidative polymerization of THF that can occur at the CE when studying a reductive process in THF at the WE.

2.12. IMPORTANCE OF BIODEGRADABLE POLYMER IN BANGLADESH

Advancement of science and technology promote us to produce materials that can withstand extreme temperatures, and durable and easy to use. But what we forget is that these advanced products do not break down naturally. When we dispose them in a garbage pile, the air, moisture, climate, or soil cannot break them down naturally to be dissolved with the surrounding. They are not biodegradable. However natural waste and products made from nature break down easily when they are disposed as waste. But as more and more non-biodegradable materials pile up, there is increased threat to the environment. To understand the seriousness of the problem caused by non-biodegradable waste, we can check about what's happening to particular places where plastic and other materials are used for almost everything. One of the most common household wastes in Bangladesh is polythene- mostly used as polythene bags for shopping and carrying light things. Since they are cheap, they are used by almost everyone from the local vegetable seller to the supermarket. The hazard that polythene causes to the environment is very serious. Keeping in mind the potential hazard of biodegradable waste, it is important for us to know in what way we can help to make sure that less non-biodegradable material is left on the planet. Become an environment friendly consumer by following the everyday tips at on how we can contribute to less non-biodegradable materials.

REFERENCES:

[16]   Nishiyama, Y., Langan, P., and Chanzy, H., "Crystal Structure and Hydrogen-Bonding System in Cellulose I β from Synchrotron X-ray and Neutron Fiber Diffraction" *Am. Chem. Soc*, 124 , 9074–82, 2002

[17]   Klemm, D., Shmauder, H.P., Heinze, T., Cellulose In Biopolymers, Polysaccharides II; Vandamme, E.J., De Baets, S., Steinbchuel, A., Eds., 6, 275-319, 2002

[18]   Tang, W.L., Khor, E., Tan, T.K., Lim, L.Y., and Tan, S.C, "Concurrent production of chitin from shrimp shells and fungi" *Carbohydr. Res.*, *332*, 305-316, 2001

[19]   Tokura, S., and Tamura, H., "Chitin and Chitosan" Compr. Glycosci. 2007, 2, 449-475

[20] Je, J.Y., and Kim, S.K., "Antioxidant activity of novel chitin derivative" Bioorg. Med. Chem. Lett., 14, 5989-5994, 2006

[21] Park, S.Y., Lee, B.I., Jung, S.T., Park, "J.H. Biopolymer composite films based on carrageenan and chitosan" Mater. Res. Bull., 36, 511-519, 2001

[22] Muzzarelli, R., Weckx, M., Bicchiega, V., " N-carboxybutyl chitosan as a wound dressing and a cosmetic ingredient" Chim. Oggi., 9, 33-37, 1991

[23] Sarkanen, K.V., and Ludwig, C.H., "Lignin: Occurrence, Formation, Structure and Reactions." ed. Sarkanen, K.V. and Ludwig, C.H. Wiley-Interscience: New York. 916, 1971

[24] Sjostrom,E.,"Wood Chemistry: Fundamentals and Application"*Academic Press:Orlando*, 293, 1993

[25] Gao, C., Stading, M., and Wellner, N., " Plasticization of a protein-based film by glycerol: A spectroscopic, mechanical, and thermal study" *Agric. Food Chem.*,*54*, 4611-4616,2006

[26] Song, Y., and Zheng, Q., "Improved tensile strength of glycerol-plasticized gluten" *Bioresour. Technol.*, *99*, 7665-7671, 2008

[27] Hizukuri, S., Takeda, Y., Maruta, N., Juliano, B. O., "Molecular structures of rice starch", *Carbohydrate Research,* 189, 227, 1989

[28] Takeda, Y., Hizukuri, S., Takeda, C., Suzuki, A., "Structures of branched molecules of amyloses of various origins, and molar fractions of branched and unbranched molecules" *Carbohydrate Research*, 165, 139, 1987

[29] Hizukuri, S.,Takeda, Y., Yasuda, M., and Suzuki, A., "Multi-branched nature of amylose and the action of debranching enzymes " *Carbohydrate Research*, 94, 205,1981

[30] Imberty, A.,Chanzy, H., Perez, S., Buleon, A., and Tran, V., "The double-helical nature of the crystalline part of A-starch."*Molecular Biology,* 201, 365, 1988

[31] Brewster, M. , Estes, K. , Bodor, N., *Pharm,*59, 231,1990

[32] Szejtli, J . J., *Inclusion Phenom,* 11, 135, 1983

[33] Hirai,S., Okada, H., and Yashiki, T, *US Patent,*4, 659,696,1987

[34] Cyclodextrin News, 7, 295, 1993

[35] Cyclodextrin News, 8, 12, 1994

[36] Cyclodextrin News, 7, 276, 1993

[37] Gardlick, J.M.,Trinh,T, Barks,T.J., Benvegnu,F., *US Patent*, 5,234,610,1993.

[38] Trinh, T., Bacon, D.R., Benvegnu,F., *US Patent,*5, 234,611,1993.

[39] Wiedenhof, N., Lammers, J.N.J.J., Carbohydr. Res.7,1,1968

[40] Vakaliu, H., Miskolczi-Torak , M., Szejtli, J., Jarai , M., Seres, G., *Hungarian Patent,* 16,98,1979

[41] Wiedenhof, N., Lammers, J.N.J.J., *Carbohydr. Res.,* 7, 1, 1968

[42] Shalaby, S.W., "Bioabsorbable Polymers. In: Encyclopedia of Pharmceutical Technology" Swarbrick, J., Boylan, J.C., 1,465-476, 1988

[43] Holland, S.J., Tighe, B.J., "Biodegradable polymers.In: Advances in Pharmaceutical Science" *Academic Press, London, 6,101*-164, 1992

[44] Hayashi, T., "Biodegradable polymers for biomedical applications" *Prog Polymer Sci,* 19,663-702, 1994

[45] Kohn. J., Langer, R., Ratner, B.D, Hoffman, A.S., Schoen, F.J., Lemon, J.E., "Bioresorbable and bioerodible materials. In: An Introduction to Materials in Medicine" *eds. Academic Press*, San Diego, 65-73, 1997

[46] Ashammakhi, N., Rokkanen, P., "Absorbable polyglycolide devices in trauma and bone surgery" *Biomaterials,*18,3-9,1997

[47] Cutright, D., Beasley, J., Perez, B., "Histologic comparison of polylactic acid sutures" *Oral Surg,* 32,165-173,1971

[48] Pathiraja, A, .Gunatillake, and Raju, A., "Biodegradable synthetic polymer for tissue engineering" Polymer for tissue engineering, 5,1-16,2003

[49] Thomson, R. C., Wake, M.C., Yaszemski, M.J., Mikos, A.G., "Biodegradable polymer scaffolds to engineer trabecular bone" *J Biomater Sci Polymer* ,7,23-38,1995

[40] Chu,C. C. "An in-vitro study of the effect of buffer on the degradation of poly (glycolic acid) sutures" *J Biomed Mater*,15,19-27,1981

[51] Chu, C. C., "Thein-vitrodegradation of poly (glycolic acid) sutures- effect of pH*" J Biomed Mater*,15,795-804,1981

[52] Chu, C., C., "Hydrolytic degradation of polyglycolic acid: tensile strength and crystallinity study" *J Appl Polym Sci*, 26, 1727-1734, 1981

[53] Holland, S.J., Tighe, B.J. "Biodegradable polymers. In: Advances in Pharmaceutical Science" *Academic Press, London*, 6,101-164, 1992

[54] Veld, P.J.A., Velner, E.M., Van DeWhite, .P, Hamhuis, J., Dijkstra, P.J., and Feijen, J. " Melt block copolymerisation of e-caprolactone and L-Lactide" *J. Polym Sci Part 1 Polymer Chem*,35, 219-226,1997

[55] Storey, R.F., Taylor, A.E., "Effect of stannous octoate on the composition, molecular weight, and molecular weight distribution of ethyleneglycol-initiated poly(ecaprolactone)" *J Macromol Sci- Pure Appl Chem,*35,723-750,1998

[56] Yang, J., Yu, J., and Ma,X., "Preparation of a novel thermoplastic starch (TPS) material using ethylenebisformamide as the plasticizer" *Starch/Starke,*58,330-337,2006

[57] Thunwall, M., Boldizar, A., and Rigdahl, M., "Extrusion processing of high amylase potato starch materials" *Carbohydrate Polymer*, 11, 419-428, 2006

[58] Torres, F.G., Arroyo,O.H., and Gomez, C., "Processing and mechanical properties of natural fiber reinforced thermoplastic starch biocomposites" Journal *of Thermoplastic Composite Materials*, 20, 207-223, 2007

[59] Wang-L., Yang, K-K., and Wang, Y-Z., "Properties of starch blends with biodegradable polymers" *Journal of Macromolecular Science*, 43, 385-409, 2003

[60] Kazuo,O., Isao, Y., Toshiaki, Y., Shin, O., Seichi, R., Yuuko, N., and Choichiro, S., "Studies on the retrogradation and structural properties of waxy corn starch*" Bulletin of the Chemical Society of Japan,*71, 1095-1100, 1998

[61] Ma, X., and J. Yu., "Formamide as the plasticizer for thermoplastic starch" *Journal of Applied Polymer Science,* 93, 1769-1773, 2004

[62] Wang, L., Shogren, R. L., and Carriere, C., "Preparation and properties of thermoplastic starch-polyester laminate sheets by coextrusion" *Polymer Engineering and Science*, 40, 499–506, 2000

[63] Kirby, A.R., Clark, S.A., Parker, R. and Smith, A.C., "The deformation and failure behaviour of wheat starch plasticized with water and polyols" *Journal of Materials science* 28(21), 5937-5942, 1993

[64] Yang, J., Yu, J., and Ma., X., "Preparation of a novel thermoplastic starch (TPS) material using ethylene bisformamide as the plasticizer" *Starch/Starke*,58,330-337,2006

[65] Thunwall, M., Boldizar, A., Rigdahl ,M. and Kuthanova,V., " On the stress-strain behavior of thermoplastic starch melts*" International Journal of Polymer Analysis and Characterization,* 11, 419-428, 2006

[66] Hwan-Man,P., Won-Ki Lee, C-Y.P., and Won-Jei Cho, C-S.H., "Environmentally friendly polymer hybrids part I: mechanical, thermal and barrier properties of thermoplastic starch/clay nanocomposites" *Journal of Materials Science 38*, (5), 909-915, 2003

[67] Schlemmer, D., De Oliveira, E. and Araujo Sales M., " Polystyrene/thermoplastic starch blends with different plasticizers" *Journal of Thermal Analysis and Calorimetry*, 87, 635-638, 2007

[68] Teixeira, E. M., Da Roz A.L. , Carvalho, A. J. F., and Curvelo, A. A. S., "The effect of glycerol/sugar/water and sugar/water mixtures on the plasticization of thermoplastic cassava starch" *Carbohydrate Polymersdoi*, 10, 1016, 2007

[69] Ma, X.F., and Yu. J.G., "Studies on the properties of formamide plasticized-thermoplastic starch" *Acta Polymerica Sinica,* 2, 240-245, 2004

[70] Yu, J., Wang,N., and Ma, X.,. "The effects of citric acid on the properties of thermoplastic starch plasticized by glycerol" Starch/Starke, 57, 494-504, 2005

[71] Torres, F.G., Arroyo,O.H., and Gomez, C., "Processing and mechanical properties of natural fiber reinforced thermoplastic starch bio-composites"*Journal of Thermoplastic Composite Materials*, 20, 207-223, 2007

[72] Dufresne, A. and M.R. Vignon, " Improvement of starch film performances using cellulose microfibrils" *Macromolecules*,31(8),2693–2696,1998

57

[73] Angles, M.N., and Dufresne, A., "Plasticized/tunicin whiskers nanocomposites materials 2: mechanical behavior" *Macromolecule,* 34(9), 2921–2931, 2001

[74] De Carvalho, A.J.F, Curvelo ,A.A.S., and Agnelli, J.A.M. , "Wood pulp reinforced thermoplastic starch composites" *International Journal of Polymeric Materials,* 51, 647-660, 2002

[75] Reis, R.L., Cunha, A.M., Allan,P.S., and Bevis,M.J., "Structure development and control of injection-molded hydroxylapatite-reinforced starch/EVOH composites" *Advances in Polymer Technology,*16, 263-277, 1997

[76] Hwan-Man, P., Won-Ki Lee, C-Y.P., and Won-Jei Cho, C-S. H., "Environmentally friendly polymer hybrids part I: mechanical, thermal and barrier properties of thermoplastic starch/clay nanocomposites" *Journal of Materials Science*, 38, 909-915, 2003

[77] Yu, L. and Christie, G., "Microstructure and mechanical properties of oriented thermoplastic starches" *Materials Science,*40,111-116,2005

[78] Van Soest, J. J. G. and Essers, P., " Influence of amylose–amylopectin ratio on properties of extruded starch plastic sheets"*Macromolecular Science Pure and Applied Chemistry*, 34, 1665, 1997

[79] Olayide, O. Fabunmi, L. G., Tabil, Jr., Satyanarayan, P., and Peter, R. C., "Developing Biodegradable Plastics from starch" *American society of agricultural and biological engineering*, 2007

[80] Mizukami,H., Takeda, Y., Hizukuri, S., "The structure of the hot-water soluble components in the starch granules of new Japanese rice cultivars." *Carbohydrate Polymers, 38*, 329, 1999

[81] Xie, W., Pan, W. and Chuang, K.,"Thermal characterization of PMR polyimides" *Thermochim. Acta*. 6, 367, 143–153, 2001

[82] Coleman, J., Khan, U. and GunKo, Y., "Mechanical reinforcement of polymers using carbon nanotubes" *Adv. Mater.,*18, 689–706, 2006

[83] Patil, A., Vaia, R. and Dai, L. "Surface modification of aligned carbon nanotube arrays for electron emitting applications" *Synth. Metals*, 154, 229–232, 6, 2005

[84] Schmidt D., Shah, D., and Giannelis, E.,"New advances in polymer/layere silicate nanocomposites" *Curr. Opin.Solid State Mater. Sci.,* 6(3), 205–212, 2002

[85] Okada, A. and Usuki, A., "Twenty years of polymer-clay nanocomposites Macromol*" Mat. Eng.,* 291, 1449–1476, 2006

[86] Powell, C. and Beall, G.,"Physical properties of polymer/clay nanocomposites" *Phy. Prop. Polym.,*6, 561–575, 2006

[87] Podsiadlo, P., Choi, S., Shim,B., Lee, J., Cuddihy, M., Kotov, N. et al., "Molecularly engineered nanocomposites: Layer-by-layer assembly of cellulose nanocrystals" *BioMacromol,* 6 ,2914–2918, 2005

[88] Hussain, F., Hojjati, M., Okamoto, M. and Gorga, R., "Review article: polymer-matrix nanocomposites, processing, manufacturing, and application: an overview" *Compos.Mater.* 6, 40(17), 1511, 2006

[89] Cho, D., Lee, S., Yang, G., Fukushima, H. and Drzal, L., "Dynamic mechanical and thermal properties of phenylethynyl-terminated polyimide composites reinforced with expanded graphite nanoplatelets" *Macromol. Mater. Eng.,* 290(3), 179–187, 2005

[90] Sevostianov, I. and Kachanov, M., "Effect of interphase layers on the overall elastic and conductive properties of matrix composites Applications to nanosize inclusion" *Solids Struct.,* 6, 44(3-4),1304–1315.2007

[91] Iijima, S. et al., " Helical microtubules of graphitic carbon" *Nature,* 6, 354(6348),56–58., 1991

[92] Holt, J., Park, H., Wang, Y., Stadermann, M., Artyukhin, A., Grigoropoulos, C., Noy, A. and Bakajin, O., "Fast mass transport through sub-2-nanometer carbon nanotubes" *Science,* 7, 312, 1034, 2006

[93] Fornasiero, F., Park, H. G., Holt, J. K., Stadermann, M., Grigoropoulos, C. P., Noy, A. and Bakajin, O. "Ion exclusion by sub-2-nm carbon nanotube pores"7, 1–6, 2008

[94] Sherman, L., "Nanocomposites: a little goes a long way" *Plast. Technol.,* 7, 45, 9, 52–54, 1999

[95] Usuki, A., Kojima,Y., Kawasumi, M., Okada, A., Fukushima, Y., Kurauchi, T. and Kamigaito, O., "Synthesis of nylon 6-clay hybrid" *Mater.,*8, 9, 10, 1179–1184, 1993

[96] Usuki, A., Kojima, Y., Kawasumi, M., Okada, A., Fukushima, Y., Kurauchi, T. and Kamigaito, O.X.,"Mechanical properties of nylon 6-clay hybrid" *Mater.* 8(5), 1185–1189, 1993

[97] Giannelis, E., "Polymer Layered Silicate Nanocomposites" *Adv. Mater,* 8, 9, 10, 11, 29–35, 1996

[98] Alexandre, M., and Dubois, P., "Polymer-layered silicate nanocomposites: preparation, properties and uses of a new class of materials" *Br. Mat. Sci. Eng,* 7, 28 , 1–63, 2000

[99] Pinnavaia, T. and Beall, G. "Polymer-clay nanocomposites" *John Wiley & Sons New York.* 7, 2000

[100] Manevitch, O., and Rutledge, G., "Elastic properties of a single lamella of montmorillonite by molecular dynamics simulation" *Phys. Chem. B,* 2, 7, 108, 1428–1435, 2004

CHAPTER THREE

EXPERIMENTAL DETAILS

3.1. EXTRACTION OF STARCH

500 g potato were weighted and cut into very tiny size using commercially available fine vegetable slicer. 1L distilled water was mixed with the paste and stirred properly using glass rod until water color changes to purple. Then, liquid portion of the potato juice was separated with fine mesh and poured into Petri dish for 3 to 4 hours at room temperature. Starch particles were settled down in the petridish. The settled starch particle was washed several times with distilled water and dried at $105^{o}C$ in the oven to remove any available water. The percent of yield of the extracted potato starch is 10 wt%. Schematic diagram of extraction of starch from potato are below.
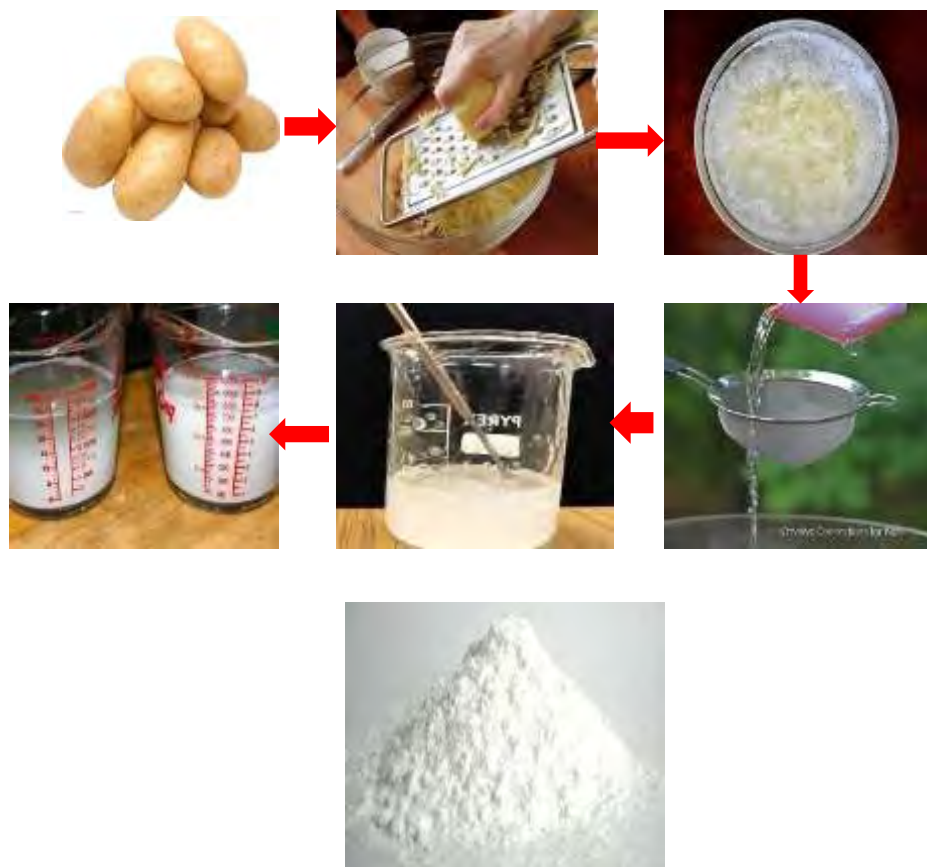

Figure: 3.1. Synthesis process of starch from plant derived source (potato)

3.2 GRAPHENE OXIDE & REDUCED GRAPHENE OXIDE PREPARATION:

Graphene Oxide (GO) will be synthesized by modified Hummer's method. Graphite fine powder, Potassium Permanganate ($KMnO_4$), $NaNO_3$, H_2O_2, H_2SO_4 was used. H_2SO_4 was added to the mixture of Graphite and $NaNO_3$. After cooling it was kept in an ice bath and $KMnO_3$ was added slowly. The mixture was heated and stirred for few hours followed by addition of DI water in an oil bath. H_2O_2 was added slowly followed by continuous stirring. After ultrasonication, GO was heated with Hydrazine Hydrate at 100^0c for 6 hours. Hydrazine Hydrate acted as a reducing agent [101-105].
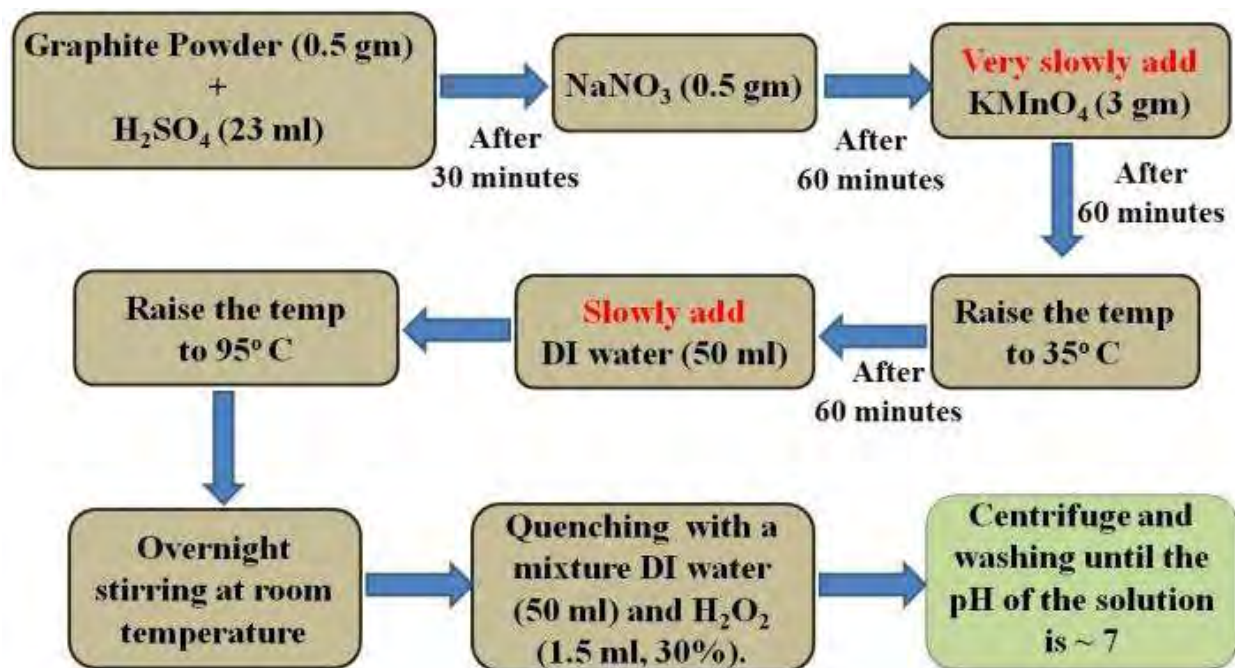

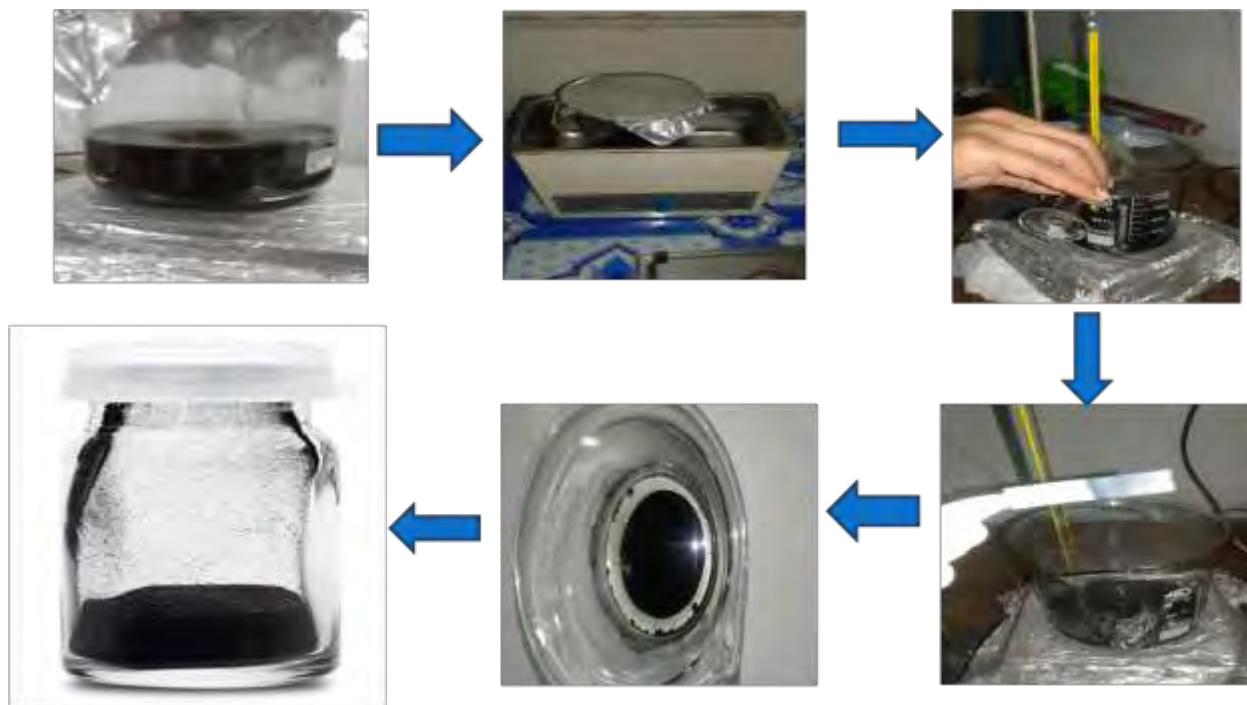Fig.ure 3.2.Synthesis procedure of GO by modified Hammer's method

Figure 3.3. Synthesis procedure of RGO from GO by chemical reduction method

3.3 PREPARATION OF STARCH-PLASTICIZER COMPOSITE FILM

3.3.1 Preparation of starch- glycerin film

800 mg extracted starch powder was dissolved in 13 mL distill water in a vial. 30 wt % glycerin was mixed with water in another vial and was added slowly into the starch solution, while stirring. The mixed solution was heated slowly in a oil bath at 70oC temperature, allowing the gradual evaporation of the solvent. Then the suspension was poured in polyethylene sheet and put into a vacuum oven at 40°C until no weight changes were observed. By maintaining the amount of suspension on the polyethylene sheet, the thickness of the starch/ glycerin film can precisely be controlled.

3.4. PREPARATION OF GO/STARCH AND RGO/STARCH NANOCOMPOSITE:

Starch is made of long chains of glucose joined together. To break down the chains, vinegar will be used. Propan-1, 2, 3-triol (glycerol) will be added to plasticize the starch. GO powder should be sonicated for 10 minutes. Mixture of Starch, vinegar, glycerol and GO will be

heated at 90^0c for 10 minutes. Then the mixture will be poured into a petridish for drying. After drying we will get GO/Starch nanocomposite film. As RGO is not soluble in water, we will disperse it in dimethyl Sulfoxide (DMSO) in an ultrasonic bath for 30 minutes. Then same procedure will be followed for the preparation of RGO/Starch nanocomposite film as GO/Starch nanocomposite‟s preparation [106-110].
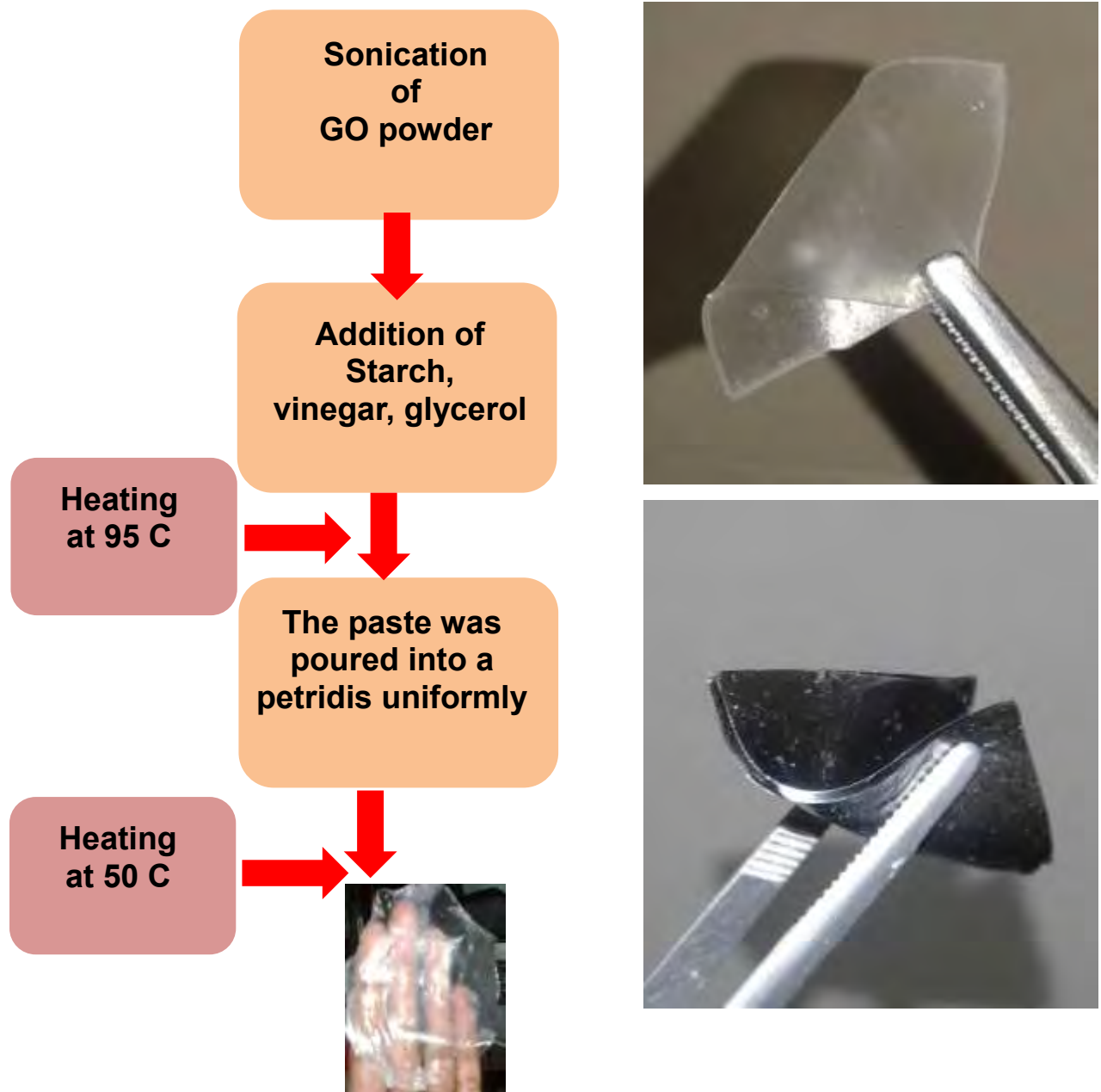
Figure 3.4 Flexible, biodegradable GO/PS and GO/RGO nanocomposite has been synthesized by solution casting process.

3.5. Characterization of GO and RGO

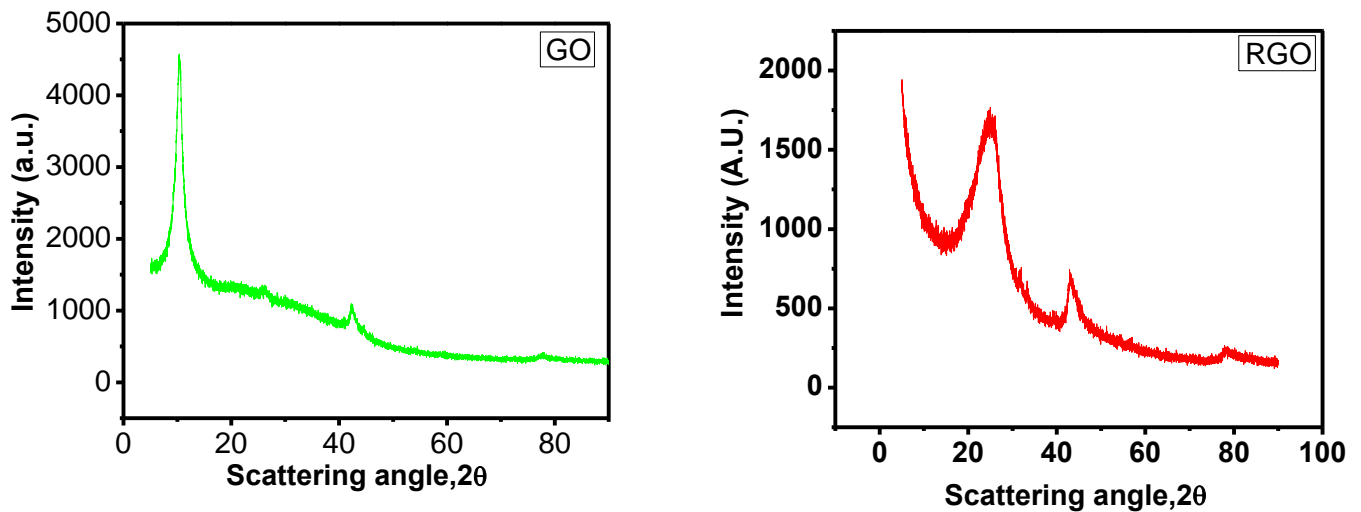## 3.5.1. Structural properties of GO and RGO

Figure 3.5: xrd patterns of GO and RGO

XRD was used to investigate the crystal phase and to determine the interlayer spacing for GO, RGO. Figure 3.5 shows the XRD spectra for the corresponding samples.

For GO, it exhibits only a sharp (001) diffraction peak at $2\theta =10.4^0$, which indicates that the graphite was perfectly oxidized into GO. This increment resulted from the intercalation of oxygen functional groups at the carbon basal plane such as epoxy, hydroxyl, and carboxyl groups during chemical oxidation reaction. Therefore, the distance between consecutive carbon layers increased.

For RGO, the peak located at 10.4° fully vanished, securing the great reduction of GO and the exfoliation of the layered RGO. However, after being chemically reduced to RGO, the (001) peak of GO disappeared and a new broad reflection peak (002) centered at $2\theta = 24.9°$ was observed that indicates the π-conjugated structure of graphene has been recover considerably at the produced RGO. The d-spacing of RGO was reduced, which proved that oxygen-containing functional groups were removed proficiently. It also said that because of having strong vander waals force between the layers RGO sheets were closely oriented. A less intense (001) peak can be seen at $2\theta = 42.60°$, which ascribed by the turbostratic band of messy carbon materials. However, this peak disappeared and a wide peak at 238 appeared which was similar with the typical diffraction peak (002 peak, 24.9) of the graphite when GO was reduced by L-AA. This difference indicated the GO was reduced to graphene successfully with some oxygen groups remained. The diffraction peak at 42.6 was attributed as the (100) plane of the carbon crystals, indicating a short range order in stacked graphene layers.

3.5.2. Chemical properties of GO and RGO

The intense of O-H band present in 3550-3000 cm^{-1} shows strong sign of intermolecular as well as intra- molecular H bonding in GO sheets. Vibrations and deformations of –OH and –COOH show at 3452 cm^{-1}. The experimental peaks of GO ensure the presence of oxygen groups
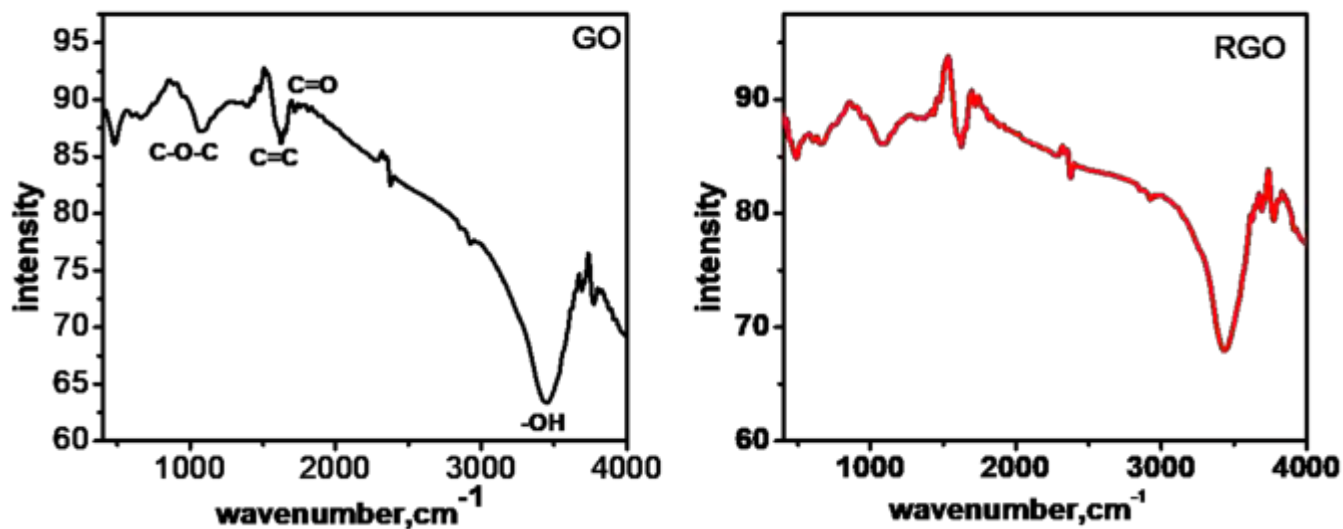

Figure 3.6 FTIR spectra of GO and RGO

in carbon framework, which include the bands at 1066 cm−1 (C−O−C, C−O stretching vibration of epoxide), and 1720 cm−1 (CO, C=O stretching of carbonyl and carboxyl groups located at edges of GO networks. A sharp peak observed at 1625 cm^{-1} is for stretching of C=C band and experimented OH groups at 1384 cm^{-1} indicates the C-O stretching.Sp^2 stretching of C-H band forms a small peak at 2926 cm^{-1}.The peak intensity of the oxygen groups decreased after being reduced and the skeleton vibration absorption peak of graphene appeared at 1475 cm^{-1}, also, the stretching vibration absorption peak of C-H at 2860 cm^{-1}, 2926 cm^{-1} could be seen clearly. These experiments suggested part of the reduction of oxygen functional groups on GO.

REFERENCES

[101] J. Guerrero-Contreras, F. Caballero-Briones / Materials Chemistry and Physics, xxx (2015) 1-12.

[102] S. Alam Bhuyan, N. Uddin „Synthesis of graphene" Int Nano Lett (2016) 6:65–83

[103] V. Singh et al. / Progress in Materials Science 56 (2011) 1178–1271

[104] S. Stankovich et al. / Carbon 45 (2007) 1558–1565

[105] *N.I. Zaaba et al. / Procedia Engineering 184 (2017) 469 – 477*

[106] Wojtoniszak, M., Chen, X. C., & Kalenczuk, R. J. (2012).Synthesis, dispersionand cytocompatibility of graphene oxide and reduced graphene oxide.Colloids and Surfaces B: Biointerfaces, 89, 79–85.

[107] Famá, L. M., Pettarin, V., Goyanes, S. N., & Bernal, C. R. (2011). Starch/multi-walled

carbon nanotubes composites with improved mechanical properties. Carbohydrate Polymers, 83, 1226–1231.

[108] T. Ma et al. / Carbohydrate Polymers *94 (2013) 63– 70*

[109] Zhu, H.; Fang, Z.; Wang, Z.; Dai, J.; Yao, Y.; Shen, F.; Preston, C.; Wu, W.; Peng, P.; Jang, N.; Yu, Q.; Yu, Z.; Hu, L. ACS Nano 2016, 10, 1369.

[110] Teodoro, A. P.; Mali, S.; Romero, N.; de Carvalho, G. M. Carbohydr.Polym. 2015,

CHAPTER FOUR

Results & Discussions

4.1. Characterization of PS/GO nanocomposite

4.1.1. Structural properties analysis

XRD was used to investigate the crystal phase of neat PS and different loadings of PS/GO nanocomposite. Figure 4.1.1 shows the XRD spectrum for PS and PS/GO
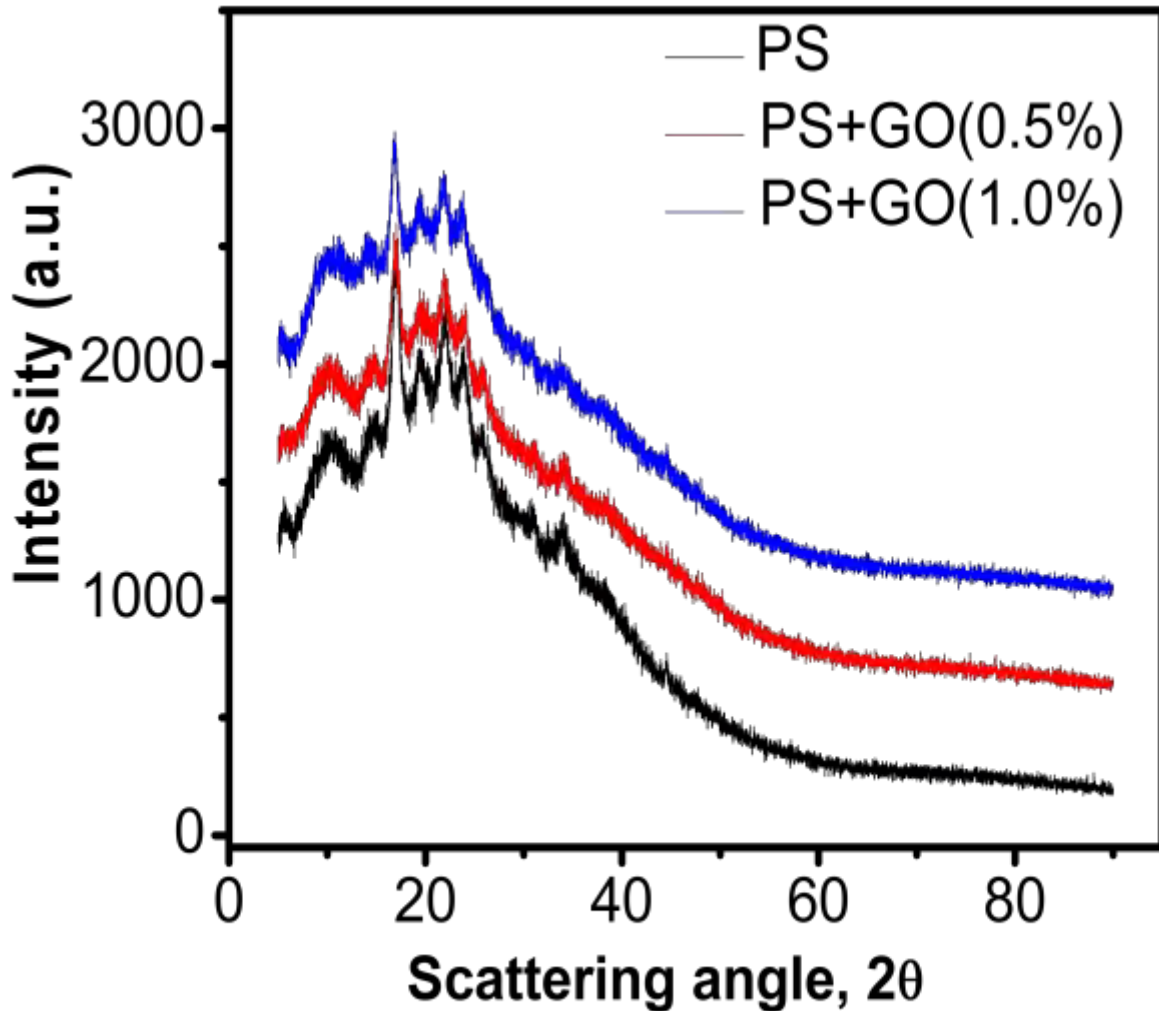

Figure 4. 1.1. XRD patterns of PS and GO/PS nanocomposites

nanocomposite. Much of the information about starch granule crystalline properties has been acquired from X-ray powder diffraction studies. Starch can be classified to A, B and C forms. In the native granular forms, the A form starch is associated mainly with cereal starches, such as maize starch and wheat starch. The X ray patterns of these starches give the stronger diffraction peaks at around 15, 17, 18 and 23°. The B form starch is usually obtained from tuber starches,

such as potato starch and canna starch. The strongest diffraction peak of the X-ray diffraction pattern appeared at 17° 2θ. And there were also a few small peaks at around 2θ values of 20, 22 and 24°. The C pattern starch is a mixture of both A and B types, such as smooth-seeded pea starch and various bean starches. XRD patterns of PS/GO composites appearing almost the same peaks as PS, signifies that PS/GO nanocomposite contain the same crystal type as PS. Additionally, in the XRD pattern of PS/GO nanocomposite the characteristic diffraction peak of GO was disappeared and the intensity of the diffraction peak was decreased [111-113]. This effect shows that GO was uniformly dispersed in PS matrix and the crystalline structure of PS was affected by the incorporation of GO component. Additionally, it is observed that the incorporation of GO (0.5%) upshift the peaks this suggest that a decrease in the *d*-spacing. Whereas for the incorporation of 1.0% GO peaks are downshifted and meaning a reduction in the *d*-spacing.

4.1.2. Structural properties (Fourier transforms infrared spectroscopy)

To investigate the chemical changes that occur in PS after the addition of filler, ATR-FTIR experiments were carried on PS sheets. Analyzing FTIR spectra can identify the interaction of hydrogen bond of starch hydroxyl groups.

Figure 4.1.2 shows the FTIR spectrum for PS and PS/GO nanocomposite. As seen from the
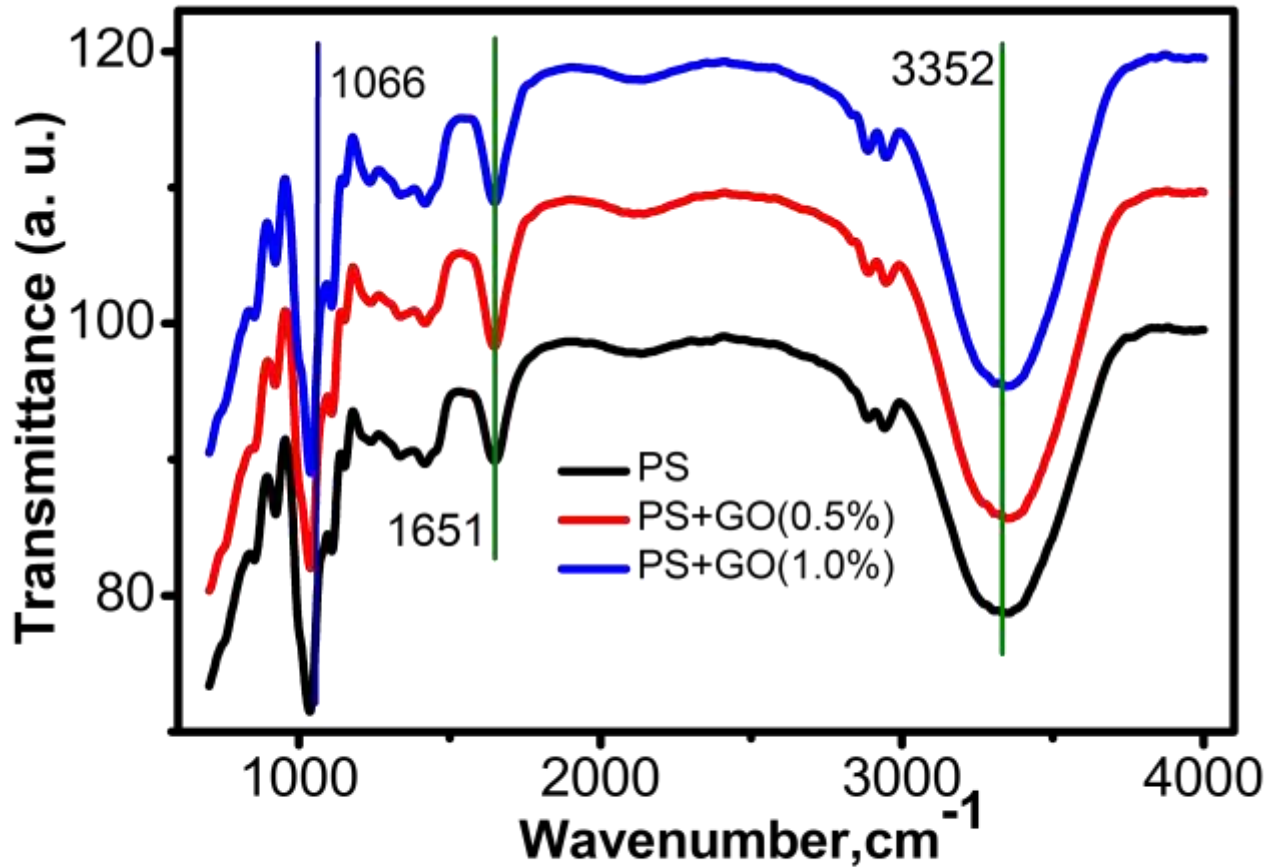

Figure. 4.1.2. FTIR spectra of PS and GO/PS nanocomposites

FTIR spectrum of neat PS nanocomposite, the region at 2950-3450 cm^{-1} refers to hydroxyl groups [114-115]. Stretching and bonding of –OH groups occurred at 3352 cm^{-1} and 1651 cm^{-1} respectively.The presence of CH_2 groups determines the existence of peak at 2941 cm^{-1}. The bands at 1153cm^{-1} and 1109 cm^{-1} were attributed to the stretching vibration of C–O in C–O–H

groups and at 991 cm^{-1} stretching of C-O in C-O-C groups. In the spectrum of the PS/GO nanocomposite the O-H bending has been shifted from 1651 cm^{-1} to 1645 cm^{-1} which indicates formation of hydrogen bonding between GO and PS in the nanocomposite. Similar type of shift towards shorter wavenumbers has also been observed for most of the peak. Additionally, the intensity of the band corresponds to the O-H group (at 3352 cm^{-1}) increases with the incorporation of GO. This suggest that the GO enhance the affinity of water to the surface [116].

4.1.3. Surface morphology analysis

To view the dispersion of GO in the starch and PS/GO nanocomposite, SEM morphology is shown in Fig.4.1.3.The SEM images of the fractured faces of the GO/PS composites are shown in the figure. GO sheets were observed to be uniformly dispersed in the PS matrix. It was
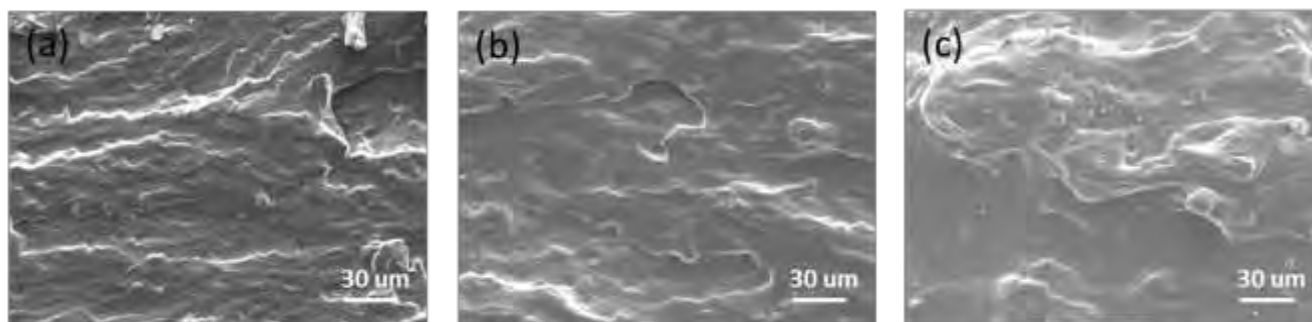

Figure. 4.1.3.FESEM images of the cross-sections of (a) PS, (b) PS/GO 0.5 wt% (c) PS/GO 1 wt%

similar to the earlier report. In addition, GO appeared to be covered by the PS matrix, which was related to stronger interfacial interactions between GO and the matrix. GO sheets with more oxygen-containing groups could form better hydrogen bond interactions with starch. A layered structure caused by the incorporation of GO [Figure b, c] were all clearly observed in the cross section of the films compared with the pure PS film [117].

4.1.4. Optical properties

Figure 4.1.4 shows the ultraviolet–visible absorbance of GO/PS composites with different GO loadings in the wavelength range 200–1100 nm. Fortunately, there was an insignificant disparity in the average thickness of the nanocomposites samples. The absorbance was surprisingly enhanced by the incorporation of GO sheets compared to the absorbance of pure PS. In close proximity to ultraviolet range (200–400 nm) there was very low absorbance in the pure
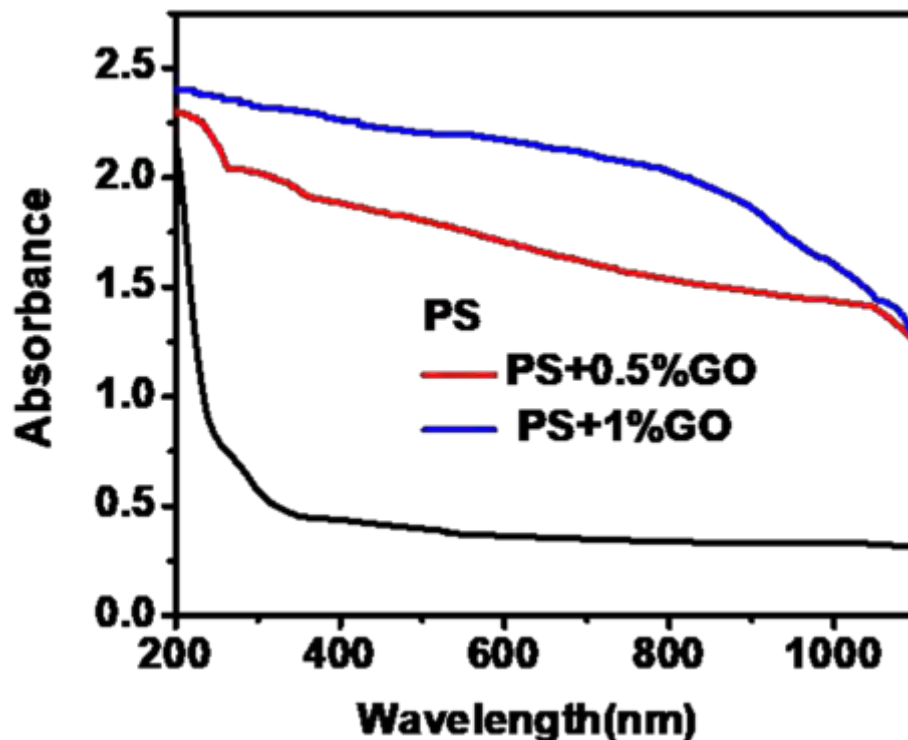

Figure. 4.1. 4. UV-vis absorption spectra of PS and PS/GO nanocomposite

PS. With increasing GO content, the UV absorbance and the intensity of the peaks increased. The absorbance value peaked above 2 for the composites with different loadings of GO, meaning that the transmittance of UV light was very low and most of the UV light was shielded. GO/PS composites could effectively protect against UV light and potentially be useful to UV-shielding materials.

4.1.5. Thermal stability analysis

Thermal analysis was performed to determine the effect of GO on the thermal decomposition behavior of starch. The thermal stability of PS film, GO/PS films were performed by thermo gravimetric analysis (TGA) is presented in Figure 4.1.5.The onset temperatures of PS film, GO/PS (0.5wt%) and GO/PS (1wt%) nanocomposites are 242^0C, 253 ^{0}C, 225^0C
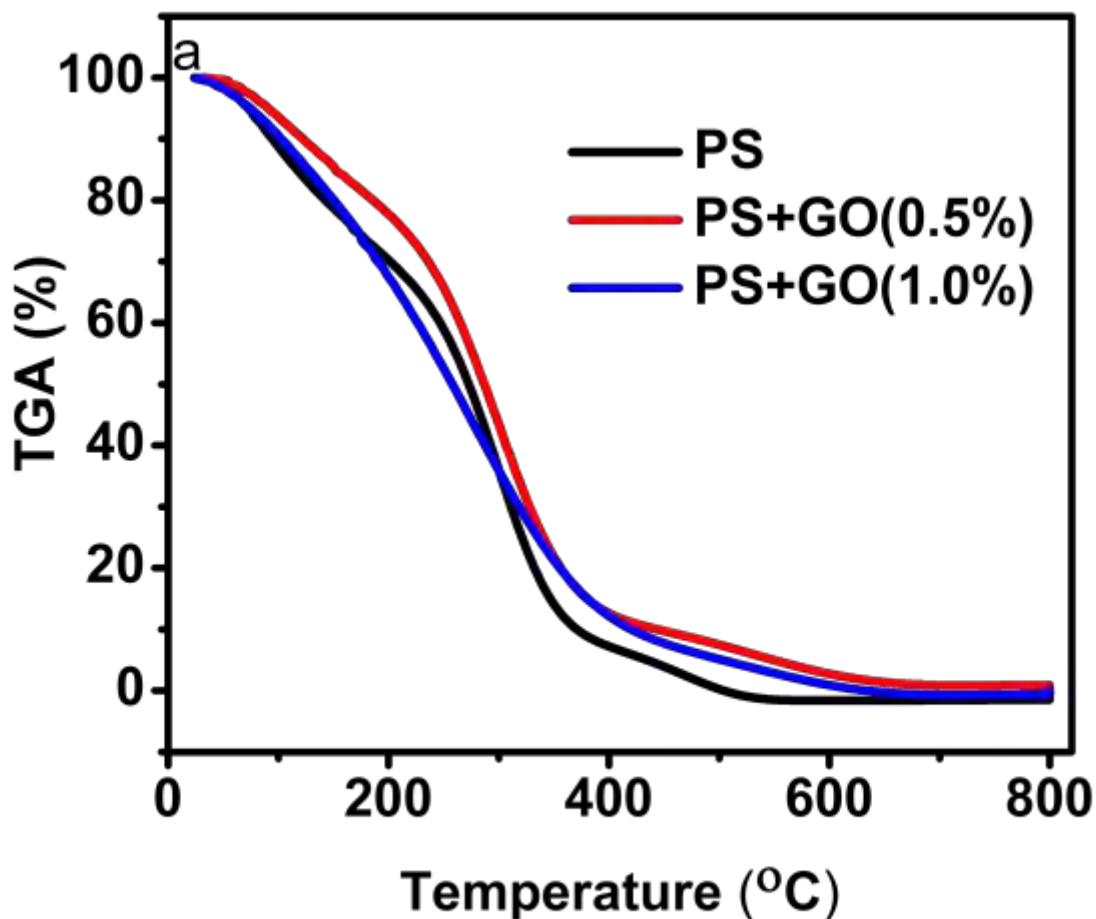

Figure 4.1.5. TGA thermograms of PS and PS/GO nanocomposites

respectively. Onset temperature is the temperature where the first detectable heat is released, obtained by extrapolation of the steepest portion of curve. It could be noted basically two main thermal events. The weight loss before the onset temperature was attributed to volatilization of both of the water absorbed by starch and glycerol plasticizer. The second stage of the weight loss in the temperature range of 220–380 ^{0}C corresponded to decomposition of starch. An

improvement in the thermal stability of the nanocomposite films could be seen with an increase of the fillers loading [118-119].

All experimental results of TGA, which was generally used to assess a material"s lifetime, are listed in the table, such as the initial decomposed temperature (IDT), the integral procedural decomposition temperature (IPDT),The temperature at 50% weight loss (T−50%) and the temperature at the maximum rate of mass loss (Tmax). It could be observed that all PS/GO-n nanocomposite films showed a higher IPDT than neat PS film. These results indicated that the decomposition temperatures of starch increased by the addition of GO. The reason might be that the mobility of PS chains was suppressed by strong hydrogen bonding interactions with GO. Usually, the better the interaction between the filler and the matrix was, the higher the thermal stability of the composites was. However, GO/PS composites containing 1wt% GO thermally degraded at lower temperature than that of 0.5% GO contents indicating that the addition of GO unexpectedly decreased the thermal stability of the composites. The decomposition of oxygen functional groups, which could weaken the interaction between GO filler and PS matrix and simultaneously accelerates the decomposition of starch matrix. In agreement with this result,the addition of GOs also decreased the thermal stability of epoxyresins.

Table 1

Thermal properties of neat PS and PS/GO-n biocomposite films

Sample	IDT (^{0}C)	IPDT(^{0}C)	T-50%(^{0}C)	T_{max}(^{0}C)
PS	242	243	273	380
PS/ GO (0.5%)	253	284	286	380
PS/ GO (1%)	225	264	258	346

4.1.6. Mechanical properties

Incorporating graphene oxide into the polymer matrix improves the polymer''s mechanical properties. The effects of graphene oxide loading on the mechanical properties of
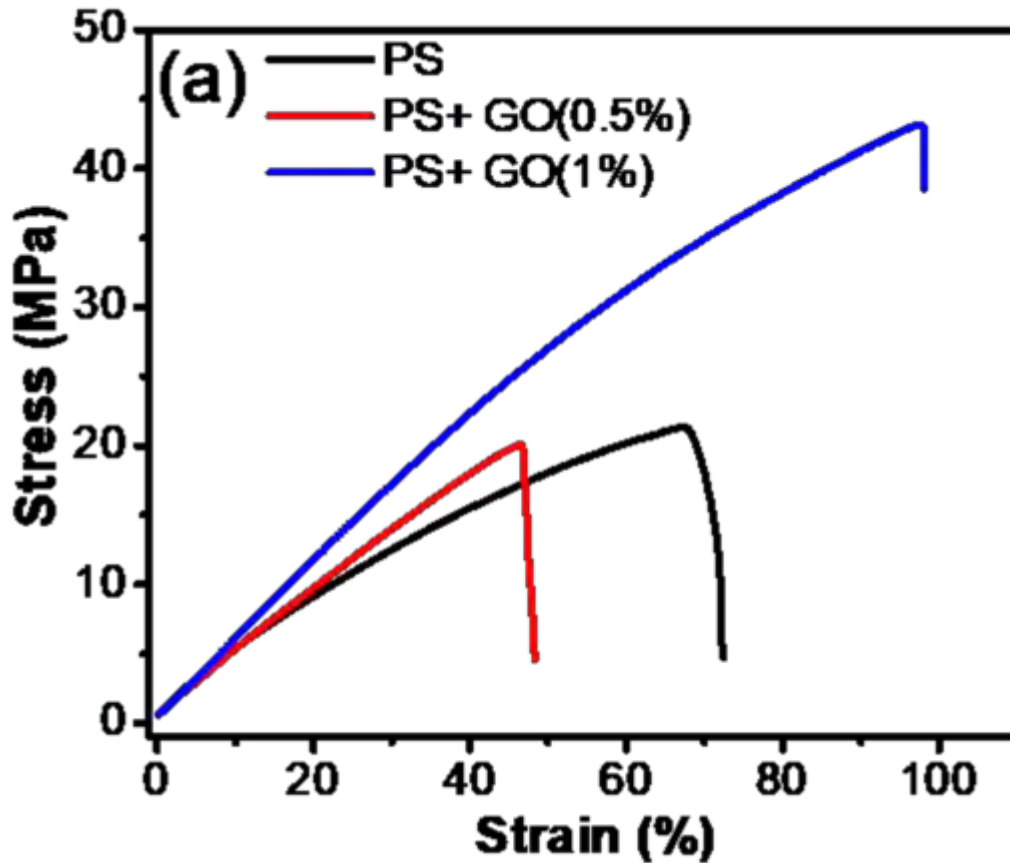

Figure 4.1.6.(a) Stress–strain curves of PS and PS/GO nanocomposites

PS/GO films are illustrated in Figure 4.6. Figure 4.6(a) shows the effects of different GO loading on the tensile properties of the nanocomposites. The tensile strength of pure PS was 20 MPa. The tensile strength reached at 42 MPa from 20 MPa at the increasing loading level of 1 wt% from 0.5% GO. Besides, the elongation at break of the GO/PS composites was increased by almost 100% when the GO loading level increased from 0.5 to 1 wt%.

Figure 4.1.6(b) shows that the young modulus of the PS/GO composites with different GO loading. A 16% increase in the tensile modulus from 40.8 MPa to 47.3MPahas been observed when 0.5wt % GO is added. A further increase in GO (1wt %) concentration resulting in a 40% rise of the tensile modulus.

From figure 4.1.6 films it is observed that the incorporation of GO simultaneously improved the strength and elongation at break of PS GO had and has a reinforcing effect on the PS matrix. This improvement in mechanical properties is related to good interfacial interaction,
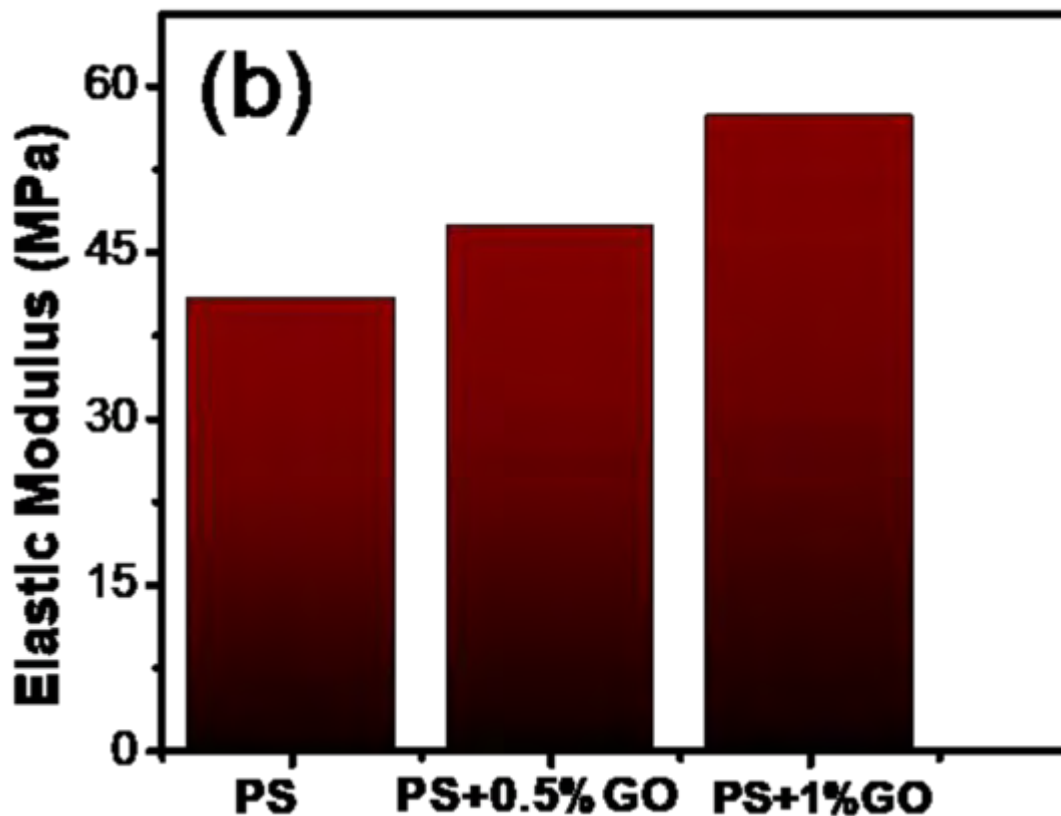

Figure 4.1.6.(b) Young's modulus of PS and PS/GO nanocomposites

which may lead to a higher efficiency of stress transfer from the PS matrix to the GO fillers [120-121].

The improvement in the mechanical properties confirm the good dispersion GO within the starch matrix resulting the strong interfacial interactions between GO and PS matrix. In consequence, when the biocomposites were under tensile stress, the fillers were difficult to disconnect from the

matrix and could resist and transfer the imposed force, leading to weaken the loading stresses of starch matrix. The abundant oxygen containing groups of GO formed hydrogen-bonding interactions with the hydroxyl groups of starch resulting in improved tensile properties.

4.1.7. Dielectric properties

Dielectric materials with high ε are viable in the field of electrical and electronic engineering. In the present study, dielectric constant (ε) of the GO filled starch nanocomposites
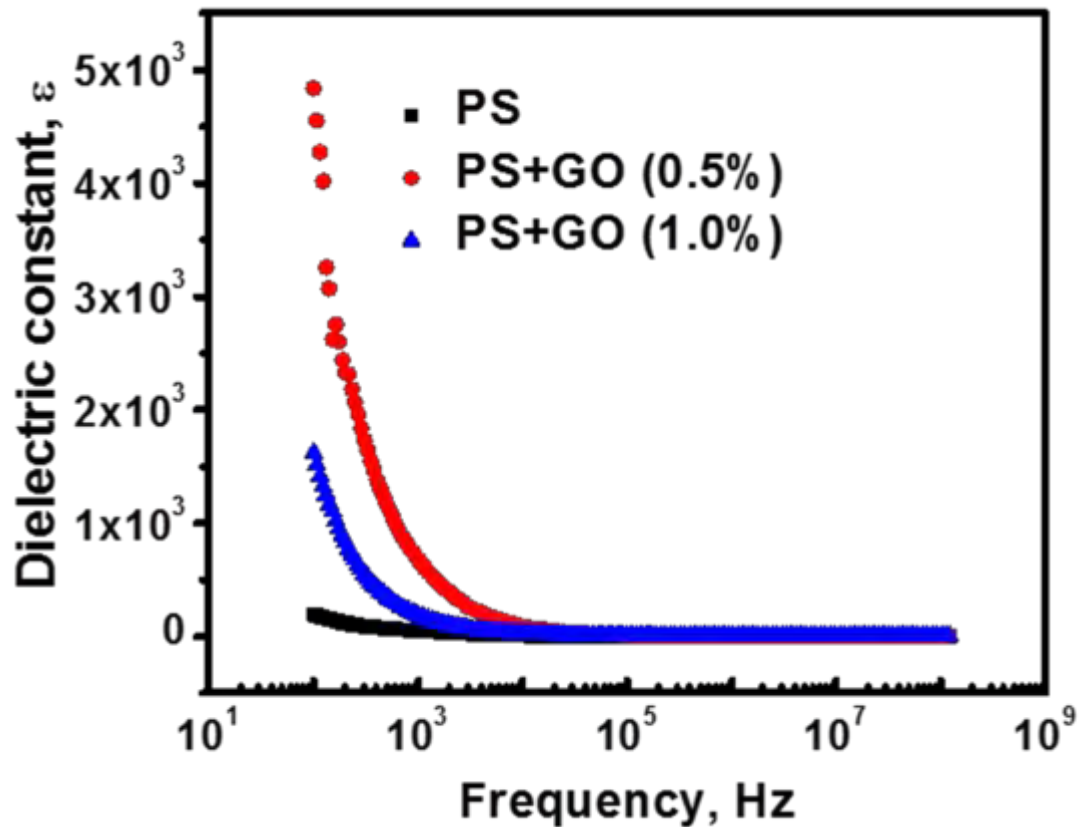

Figure 4.1.7 (a) Dielectric constant of PS/GO nanocomposite

showed interesting electrical properties, when compared to the pure matrix. Dielectric constant was calculated using the following formula, $C = \varepsilon_r \varepsilon_0 A / d$ Where d is the thickness of the sample, A is the area; C is the parallel capacitance value, ε_0 is a constant.

Figure 4.1.7(a) shows the dielectric constant of PS and PS/GO nanocomposite with different loadings at room temperature over the frequency range of 10^2 to 10^8 Hz. At frequency 100 Hz pure PS samples shows a dielectric constant about 100 but incorporation of 0.5% GO it enhances at large scale which is 50 times to the pure samples. But for 1% loadings dielectric constant is shown to be decreased to 1600.

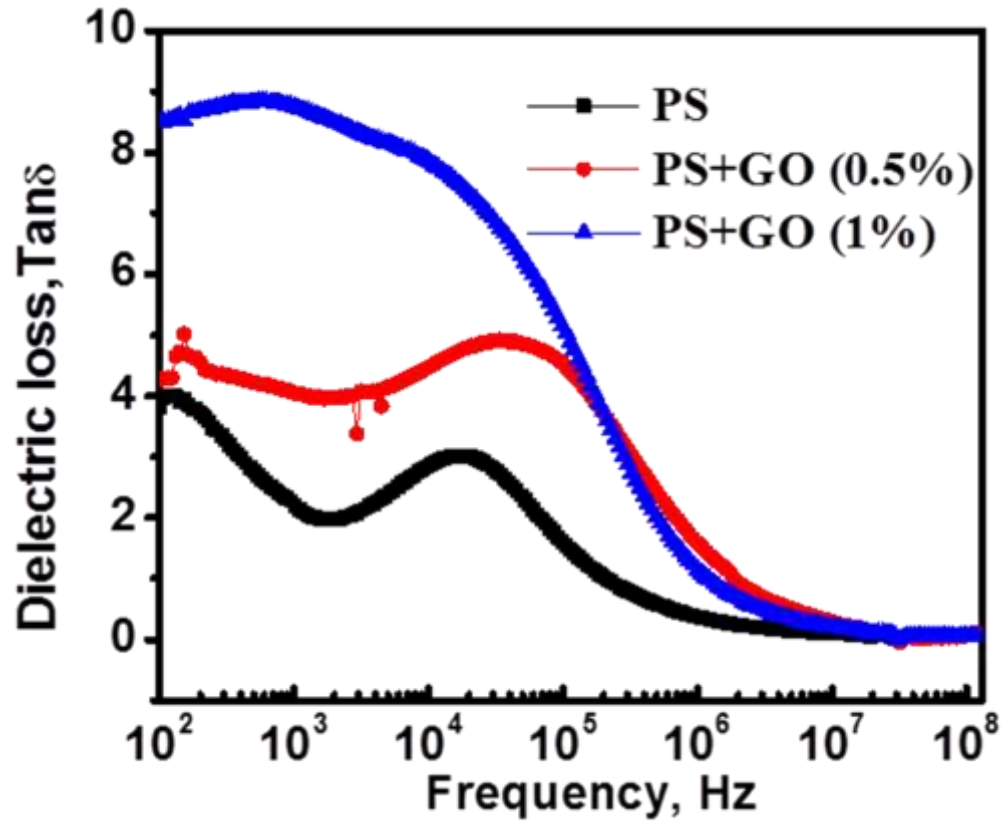From the Figures, we observed the loading of GO have significant effect on the

Figure 4.1.7 (b) Dielectric loss of PS/GO nanocomposite

improvement of the dielectric property. It was found that both ε and tan δ were influenced by frequency. GO loaded samples (0.5 and 1wt%) shows increment in the dielectric constant value at the low frequency region 100 Hz. The increase in the dielectric constant of the composite with the GO is attributed to interfacial polarization occurring at the interface between the PS and GO [122-123].In the present study, we observed interfacial and space charge polarization in the GO loaded matrix. GO contains polar functional groups, like –OH, –CHO,–CO, and –COOH, which

ensures good bonding and appropriate local electrical contacts that may lead to a strong interfacial polarization and play a role in enhancing dielectric constant, whereas, this polarization in the pure sample may be due to the immiscible phase of the polymer matrix. The spatial polarization arising from the trap states results an accumulation of charge carriers and leading to an increase of the value of dielectric constant. This interfacial polarization, also known as the Maxwell-Wagnar effect, is responsible for the enhancement of dielectric constant observed at low frequency. When an electric field is applied to the composite film, charge carriers originating from the external electrode migrate and accumulate at the interface due to the
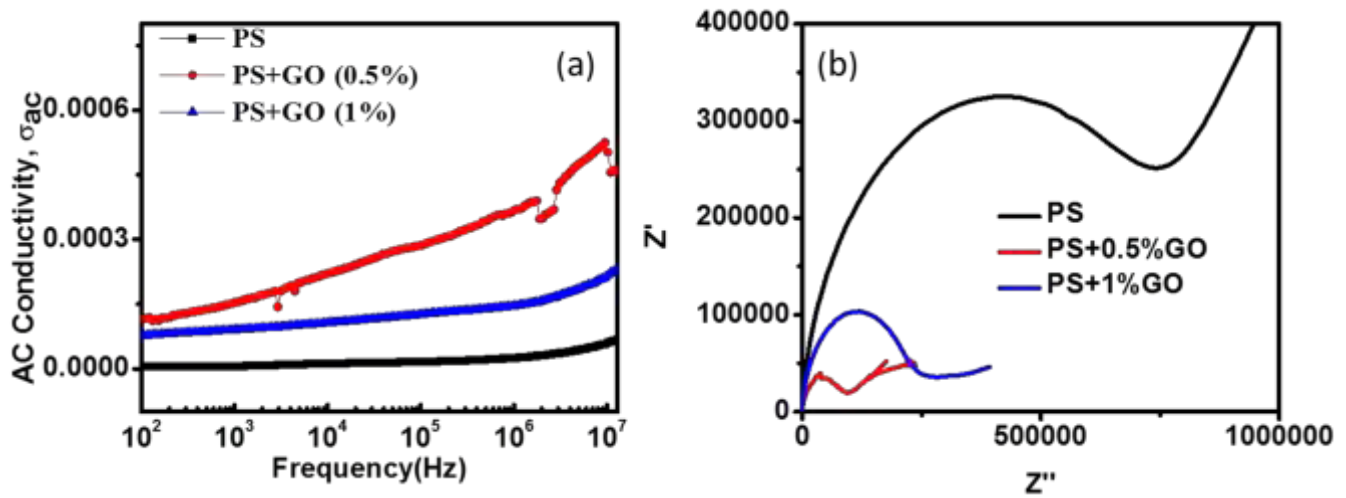

Figure 4.8 (a)AC conductivity (b) cole-cole plot of PS/GO nanocomposite

difference in relaxation time between the two components. The accumulated charge carriers can induce a polarization, ultimately resulting in an increased dielectric constant. Besides these factors, defects also play an important role; there are numerous lattice and/or topological defects and interfaces, which can bring changes in positive and negative space charge distributions, creating conditions for the formation of numerous dipole moments which enhance dielectric constant. The decrease in dielectric constant occurs because of the presence of higher loadings of GO, which have greater surface area and electrical resistance [124-125].

Dielectric constant decreased with increasing frequency at all wt%. In the higher frequency region, a gradual decrease in dielectric constant was noticed. The overall decrease in the value of dielectric constant of the composite with increase of frequency could be due to the induced polarization process, which essentially does not follow the changes in ac frequency rapidly and causes to decrease its value gradually with increase of frequency. The occurrence of the polarization process in composite may be due to the existence of a large number of trap states at the grain boundaries of the synthesized samples. These trap states are generated due to the presence of defects/vacancies such as, oxygen vacancies, dangling bonds, micro porosities etc. These trap states can induce charges with different time constants. At higher frequencies, the induced charges can no longer be able to rotate with a sufficient speed and, therefore, their frequency lags behind the applied ac signal, resulting decrease in the value of dielectric constant.

Figure 4.1.**7** (b) shows the dielectric loss of the composites. 1wt%GO loadings in starch shows a dissipation factor of 9 from lower frequency to 10^5 Hz then decrease exponentially at higher frequencies and for 0.5% loadings dissipation factor remains constant at 5 from 10^2-10^5 Hz and then decrease exponentially.

Dielectric losses are caused by Maxwell-Wagner polarization, ionic conduction, dipole, electronic, and atomic mechanisms. The dielectric loss consists of two parts: One is due to Debye-type relaxation, and the other originates from the leakage current that happens near percolation. The leakage current usually leads to a large loss factor given their small percolation threshold.

However, it should be noted that tan δ of composites with0.5wt% of GO was slightly higher than that of the others at the frequency range of 10^5 Hz. This is reasonable because the highly ordered layered structure of the composite was corrupted. For all the samples dielectric loss became minimum at 10 MHz. The increase in dissipation factor for PS/GO (1%) may be due to starch implicates a percolation network with GO aggregation, which causes a marked increase of leakage currents and in turn to a dielectric loss in the system. Also, the values of dielectric loss are high at lower frequencies as compared to higher frequencies. It is mainly due to interfacial polarization relaxation in the composites. On the other hand, dispersion of GO in PS matrix also significantly influences the dielectric properties. Good dispersity of GO leads to higher dielectric

constant and lower dielectric loss. As a result, both the dielectric constant and dielectric loss of GO/PS composite are higher than that of neat PS.

4.1.8. Electrochemical properties

To explore the effect of GO on the capacitative behavior of the nanocomposite cyclic voltagrams (CV) were recorded. To assess the power capability of the nanocomposite CV measurements were performed at different sweep rates of $5mVs^{-1}$, $10mVs^{-1}$, $20mVs^{-1}$,$30mVs^{-1}$,$50mVs^{-1}$ and $80 mVs^{-1}$using 0.1 M KCL as the electrolyte in a potential window of 1V. In all cases the area of the CV curve increases with the scan rate [126-127].

For all scan rates the CV curves for PS exhibit nearly rectangle cyclic voltammogram whereas a distorted rectangular shape is observed for the GO and PS/GO composite. Such deviation can be attributed to the pseudocapacitance originating from oxygen groups on the surface of the GO and presence of uncompensated resistance due to the GO flake in the system. Additionally, the cyclic voltammograms for GO, and GO/PS composite exhibit a sharp rise in current at low voltage which drops sharply at the vertex potential indicating the good electrochemical stability of the electrode material. Figure 4. 9 shows the CV measurements for PS, GO, PS+0.5% GO and PS+1%GO at a scan rate of $20 mVs^{-1}$.Notably, the quasi-rectangle area of CV curves of PS /GO was larger than that of pure PS and GO, which indicated that GO-PS composites exhibited better capacitance performance. This result implied that GO played key roles in speeding up carriers" transportation along the PS networking chains. Figure 4.11 shows the galvanostatic charge-discharge (GCD) curves of PS and PS/GO nanocomposite at a constant current density of $0.1mA/cm^2$.Thedischarge time of PS/5%GO composite based device was 7000 s which is much longer compared to PS and PS+1%GO nanpcomposite.

The charge/discharge plots of PS/GO (0.5%) and PS/GO (1.0%)   nanocomposites at different current densities are studied. It was observed that the charging/discharging curve
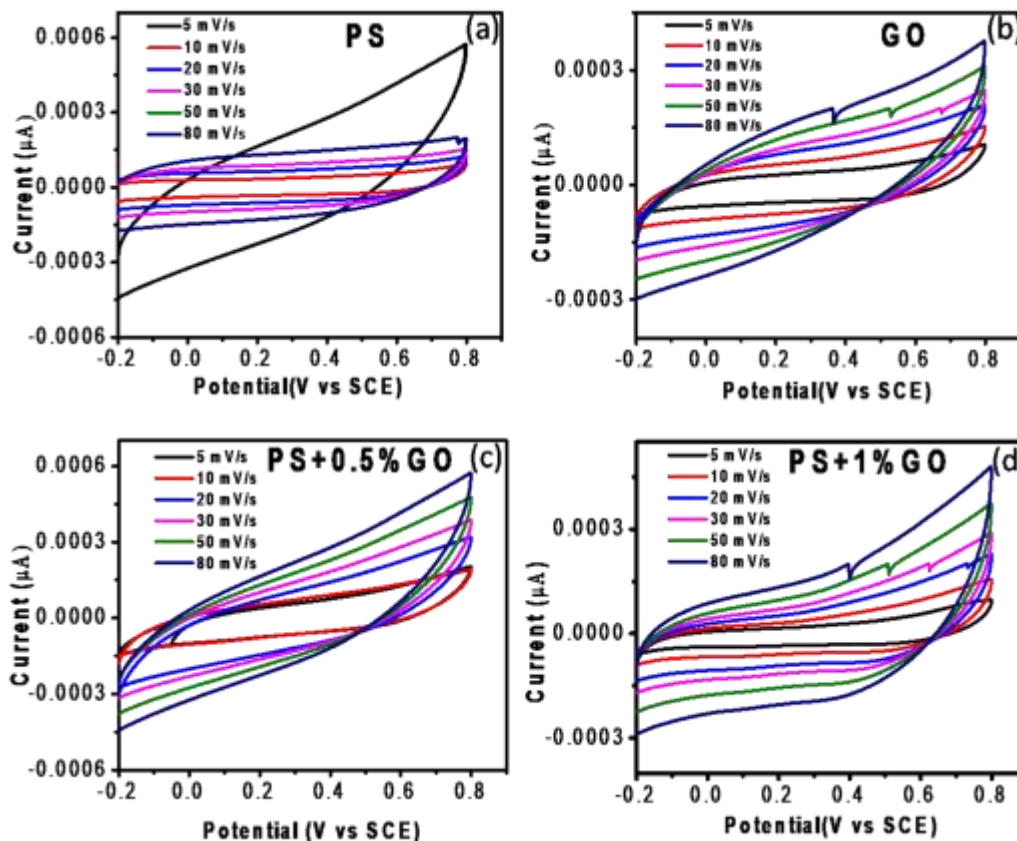

Figure 4.9. CV curves PS, GO and GO/PS at various scan rate

significantly depends on the current densities and the charging/discharging time decreases with the increase of current density. This suggest that, at low current density the ions diffuse through the materials whereas at higher current density the movement of the ions through the composite are hindered.
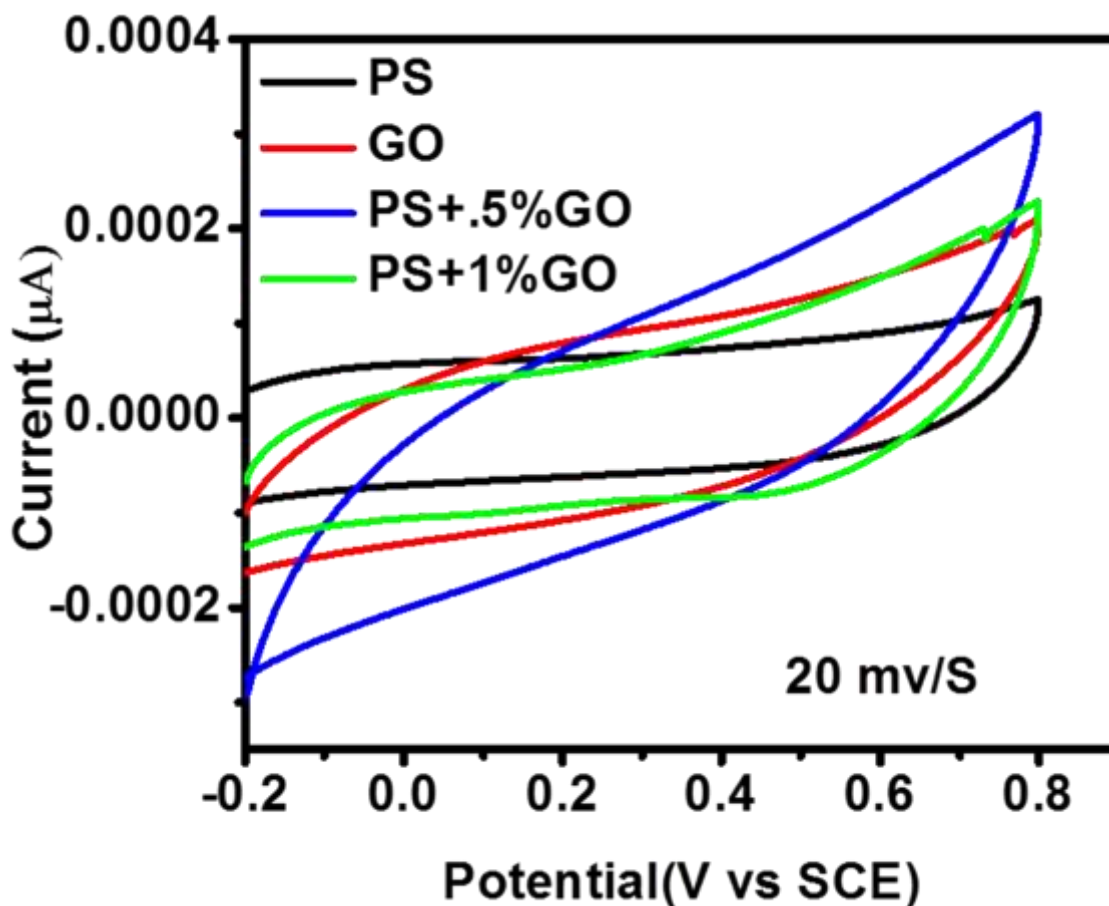
Figure 4.10. CV curves of PS, GO and GO/PS electrodes at 20 mv/S

The specific capacitances of the different nanocomposites were estimated from their respective GCD curve using the formula $C_s = I\Delta t/m\Delta V$. Where, I, t, V, and m are the constant current (A), discharge time (s), total potential deviation (V) and the mass of the active materials within the electrode (g), respectively. The first discharge specific capacitances of PS, GO, PS+0.5%GO,PS+1%GO composite electrodes were found to be 2.4F/g, 10.83F/g, 116.25F/g and 76.15F/g respectively.

The discharging curve PS/GO (0.5%) showed two voltage range. A short discharge occurred between 0.8 V to 0.4V due to the electric double layer capacitance originating from the
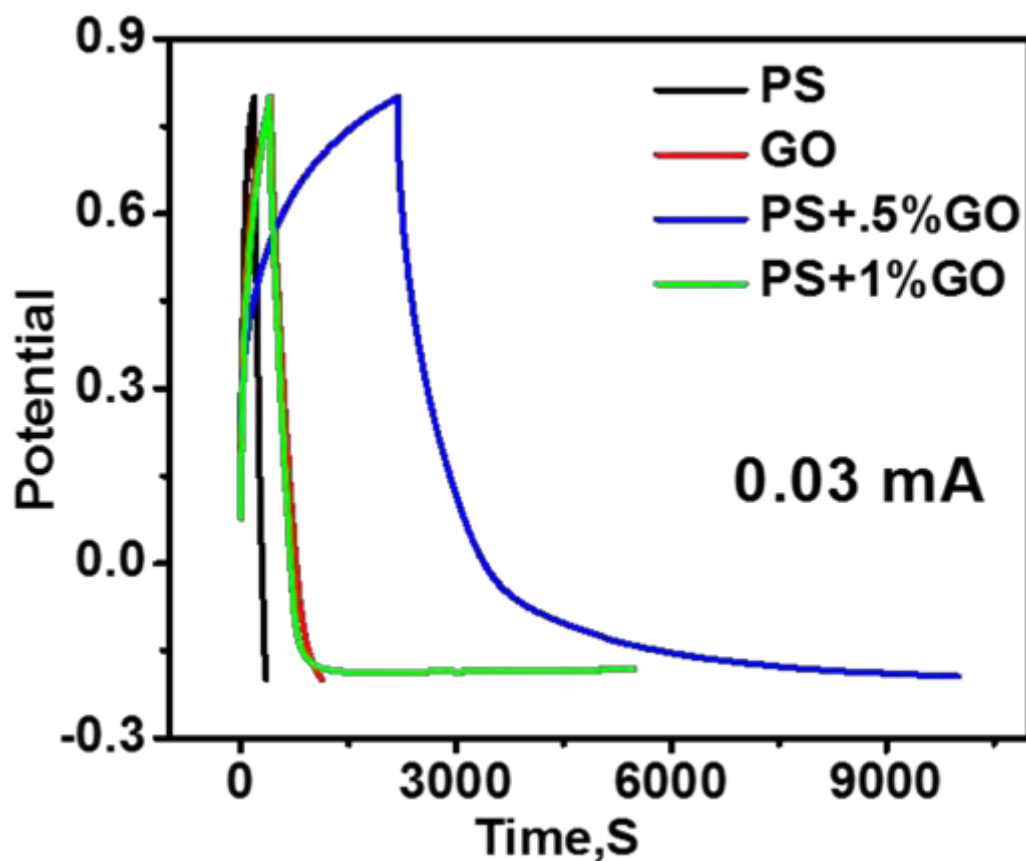

Figure 4.11.Galvanostatic charge-discharge curves of PS, GO and GO/PS electrodes at 0.1 mA /cm^2

charge separation at electrode-electrolyte interface. A longer discharge occurred between 0.4V to -0.2V which may be attributed to the combined effect of electric double-layer capacitance and Faradaic capacitance [128-129].However, the sharp IR drop at the initial discharge can roughly reflect the internal resistance of the electrode. The IR drop of PS+0.5%GO was much lower than that of the others. This result reflected that the internal resistances of the PS+0.5%GO was much lower than that of the others. Low internal resistance is of great importance in energy storing devices; for less energy will be wasted to produce unwanted heat during charging-discharging processes. Thus, PS+0.5%GO was more suitable for fabricating and power-saving supercapacitors. All the specific capacitance data of these composites at different current densities are summarized in Table 1. It can be observed that the capacitance of PS+0.5%GO was

always higher than that of pure PS, GO in all current densities. The specific capacitance of PS+0.5%GO was 116.25 F/g at a discharge current of 0.1mA/cm^2 and was still kept soar at 9.5 F/g even at a discharge current density of 0.35mA/cm^2.Meanwhile, PS+1%GO has slightly lower specific capacitances at all current densities compared toPS+0.5%GO but higher than that of pure PS, which is consistent with the CV curves discussed above. This result is also consistent to dielelectric constant, discussed previously [130-132].

Table 2:

SAMPLES	0.1 mA/cm^2	0.18 mA/cm^2	0.35 mA/cm^2
PS	2.4	1.9	1.4
GO	10.83	7.1	4.5
PS+0.5%GO	116.25	28.8	9.5
PS+1%GO	76.15	6.125	3.35

These data suggest that the significantly enhanced specific capacitances of PS/GO nanocomposite originating from the synergistic effect of PS and GO. Such an enhancement in the capacitance can be attributed to a number of factors. GO with higher specific surface area increases the effective interfacial area between the nanocomposite and electrolyte whereas the layered structure of GO reduces the diffusion length of the electrolyte ions. This improves the specific capacitance by increasing the electroactive region. Additionally, due to the hydrophilicity nature of GO the ions can easily move to the electrode/electrolyte interface for PS/GO nanocomposite resulting in increased action site and high specific capacitance. However, agglomeration in of GO sheets may occur when the GO contents are increased, this can reduce the accessible surface area accessible for ion exchange leading to a decreased specific capacitance. Also the XRD results suggest that the interlayer spacing increases with the increase of GO content which is also responsible for the decrement of the specific capacitance for higher GO content.

4.2 Characterization of PS/RGO nanocomposite

4.2.1. Structural properties analysis

XRD was used to investigate the crystal phase of neat PS and different loadings of PS/GO nanocomposite. Figure 4.2.1 shows the XRD spectrum for PS and PS/RGO nanocomposite. XRD patterns of PS/RGO composites appearing almost the same peaks as PS/GO, signifies that PS/RGO nanocomposite contain the same crystal type as PS/GO. The recrystalisation of amylose in starch during plasticizing process is due to the lysophosholipids forming complexes with ingredients such as glycerol. Dehydration of the amylose leads to recrystallization which forms a single helix crystal and results in a stronger but more brittle
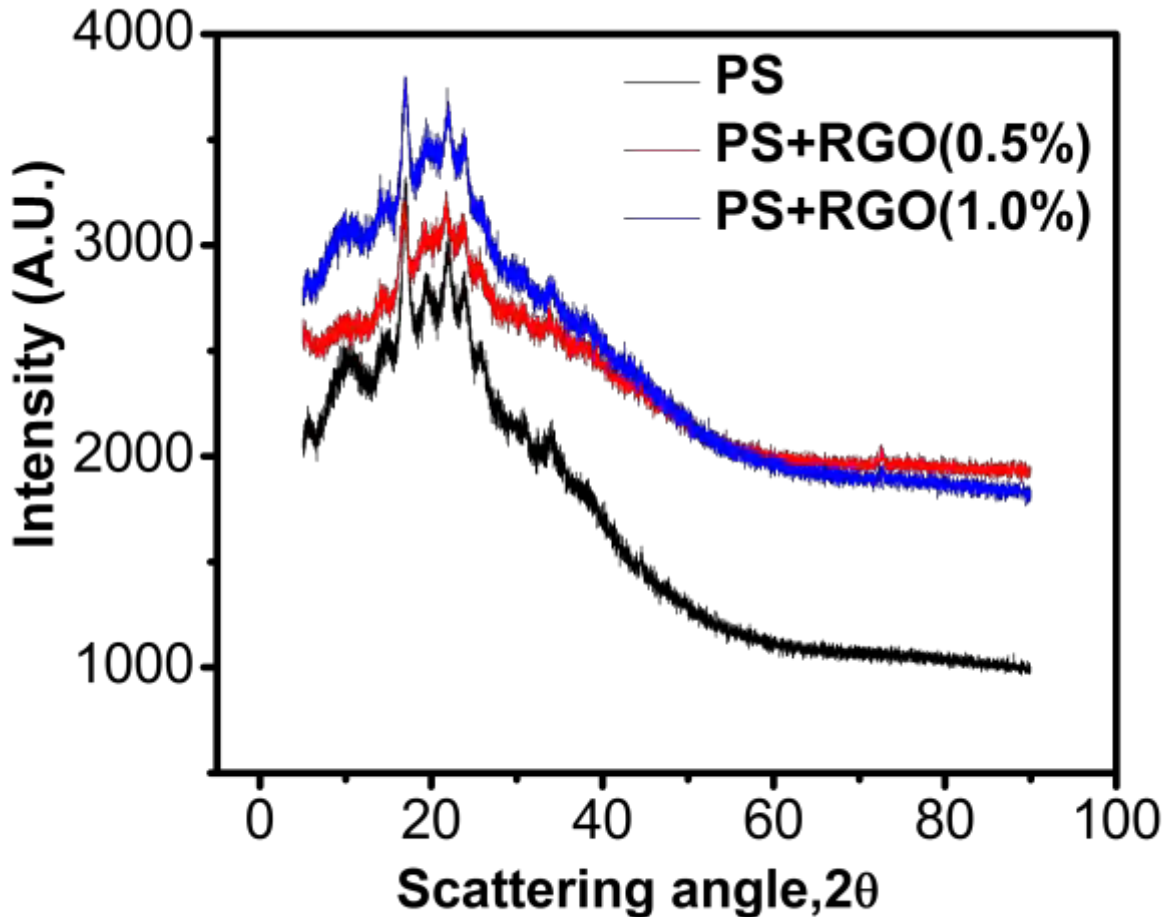

Figure.4.2. 1. XRD patterns of PS and RGO/PS nanocomposites

material. Gelation of starch occurs by disrupting the crystalline structure freeing the starch

helices, producing amorphous thermoplastic starch. Heating the mixture of starch and the plasticizer is important to make the starch granules swell and amylose disperses out of the starch granules, while amylopectin is held in. Thus the gelation breaks down starch-starch –OH bonds and forms new interactions between starch and the plasticizer. For gelation, the small size of RGO smoothly stack into starch chains and formed hydrogen bonding with PS, which limited the mobility of polymer chains and led to a significant slowing down of the re-crystallization of PS. In addition, the typical peak of RGO completely disappears in the composites, which may be covered by the diffraction peaks of Starch.

4.2.2. Structural properties (Fourier transforms infrared spectroscopy)
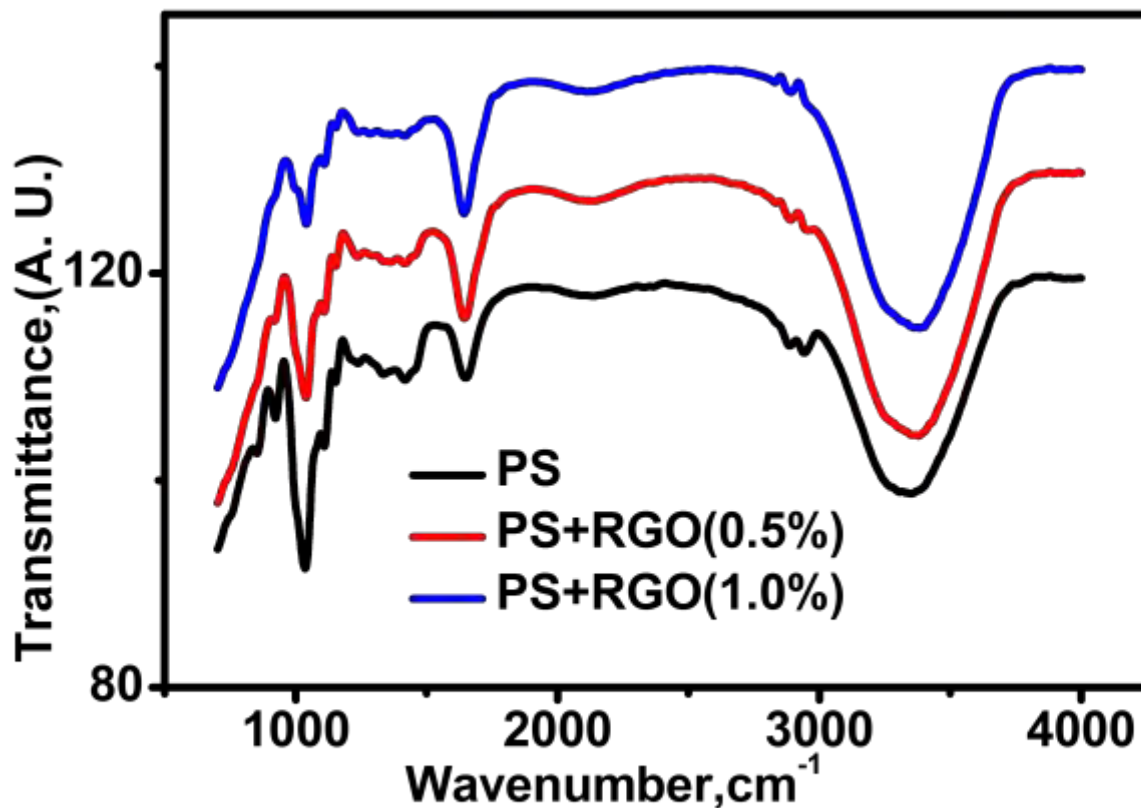

Figure 4.2.2. FTIR spectra of PS and RGO/PS nanocomposites

To investigate the chemical changes that occur in PS after the addition of filler, ATR-FTIR experiments were carried on PS sheets. Analyzing FTIR spectra can identify the interaction of hydrogen bond of starch hydroxyl groups. Figure 4.2.2 shows the FTIR spectrum for PS and PS/GO nanocomposite. As seen from the FTIR spectrum of neat PS nanocomposite, the region at 2950-3450 cm^{-1} refers to hydroxyl groups. Stretching and bonding of –OH groups occurred at 3352 cm^{-1} and 1651 cm^{-1} respectively.The presence of CH_2 groups determines the existence of peak at 2941 cm^{-1}. The bands at 1153 cm^{-1} and 1109 cm^{-1} were attributed to the stretching vibration of C–O in C–O–H groups and at 991 cm^{-1} stretching of C-O in C-O-C groups. In the spectrum of the PS/GO nanocomposite the O-H bending has been shifted from 1651 cm^{-1} to 1645

cm^{-1} which indicates formation of hydrogen bonding between GO and PS in the nanocomposite. When GO reduced to RGO, the oxygen containing groups are removed mostly. In the presence of starch, parts of carbon bonds kept and removed oxygen groups were replaced with oxygen atoms of hydroxyl groups. The more C-O-C bands at the region 1200-1500cm^{-1} in RGO/PS than PS indicated the formation of C-O-C bonds in RGO/PS films.

4.2.3 Surface morphology analysis

The SEM images of the fractured faces of the RGO/PS composites are shown in Fig 4.2.3.RGO sheets were observed to be uniformly dispersed in the PS matrix in the figure. RGO appeared to be covered by the PS matrix, which was related to stronger interfacial Interactions between RGO and the matrix. A layered structure caused by the incorporation of RGO was clearly observed in the cross section of the films compared with the pure PS film.PS/RGO nanocomposite films, a 3D network structure with a few folds is presented. It is clear that the RGO nanosheets are homogeneously coated by starch, indicating that PS was successfully polymerized on the surfaces of RGO nanosheets to form sandwich-like structures. The cross-section of PS/RGO nanocomposite film presents a layer-by-layer formation, which is probably caused by the flow-assembly effect of RGO sheets.
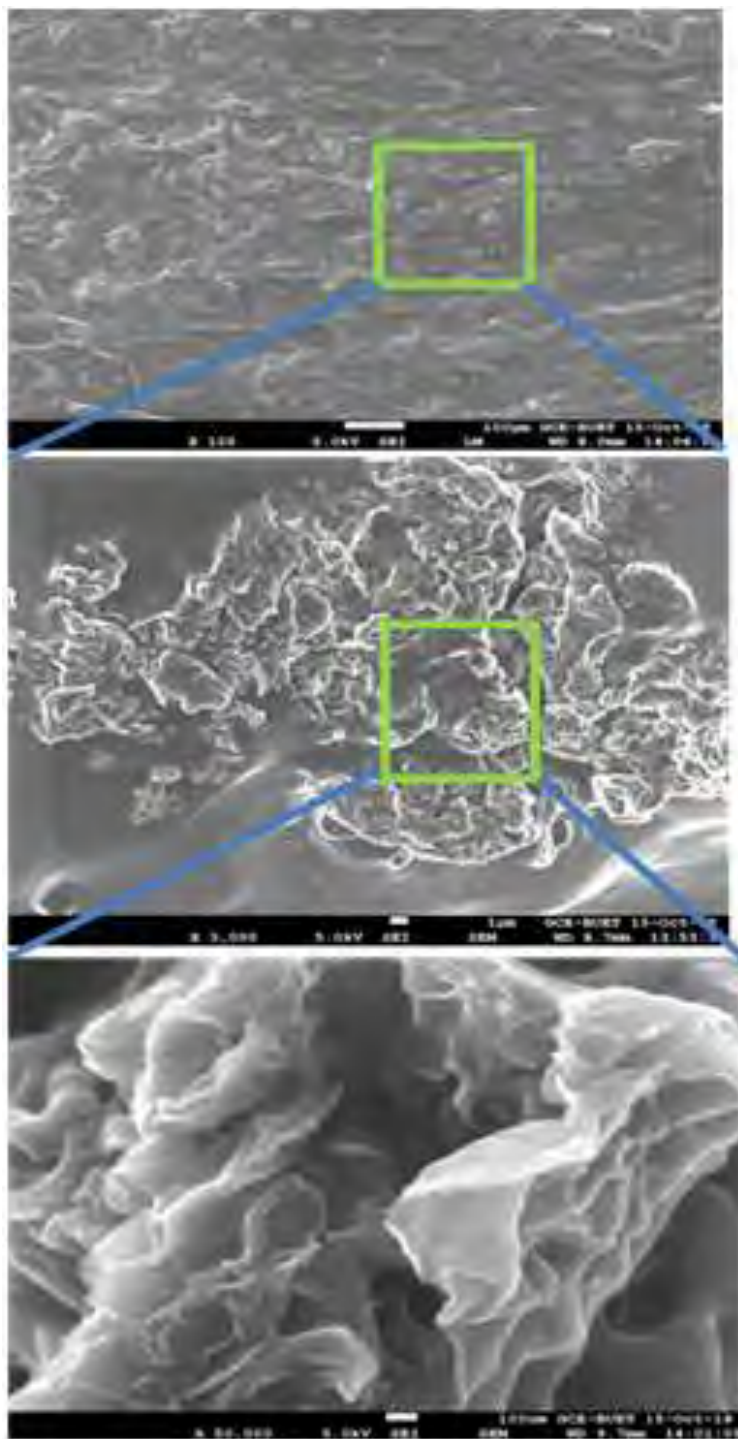
Figure 4.2.3. FESEM spectra of PS and RGO/PS nanocomposites

4.2.4. Optical properties

Figure 4.2.4 shows the ultraviolet–visible absorbance of RGO/PS composites with different GO loadingsin the wavelength range 200–1100 nm. Fortunately, there was an insignificant disparity in the average thickness of the nanocomposites samples. The absorbance
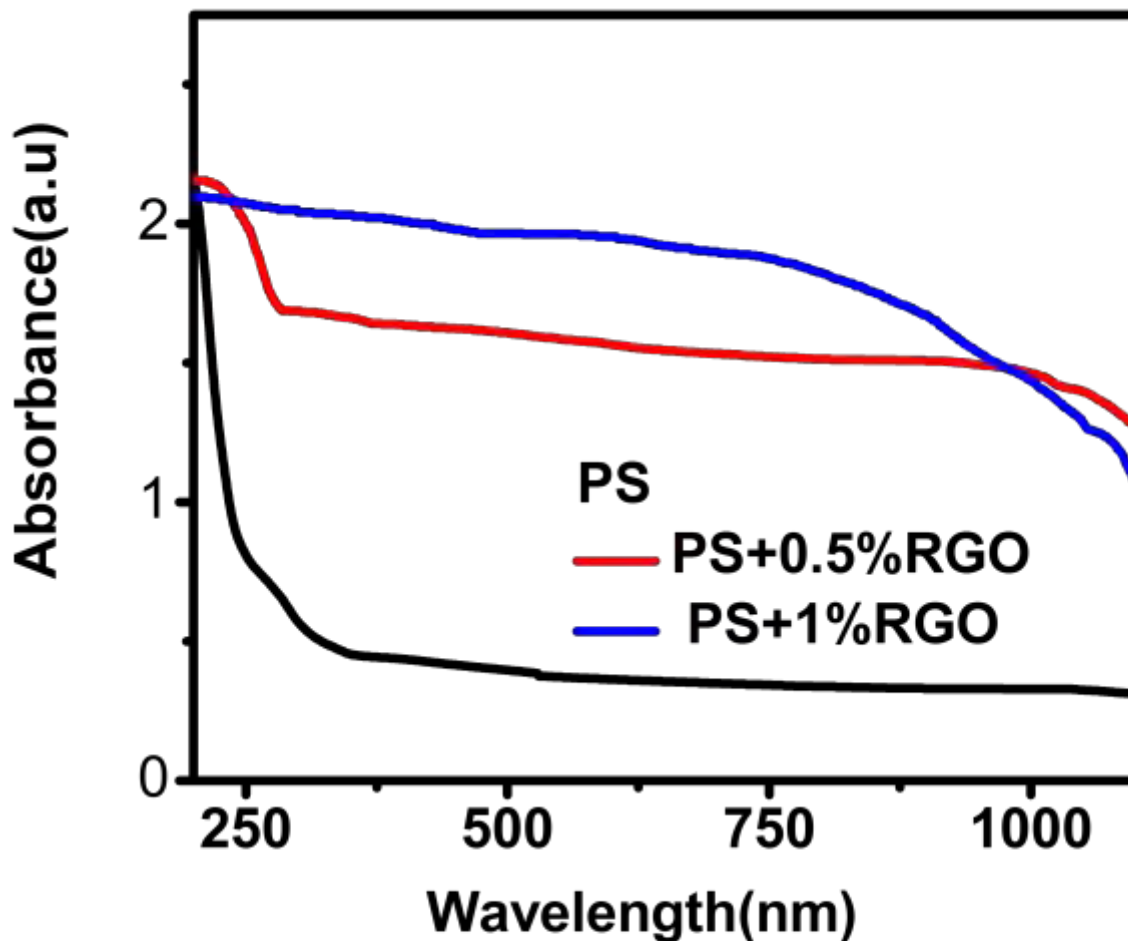

Figure 4.2..4. uv-vis spectra of PS/RGO nanocomposite

was surprisingly enhanced by the incorporation of RGO sheets compared to the absorbance of pure PS. In close proximity to ultraviolet range (200–400 nm) there was very low absorbance in the pure PS. With increasing RGO content, the UV absorbance and the intensity of the peaks

increased. The absorbance value peaked above 2 for the composites with different loadings of RGO, meaning that the transmittance of UV light was very low and most of the UV light was shielded. RGO/PS composites could effectively protect against UV light and potentially be useful to UV-shielding materials.

4.2.5. Thermal stability analysis

The thermal stability of PS film, RGO/PS films were performed by thermo gravimetric analysis (TGA) shown in Figure 4.2.5. Thermal analysis was performed in order to determine if
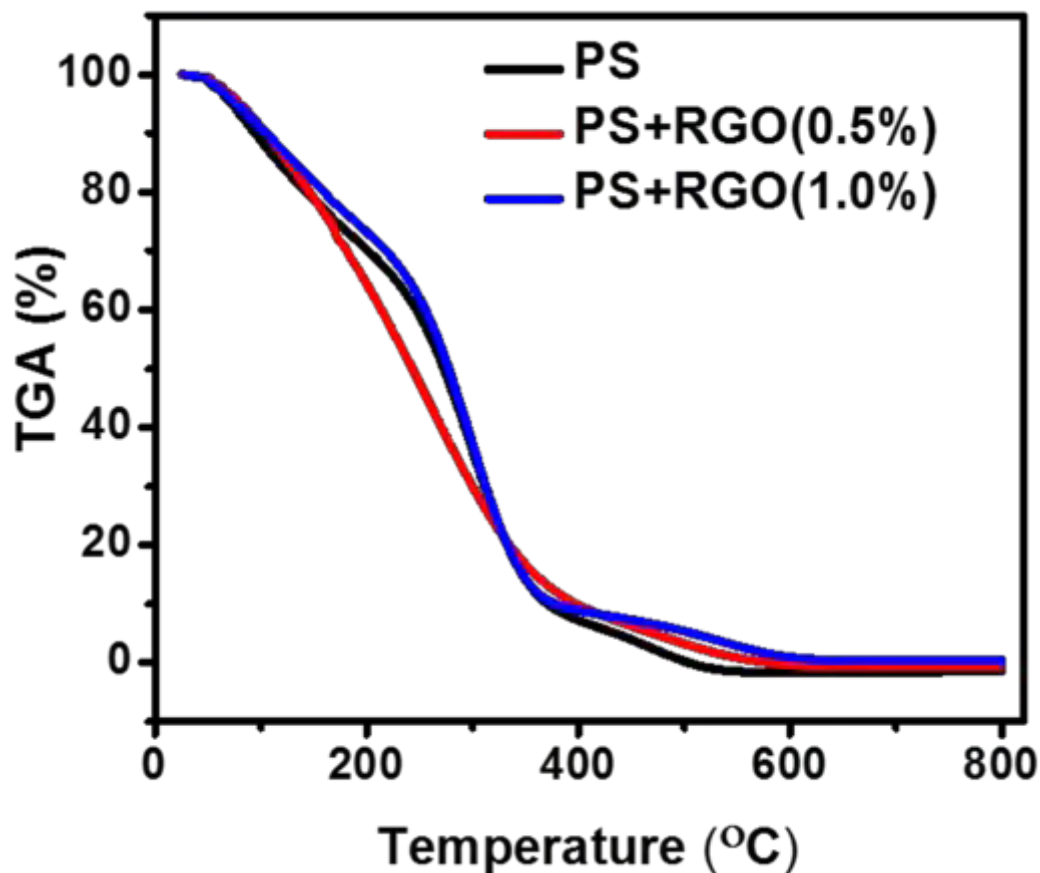

Figure 4.2.5. TGA thermograms of PS/RGO nanocomposite

the addition of RGO could produce any change on the thermal decomposition behavior of starch. The onset temperatures of PS film, RGO/PS (0.5%) film and RGO/PS (1%) films are 242 C, 200 C, 250C respectively. Onset temperature is the temperature where the first detectable heat is released, obtained by extrapolation of the steepest portion of curve. It could be noted basically two main thermal events. The weight loss before the onset temperature was attributed to volatilization of both of the water absorbed by starch and glycerol plasticizer. The second stage of the weight loss in the temperature range of 220–380 ∘C corresponded to decomposition of starch. An improvement in the thermal stability of the nanocomposite films could be seen with an increase of the fillers loading. Meanwhile, all experimental results of TGA, which was generally accepted and used to assess a material‟s lifetime, are listed in table. Such as the initial decomposed temperature (IDT), the integral procedural decomposition temperature (IPDT),the temperature at 50% weight loss (T−50%) and the temperature at the maximum rate of mass loss (T_{max}). It could be observed that all PS/RGO-n nanocomposite films showed a higher decomposition temperature than neat PS film. These results indicated that the decomposition temperatures of starch increased by the addition of RGO. The reason might be that the mobility of PS chains was suppressed by strong hydrogen bonding interactions with RGO.

Usually, the better the interaction between the filler and the matrix was, the higher the thermal stability of the composites was. From the result, it is observed that decomposition temperature is increased with the increasing loadings of RGO in the PS matrix.

Table 3

Thermal properties of neat PS and PS/RGO-n biocomposite films

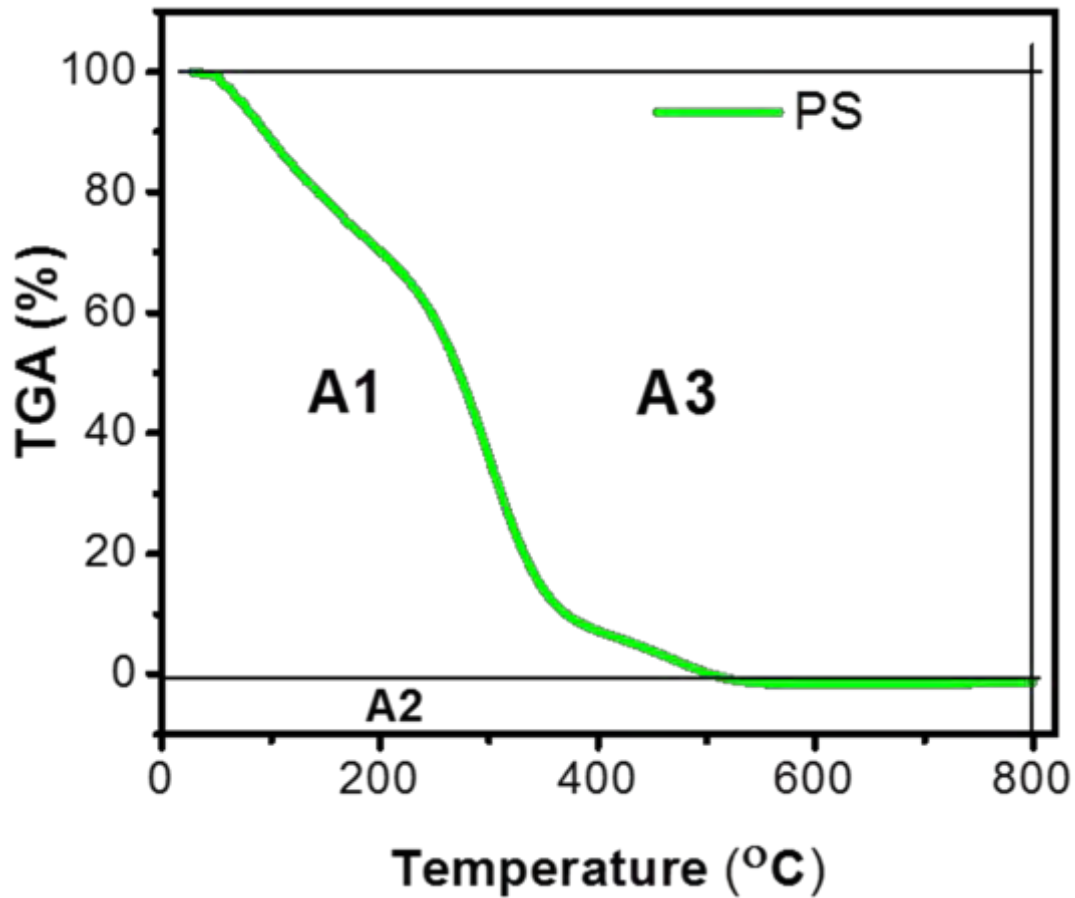| Sample	IDT	IPDT	T-50%	T_{max}
PS	242	242	270	380
PS+ RGO (0.5%)	200	249	243	395
PS+ RGO (1%)	250	266	275	385

Figure.4.2.6 shows the schematic representation of *A1, A2, and A3 for A* and K*.*

The integral procedural decomposition temperature (IPDT) can be used to assess a material''s lifetime. Figure5.6. shows the calculation procedure of IPDT.

The IPDT is calculated as follows: $IPDT=A^*K^*(T_f-T_i)+T_i$

whereA^* is the area ratio of the total experimental curve divided by the total TGA thermo gram $[(A1 + A2)/(A1 + A2 + A3)]$, K^* is the coefficient of A^*

$[(A1 + A2)/A1]$, Ti is the initial experimental temperature (25 °C in this work), and $Tf$is the final experimental temperature (800 °C).

4.2.6. Dielectric properties

Dielectric materials with high ε are viable in the field of electrical and electronic engineering. Polymer nanocomposites containing conductive carbon fillers have been widely used as potential high dielectric materials for various applications, such as embedded capacitors, electro active polymers for artificial muscles, active control in aeronautics and flexible batteries. High- k materials can store a significant amount of electrical charge. In the present study, dielectric constant (ε) of the RGO filled starch nanocomposites showed interesting electrical properties, when compared to the pure matrix. Dielectric constant was calculated using the following formula, $C= \varepsilon_r\varepsilon_0 A /d$ Where d is the thickness of the sample, A is the area; C is the parallel capacitance value, ε_0 is a constant.

Figure 4.2.7(a) shows the dielectric constant of PS and PS/RGO nanocomposite with different loadings at room temperature over the frequency range of 10^2 to 10^8 Hz. At frequency 100 Hz pure PS samples shows a dielectric constant about 195 but incorporation of 0.5% RGO it enhances at large scale which is 40 times to the pure samples and for 1% loadings of RGO dielectric constant is shown to be increased to 300 times.

The high dielectric constants of these materials originate from the displacement of ionic centers in the crystalline structure under the influence of an external electric field, resulting in asymmetrical shift of the ionic centers and polarization in the crystalline lattice. Ceramic dielectrics suffer from inherent brittleness which can be mitigated by adding powder form of these materials to polymers to fabricate flexible dielectric polymer composites. However, more than 30 wt% ceramic fillers are needed to obtain relatively high dielectric constant, which often causes deterioration of the mechanical properties of the composites. In contrast, polymer
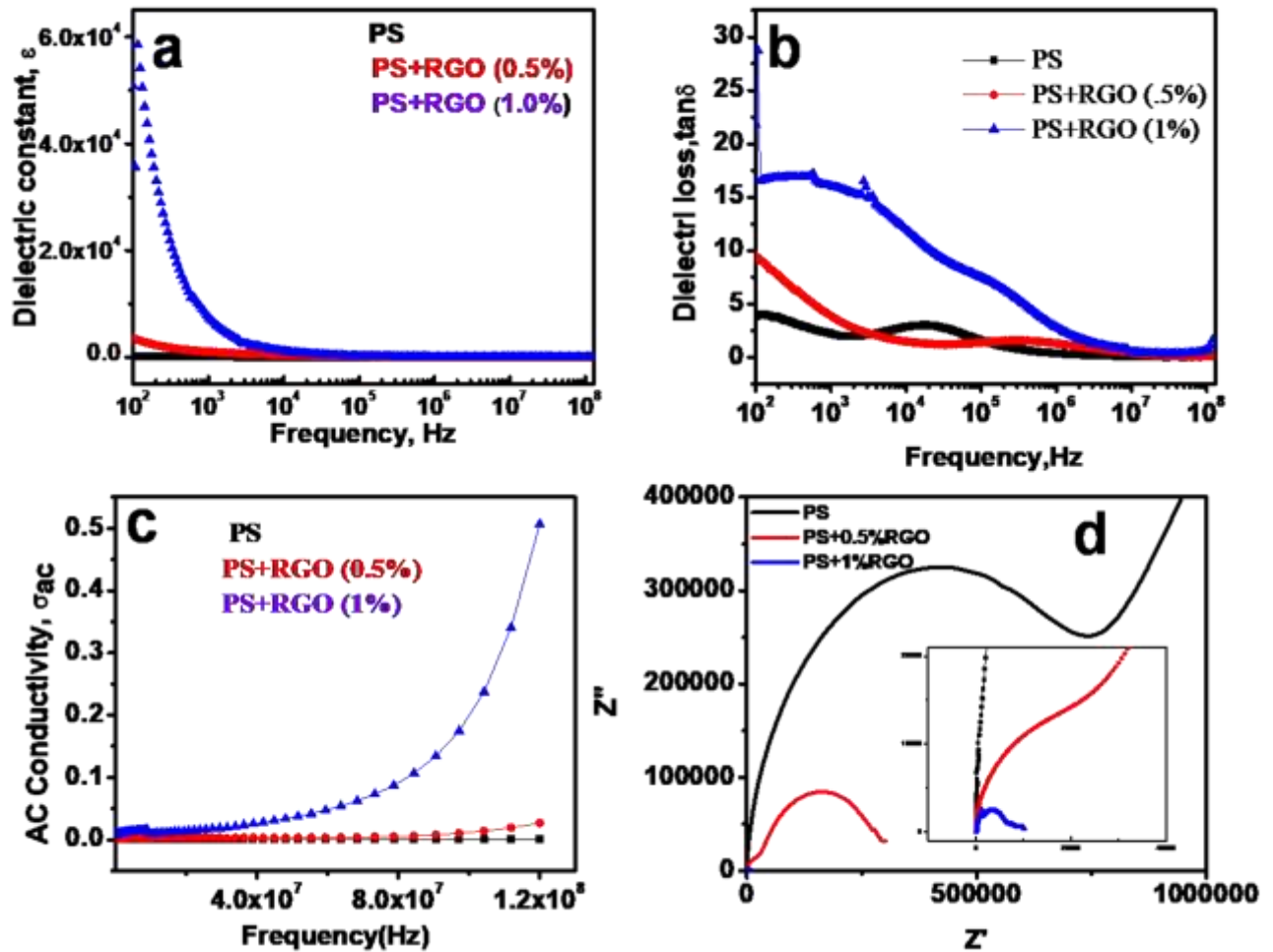
Figure 4.2.7 (a) Dielectric constant, (b) dielectric loss, (c) AC conductivity and (d) impedance of PS and PS/GO nanocomposites

nanocomposites consisting of carbon fillers can deliver high dielectric constants at much lower filler contents, while enjoying the advantages of high flexibility, processability and mechanical properties. The good potential of carbon filler/polymer nanocomposites as high- k materials arises mainly from the conductivity mismatch between the fillers and matrix. According to the Maxwell-Wagner-Sillars (MWS) principle, the disparity between the conductivities of two adjacent materials results in polarization and charge accumulation at their interfaces. Therefore,

the dielectric properties of nanocomposites are determined largely by the nature of the filler/matrix interface, the filler surface area and the inherent conductivity of the fillers. More importantly, the orientation of the fillers in a certain direction also plays a very important role in obtaining high dielectric constants. The neat PS showed negligible k -values at all frequencies studied. It appears that the dielectric properties of nanocomposites follow a percolative pattern. Above the electrical percolation threshold, the conductive networks formed by the nanofillers contribute synergistically to storing the electrical charge at the irinterfaces with the insulating polymer, hence a high- k nanocomposite.

Therefore, the dielectric constants drastically improved, reaching a value as high as 4000 in the composite with 0.5wt% RGO and 60000 for the 1wt%. The dielectric constants were dependent on frequency, showing parabolic decreases with an increase in frequency. This observation is a reflection of several important structural and material characteristics of the fillers and composites produced, including (i) ultralarge size of RGO sheets, (ii) excellent dispersion of RGO in the PS, (iii) preservation of the stability and superior dispersion even after reduction in the entirely in situ process, and (iv) self -alignment of the RGO sheets into a layered structure. Among the above mechanisms, the self-alignment into a layered structure is of particular importance. As the main mechanism of dielectric permittivity in these nanocomposites, the MWS polarization across the RGO/PS interface indicates that any pair of adjacent conductive RGO sheets separated by an insulating PS thin film can serve as a nanoscale capacitor. The anisotropic nature of the aligned RGO/epoxy composites may also present anisotropic dielectric properties between the plane and perpendicular directions. This is because the polarization intensity is directly proportional to the displacement between positive and negative charges under an external electric field which is higher in the plane direction, confi rming that the anisotropic intensity of interfacial polarization mostly contributed to the anisotropic dielectric constant.

Dielectric permittivities of GO and RGO papers were also investigated to compare the results with those of the nanocomposites, the dielectric constants of GO were much lower than the RGO counterparts due to the electrical insulating nature of GO sheets which prohibited the necessary interfacial polarization, while those of RGO papers were even higher than the corresponding polymer nanocomposites.

Dielectric losses are caused by Maxwell-Wagner polarization, ionic conduction, dipole, electronic, and atomic mechanisms. The dielectric loss consists of two parts: One is due to Debye-type relaxation, and the other originates from the leakage current that happens near percolation. The leakage current usually leads to a large loss factor given their small percolation threshold. However, it should be noted that tan δ of composites with0.5wt% of GO was slightly higher than that of the others at the frequency range of 10^5 Hz. This is reasonable because the highly ordered layered structure of the composite was corrupted. For all the samples dielectric loss became minimum at 10 MHz. The increase in dissipation factor for PS/GO (1%) may be due to starch implicates a percolation network with GO aggregation, which causes a marked increase of leakage currents and in turn to a dielectric loss in the system. Also, the values of dielectric loss are high at lower frequencies as compared to higher frequencies. It is mainly due to interfacial polarization relaxation in the composites. On the other hand, dispersion of GO in PS matrix also significantly influences the dielectric properties. Good dispersity of GO leads to higher dielectric constant and lower dielectric loss. As a result, both the dielectric constant and dielectric loss of GO/PS composite are higher than that of neat PS.

4.2.7. Electrochemical properties

To explore the effect of RGO on the capacititive behavior of the nanocomposite cyclic voltagrams (CV) were recorded. To assess the power capability of the nanocomposite CV measurements were performed at different sweep rates of $5mVs^{-1}$, $10mVs^{-1}$, $20mVs^{-1}$, $30mVs^{-1}$, $50mVs^{-1}$ and $80 mVs^{-1}$ using 0.1 M KCL as the electrolyte in a potential window of 1V. In all
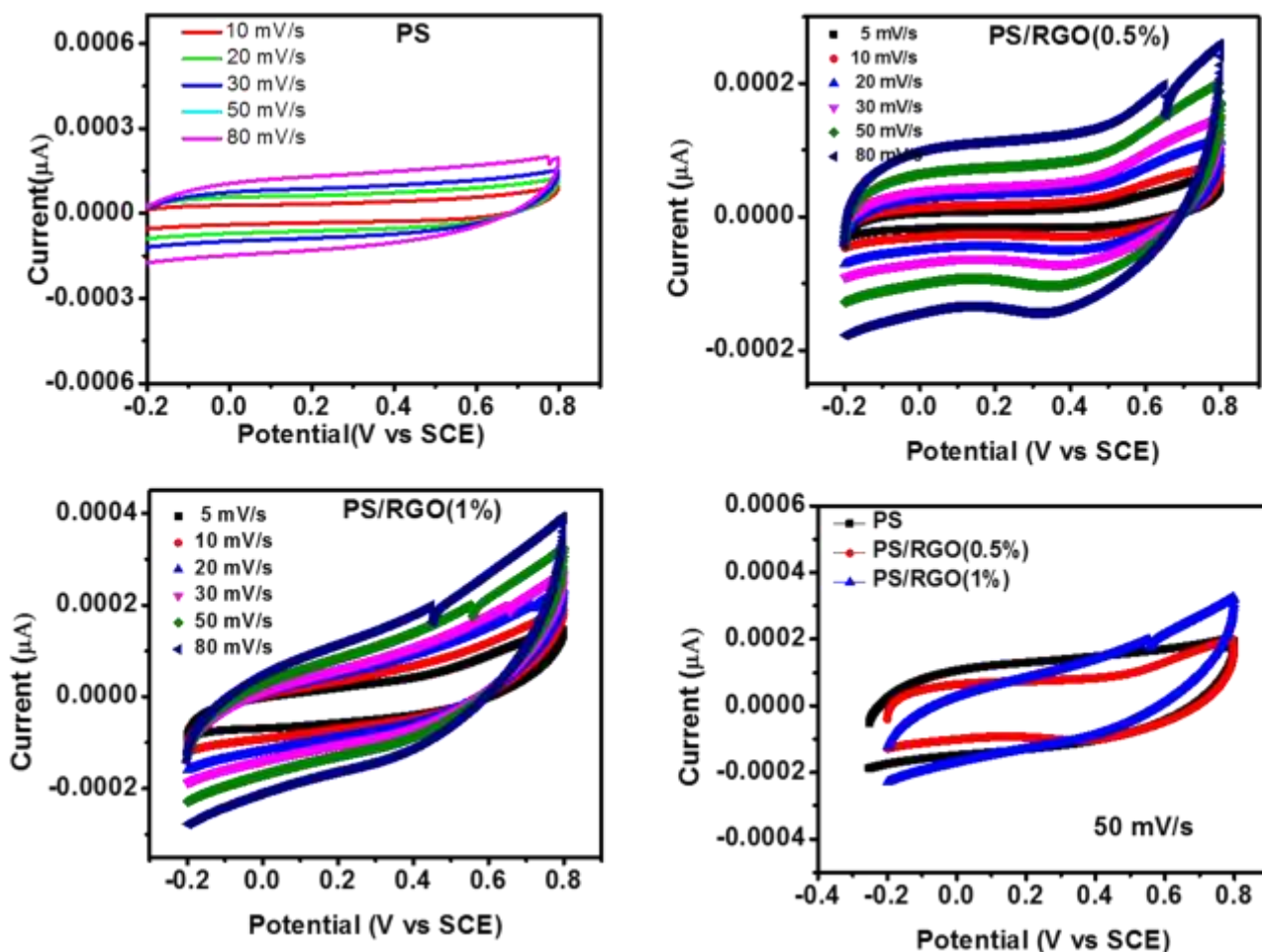

Figure 4.2.8. CV curves of PS, RGO and RGO/PS at various scan rates

cases the area of the CV curve increases with the scan rate.

For all scan rates the CV curves for PS exhibit nearly rectangle cyclic voltammogram whereas a distorted rectangular shape is observed for the RGO and PS/RGO composite. Such deviation can be attributed to the pseudocapacitance originating and electric double layer capacitance of RGO in polymer matrix.

Additionally, the cyclic voltammograms for RGO and RGO/PS composite exhibit a sharp rise in current at low voltage which drops sharply at the vertex potential indicating the good electrochemical stability of the electrode material.

Figure 4.2.8 shows the CV measurements for PS, RGO, PS+0.5%R GO and PS+1%RGO at a scan rate of 50 mVs^{-1}.Notably, the quasi-rectangle area of CV curves of PS /RGO was larger than that of pure PS but a bit less than only RGO, which indicated that RGO-PS composites exhibited better capacitance performance pure PS . This result implied that RGO played key roles in speeding up carriers" transportationalong the PS networking chains.

 Figure 4.2.9shows the galvanostatic charge-discharge (GCD) curves of PS and PS/RGO nanocomposite at a constant current density of 0.1mA/cm^2.The discharge time of PS/1%RGO composite based device was much longer compared to PS and PS+0.5%RGO nanpcomposite specific capacitances of the different nanocomposites were estimated from their respective GCD curve using the formula $C_s= I\Delta t/m\Delta V$. Where, I, t, V, and m are the constant current (A), discharge time (s), total potential deviation (V) and the mass of the active materials within the electrode (g), respectively.
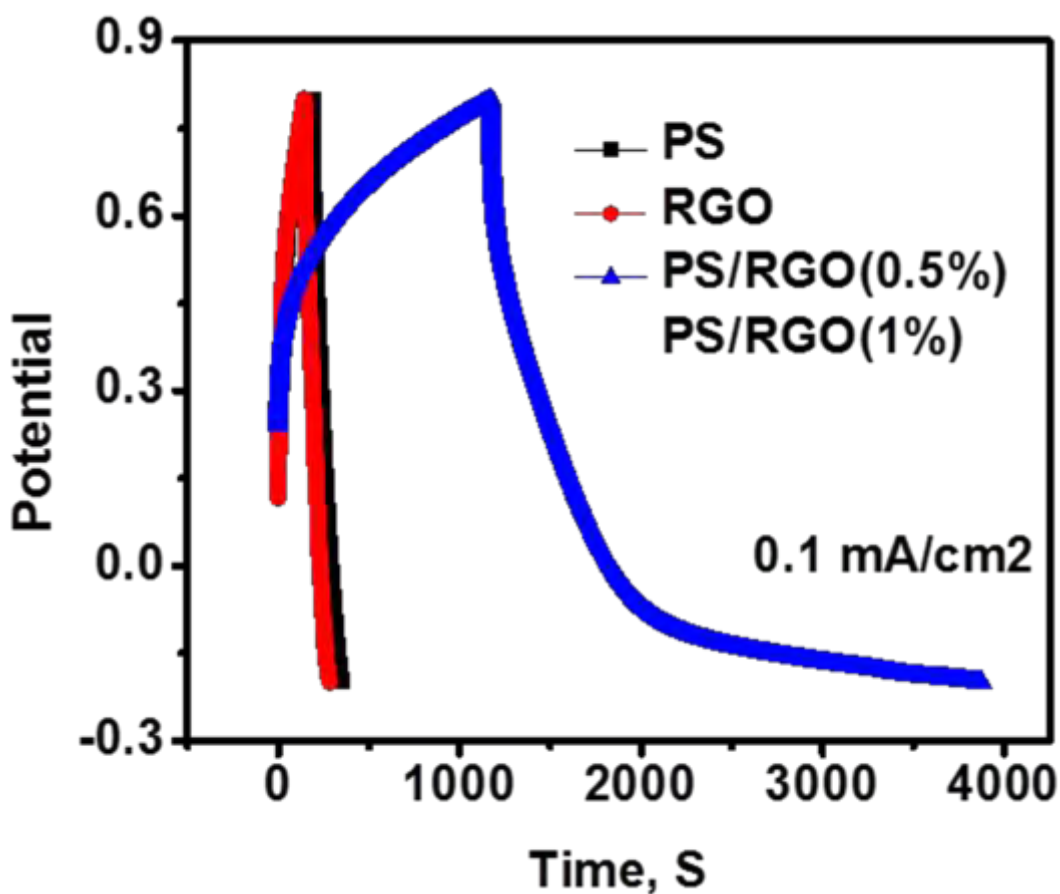
Figure 4.2.9.Galvanostatic charge-discharge curves of PS, RGO and RGO/PS electrodes at 0.1 mA /cm^2

However, the sharp IR drop at the initial discharge can roughly reflect the internal resistance of the electrode. The IR drop of PS+1%GO was much lower than that of the others. This result reflected that the internal resistances of the PS+1%RGO was much lower than that of the others. Low internal resistance is of great importance in energy storing devices; for less energy willbe wasted to produce unwanted heat during charging-dischargingprocesses. Thus, PS+1%RGO was more suitable for fabricating and power-saving supercapacitors.All the specific capacitance data of these composites at differentcurrent densities are summarized in Table 1. It can be observedthat the capacitance of PS+1%RGO was always higher thanthat of pure PS, RGO in all current densities.

References

[111]   Han, D. L., Yan, L. F., Chen, W. F., & Li, W. (2010). Preparation of chitosan/grapheneoxide composite film with enhanced mechanical strength in the wet state. CarbohydratePolymers, doi:10.1016/j.carbpol.2010.08.038

[112]   Hoover, R., & Ratnayake, W. S. (2002). Starch characteristics of black bean, chick pea,lentil, navy bean and pinto bean cultivars grown in Canada. Food Chemistry, 78,489–498.[113]   R. Li et al. / Carbohydrate Polymers *84 (2011) 631–637*

[114]   Chandra, S., Sahu, S., & Pramanik, P. (2010).A novel synthesis of graphene by dichromateoxidation. Materials Science and Engineering B, 167, 133–136.

[115] Chen, Y., Cao, X. D., Chang, P. R., & Huneault, M. A. (2008). Comparative study onthe films of poly(vinyl alcohol)/pea starch nanocrystals and poly(vinyl alcohol)/native pea starch. Carbohydrate Polymers, 73, 8–17.

[116]   Chung, Y. L., Ansari, S., Estevez, L., Hayrapetyan, S., Giannelis, E. P., & Lai, H. M. (2010) Preparation and properties of biodegradable starch–clay nanocomposites. CarbohydratePolymers, 79, 391–396

[117]   T. Ma et al. / Carbohydrate Polymers *94 (2013) 63– 70*

[118] Khurana, P., Aggarwal, S., Narula1, A. K., & Choudhary, V. (2003). Studies on thecuring and thermal behaviour of DGEBA in the presence of bis(4-carboxyphenyl)dimethyl silane. Polymer International, 52, 908–917.

[119] Ma, X. F., Chang, P. R., Yu, J. G., & Stumborg, M. (2009). Properties of biodegradablecitric acid-modified granular starch/thermoplastic pea starch composites.Carbohydrate Polymers, 75, 1–8.

[120]   Loos MR, Yang J, Feke DL, Manas-Zloczower I, Unal S,Younes U (2013) Enhancement of fatigue life of polyurethanecomposites containing carbon nanotubes. ComposPart B: Eng 44:740–744

[121]   Ma, X. F., Chang, P. R., Yu, J. G., & Stumborg, M. (2009). Properties of biodegradablecitric acid-modified granular starch/thermoplastic pea starch composites.Carbohydrate Polymers, 75, 1–8.

[122]   Jen-Yu Wang,‡ Shin-Yi Yang,‡ Yuan-Li Huang J. Mater. Chem., 2011, 21, 13569–13575

[123] Xiao-Juan Zhang,a Guang-Sheng Wang,* J. Mater. Chem. A, 2013, 1, 12115–12122

[124]   S. He, G. S. Wang, C. Lu, X. Luo, B. Wen, L. Guo andM. S. Cao, J. Mater. Chem.A, 2013, 1, 4685.

[125]   W. L. Song, M. S. Cao, M. M. Lu, J. Liu, J. Yuan and L. Z. Fan,J. Mater. Chem. C, 2013, 1, 1846.

[126] W. Wu et al. / Electrochimica Acta 139 (2014) 117–126

[127]   Q. Wu, Y. Xu, Z. Yao, A. Liu, G. Shi, Supercapacitors based on flexiblegraphene/polyaniline nanofiber composite films, ACS Nano 4 (2010) 1963.

[128]   K. Zhang, L.L. Zhang, X. Zhao, J. Wu, Graphene/polyaniline nanofiber compositesas supercapacitor electrodes, Chemistry of Materials 22 (2010) 1392.

[129] J. Zhang, X. Zhao, Conducting polymers directly coated on reduced grapheneoxide sheets as high-performance supercapacitor electrodes, The Journal ofPhysical Chemistry C 116 (2012) 5420.

[130]   L. Mao, K. Zhang, H.S.O. Chan, J. Wu, Surfactant-stabilized graphene/polyanilinenanofiber composites for high performance supercapacitor electrode, Journalof Materials Chemistry 22 (2012

[131]   J. Xu, K. Wang, S.-Z.Zu, B.-H.Han, Z. Wei, Hierarchical nanocomposites ofpolyaniline nanowire arrays on graphene oxide sheets with synergistic effectfor energy storage, ACS Nano 4 (2010) 5019.

[132]   Z. Gao, W. Yang, J. Wang, B. Wang, Z. Li, Q. Liu, M. Zhang, L. Liu, A New Par-tially Reduced Graphene Oxide Nanosheet/Polyaniline Nanowafer Hybrid as Supercapacitor Electrode Material, Energy & Fuels 27 (2012) 56) 80.

CHAPTER FIVE

CONCLUSION

&

SUGGESTIONS FOR FUTURE WORK

5.1 Conclusion

The aim of this research work was to produce biodegradable starch/GO & starch/RGO composite film. For that reason, natural biodegradable polymer starch granules were successfully extracted from potato. Glycerol is used as plasticizers and GO and RGO were used as nanofiller with native starch to enhance the mechanical, optical dielectric and electrochemical properties of starch based nano-composite films. GO/PS and RGO/PS composites were prepared using a casting process because both GO and RGO suspensions were stable in water. This stability was ascribed to the hydrophilic oxygen containing groups and the thin layers. The abundant oxygen containing groups of GO and the residual oxygen-containing groups of RGO could form hydrogen bond interactions with starch. These interactions and the unidirectional, uniform dispersion of GO/RGO sheets in the PS matrix played important roles in improvements to various properties. GO and RGO added functional properties to the PS matrix such as UV absorbance for the composites and electrical conductivity for RGO/PS composites. The GO/PS and RGO/PS composites with desirable mechanical properties are some of the most promising candidates for advanced UV shielding, biochemical, or electrochemical materials. In addition, GO and RGO sheets could also be used as fillers for other natural polysaccharide matrix.

5.2. Suggestions for future work

The following characterization can be performed to better understand the properties of GO/PS and RGO/PS nanocomposite

- ➢ Raman spectroscopy can be used to provide a structural fingerprint of the nanocomposite.

- ➢ X-ray Photoelectron Spectroscopy (XPS) can be performed to view the chemical bonds, state and composition.

- ➢ The effect of high concentration of GO and RGO on the dielectric and electrochemical properties of PS/GO and PS/RGO nanocomposite will be studied